European Commission
Information Society and Media

SEVENTH FRAMEWORK PROGRAMME

Specific Targeted Research Projects

SOLDER

Spectrum OverLay through aggregation
of heterogeneous DispERsed Bands

FP7 Contract Number: 619687

WP3 – Aggregation of Heterogeneous dispersed spectrum bands in HetNet and h-RATs

D3.2
Innovative solution for Carrier aggregation in h-RATs, LTE-A and beyond

Contractual Date of Delivery:	31 October 2015
Actual Date of Delivery:	
Responsible Beneficiary:	TCS
Contributing Beneficiaries:	ISI/ATHENA RC, EURECOM, IS-WIRELESS, KCL, SEQ, TCS
Security:	Public
Nature	Report
Version:	1.0

Document Information

Document ID: D3.2.doc
Version Date: 31 October 2015
Total Number of Pages: 97

Abstract

This report is the second report of the WP3. It captures the intermediate outcomes of the technical activities, related to carrier aggregation. Use cases already defined in D2.1 are considered, i.e. aggregation of LTE carriers in homogeneous or heterogeneous environment, aggregation of LTE and WiFi, consideration of TV white space spectrum. As multiple scenarios are covered, the WP3 has distributed activities to provide a good coverage of these various scenarios. Intermediate outcome are provided, both in terms of simulation and with respect to foreseen implementation, anticipating WP4 activity.

Keywords

Carrier aggregation, Link adaptation, Radio resource management, system capacity, TVWS, WiFi, LTE, LTE-U, 5G.

Authors

Name	Organisation	Email
Fotis Foukalas	ISI/AthenaRC	Foukalas@isi.gr
Apostolis Galanopoulos	ISI/AthenaRC	agalanop@isi.gr
Christos Tsinos	ISI/AthenaRC	tsinos@isi.gr
Theodoros Tsiftsis	ISI/AthenaRC	tsiftsis@isi.gr
Oliver Holland	KCL	oliver.holland@kcl.ac.uk
Adnan Aijaz	KCL	adnan.aijaz@kcl.ac.uk
Shuyu Ping	KCL	shuyu.ping@kcl.ac.uk
Mateusz Buczkowski	ISW	m.buczkowski@is-wireless.com
Sylvain Traverso	TCS	sylvain.traverso@thalesgroup.com
Guillaume Vivier	SEQ	gvivier@sequans.com
Florian Kaltenberger	EUR	florian.kaltenberger@eurecom.fr
George Arvanitakis	EUR	george.arvanitakis@eurecom.fr

Document History

Revision	Date	Modification	Authors
0.1	2015-03-18	Creation of the document	Sequans

0.2 – 0.54*	From 2015-04-24 to 2015-10-30	Iteration on content and several reviews	All authors
1.0	2015-10-31	Version 1.0 created	Thales

*see BSCW for full history

Executive Summary

D3.2 is the second report of the WP3 dealing with carrier aggregation (CA) for LTE-A and beyond. It reports the outcome of tasks T3.1, T3.2 and T3.3. It covers the usage of carrier aggregation in various scenarios defined in D2.1 (see Annex B), from “classical LTE” deployment, either homogeneous or heterogeneous, to more advanced scenario such as aggregation with WiFi, consideration of TV White Space or new waveform.

The report starts with the investigation of the enhancement of CA where we consider the specific problem of scaling the number of component carriers from 5 to 32. We identify a proposal to simplify the potential burden of DL signaling. This evolution is mostly pertinent in context of Licensed Assisted Access or the use of higher frequency bands which is actually envisaged in 5G.

Then, we propose a solution to address the objective of selective usage of a large number of non-continuous spectrum bands in HetNets dealing with the heterogeneous channel characteristics through the channel feedback adaptation. The proposed solution tackles with the large amount of channel estimation and allocation in multi-user CA in HetNets. To this end, low-complexity and low-feedback rate algorithm is devised and evaluated.

The report presents also the work related to the problem of radio resource management, and more specifically the topic of scheduling. We address the issue of achieving higher and more fair throughputs in the environment with aggregated carriers. The proposed algorithms can be successfully used in homogeneous or heterogeneous deployment, and allows to obtain higher throughput than traditional Proportional Fair algorithm without degradation in terms of dropped packets.

We study a means for aggregation of LTE in licensed spectrum with LTE in TV white space from the MAC layer point of view. The proposed solution consists in developing optimisation methods and algorithms with alternative purposes being to save transmission power and maximise capacity. We show through simulation results that considerable reductions in transmission power could be obtained as well as an increase in capacity.

After the use of LTE in TV white space, the report investigates LTE in the unlicensed 5GHz spectrum as envisaged by the standardisation in context of LTE-U. We propose to modify the LTE frame structure to define a burst which accommodates the constraints of operation in unlicensed bands. Furthermore, we extend the cognitive radio concept to the Licensed Assisted Access scenario thanks to the use of the learning and double Q-Learning techniques for the carrier selection and discontinuous transmission. The subcarrier allocation for a licensed/unlicensed CA MIMO system is also addressed proposing solution that provides both blind learning and interference nulling.

We present also some pioneering results on what is achievable in TV white space through CA, and fundamental observations on aggregation of discontiguous and contiguous channels affecting aspects such as RF design of devices for instance.

As an alternative to the LTE-U scenario, operators and also the 3GPP is working on a tighter integration between LTE and WiFi without modifying the actual access technology. We study the benefits of this scenario from a system level perspective taking the particular physical layer properties of the two RATs into account. The proposed model allows for the performance analysis of those different networks using closed form expressions. Using these newly developed tools, we show that the max-throughput criterion, which takes the different characteristics of the two RATs into account, performs better than simple offloading and max-SINR association criteria.

This report deals also with the CA of WiFi in unlicensed spectrum with LTE in TV white space where a first complete solution is proposed. We study an optional and useful case for aggregation management involving geolocation databases. The proposed solutions are novel and

highly-practical in terms of their alignment with regulatory directions and standards directions in the development of systems.

Finally, we tackled issues that arise using FBMC waveform as a PHY CA component when realistic transmitter front-end is taken into account. To this end, we first propose an efficient calibration technique to compensate for analog non idealities such as IQ imbalance and DC-offset. Then we present and develop two different PAPR reduction techniques for contiguous and discontiguous CA scenarios.

1. Introduction

SOLDER project addresses carrier aggregation in many forms. Following the definition and classification of use cases and scenarios provided by WP2 (see Annex B of D2.1) and initially considered in D3.1, this report proposes innovative solutions for these scenarios. New ideas could be found in this report as well as elaboration of ideas already been introduced in D3.1. D3.2 lists below significant solutions described in the DoW as the objectives of the project. All partners fully active achieved to complete most of them. Moreover, part of the proposed techniques in the report is being transferred to WP4 for validation on prototype. D4.1 in particular received significant input in M18 of the project regarding the developed solutions in WP3. In addition to that, the D4.2 is also driven by the D3.2 solutions giving input to the particular building block development. Notably, not all of the solutions listed in this document are going to be developed for demonstration purposes and proof of the SOLDER concept. A few of them are studies using mathematical modelling and simulations to provide more comprehensive results achieving most of the objectives of the project.

In order to limit the length of the deliverable, we deliberately try to reduce the replication of material that we have already published as part of our SOLDER work, and provide the full publications as appendices for more detailed information. The deliverable is structured as follows. Section 2 addresses the common case of LTE CA, using licensed spectrum; in context of homogeneous deployment. Sections 3 and 4 discuss the heterogeneous case, wherein aggregation of carrier from a small cells (e.g. femto and pico) and larger cells (e.g. macro and micro) in an overlay deployment is carried out, from MIMO/link adaptation and radio resource management standpoint. Then, Section 5 deals with LTE in licensed spectrum aggregated with LTE in TVWS (TV White Space) where a downlink spectrum aggregation scenario is considered. Section 6 studies the use of CA to enable LTE in unlicensed spectrum, which scenario is directly the case of LAA (Licensed Assisted Access) as currently being defined in the standardisation. As an alternative to the previous scenario, the case of the aggregation of LTE and WiFi without modifying the actual technology is presented in section 8. Aggregation of TVWS channels is discussed in Section 7, whereas section 9 is dedicated to the solutions for the aggregation of WiFi in conventional unlicensed spectrum with LTE in TV white space.Section 10 describes activities about FBMC as a candidate of 5G waveform that could be also a key component for spectrum aggregation. Finally section 11 presents the list of the techniques which are being prototyped.

2. LTE (Licensed) + LTE (Licensed) – Homogeneous deployment

This scenario corresponds to the baseline of CA, or more exactly to the original scenario as defined by 3GPP to introduce CA. The standard is still improving the toolbox of features to support CA even if the new features are not necessarily motivated by such original deployment scenario. We therefore present in this section a contribution related to a work item of LTE Rel. 13, which consists of increasing the maximum number of aggregated carrier. The full contribution is available in Appendix 2.1.

On the other hand, due to the rapid network deployment and increased demands for resources in densely populated areas it became more pertinent to develop algorithms related to the heterogeneous deployment of the network. Therefore, we elaborated on the work that has been presented in the D3.1 in section regarding homogeneous deployment and extend it into the HetNet case. In some cases, like section 4 of this document, proposed solutions can be applied to the HetNet deployment or homogeneous deployment.

2.1 LTE Carrier Aggregation Enhancement Beyond 5 Carriers

As of 2014, the 3GPP has started to introduce the idea to extend CA to more carriers (the maximum number of aggregated carriers was originally set to 5, in order to meet the requirement of IMT-Advanced).
A new work item (WI) was created, entitled “LTE Carrier Aggregation Enhancement Beyond 5 Carriers”, (LTE_CA_enh_B5C) [1]. This WI is supposed to be completed in Dec 2015, at least for the core part, the performance part showing often a shift of 1 or 2 quarter in the standardisation process. The rationale behind this work item was the following:

- 3GPP already defined bands with more than 5 carriers available (e.g. in the 3.5GHz spectrum). To fully benefit from these bands, it could be of interest to define CA schemes with more than 5 carriers.
- LAA had a lot of traction and will allow LTE device to operate in the 5GHz unlicensed spectrum. This spectrum is quite wide (80 or 160MHz depending on local regulation) and there could be the possibility to find more than 5 carriers in such band (adding up the licensed bands too).

Although not mentioned at the time of the creation of the WI, one motivation could be found in the perspective of 5G context. Indeed, many players discuss the introduction of much higher bands (mmwaves, from 20GHz to 60GHz, sometimes up to 100GHz). In these bands, the available bandwidth can be significant larger than in the sub 6GHz frequency and therefore, there is a need to enable CA with much larger number of component carriers.

The work item set the goal to extend CA principles from 5 to 32 carriers. Several problems arise when scaling up the number of CC from 5 to 32. At high level one could mention:

- Problem on the UL: in default CA, the signaling is supposed to be transmitted on the control channel of the primary cell. With the increase of the number of (DL) CC, the load on the PUCCH of the PCell is becoming significant that could even degrade the performance of the whole system (CA or non-CA devices have to share the same resource for PUCCH).
- Problem on the DL: the system should find an efficient way to signal to the user the allocation of the CC, possibly reusing both self-scheduling and cross-scheduling approaches.

For the UL control channel capacity, one solution is given by the Dual Connectivity feature still being improve at the standard level ([1][2]), which allows the terminal to have UL control connection on two sets of cells. A quick extension of this principle could allow indeed to share the PUCCH load on multiple cells (not anymore the PCell only). For the DL signaling enhancement problem, we proposed to the standardization a new approach to mitigate the issue. This proposal has been made during the RAN1#82bis meeting in the contribution R1-155917 [4], also provided in Appendix 2.1.

The main point of this contribution is to enhance the principle of Downlink Control Information (DCI) blind decoding to improve the capability of the receiver to blindly decode a large number of DCI (since each CC convey its own DCI), while keeping its complexity reasonable. Indeed, when the number of DL CC is increased, the terminal has to monitor more PDCCH to be able to dynamically detect the possible allocation of data on each CC. The enhance DCI we proposed is actually an “Auxiliary DCI”, a-DCI which includes information that could accelerate the decoding of DCI on other CC by reducing the size of the search space. In other words, we proposed to move from a total blind decoding to a not-totally-blind decoding once the first DCI is decoded. Depending on the level of information provided on this a-DCI, we evaluated the gain on the decoding of the other CCs. The gain can be expressed in terms of number of blind decoding to perform and vary from 60 to 90%. See [4] for more information.

Despite the interest of this proposal, it was not accepted in the standardization process: an alternative based on higher layer signaling was made and preferred to our PHY layer proposal.

2.2 Achievement

Solder gave the opportunity to investigate tools and enhancement of CA. We have considered the specific problem of scaling the number of CC from 5 to 32 and identified a proposal to simplify the potential burden of DL signaling. We submitted our proposal to the standardization that unfortunately preferred to consider another alternative. In any case, this contribution allowed us to better understand the possible constraints in context of implementing such evolution. At last, this evolution from 5 to 32 CC is mostly pertinent in context of LAA or the use of higher frequency bands such as the one envisaged in 5G.

3. LTE (Licensed) + LTE (Licensed) – HetNet deployment (PHY layer)

3.1 Overview

In the spirit of supporting a large number of CC, and as introduced in the previous deliverable D3.1 and discussed also above in the context of [1], this section investigate from a theoretical standpoint the issue of feedback from the UE to the network to ease link adaptation and resource allocation. We provide a solution that can manage the channel allocation for a large number of CCs in HetNets. The solution relies on the simulation of a CA MIMO system that is able to send back information using heterogeneous channel feedback reports per channel, i.e. CC. Having provided a low-complexity feedback report solution for the CA MIMO system, we provide additionally a low-feedback rate channel allocation assuming multi-users in HetNet. The solution is provided with stable matching (SM) that solves the formulated channel allocation problem more efficiently compared to Hungarian method (HM) in terms of complexity. The sections below provide adequate details about the proposed “Low-Complexity and Low-Feedback Rate Channel Allocation for CA in HetNets”, whereas the submitted full journal version with all the details can be found in the Appendix 3.2.

3.2 Low-Complexity and Low-Feedback-Rate Carrier Aggregation in HetNets

3.2.1 Low Complexity Heterogeneous Channel Feedback Calculation

In this section, we provide a low complexity heterogeneous channel feedback calculation for MIMO link adaptation based on PMI/RI selection. .The input-output relation in the k-th sub-carrier of the i-th sub-band (SB) is given by:

$$\boldsymbol{y}_{ikn} = \boldsymbol{G}_{ikn}^{H}\boldsymbol{H}_{ikn}\boldsymbol{W}_{i}\boldsymbol{x}_{ikn} + \boldsymbol{w}_{ikn}, 1 \le k \le K, 1 \le n \le N, \quad (1)$$

where $\boldsymbol{H}_{ikn}$ is the $R_x \times T_x$ channel matrix, $\boldsymbol{W}_i \in F$ and $\boldsymbol{G}_{ikn}$ are the $L \times T_x$ pre- and $R_x \times L$ post-coding matrices, L is the number of transmitted symbols, $\boldsymbol{x}_{kn}$ is the $L \times 1$ transmitted symbols vector, $\boldsymbol{y}_{kn}$ is the $R_x \times 1$ received symbols vector, $\boldsymbol{w}_{ikn}$ is the $R_x \times 1$ white noise random variable vector, I is the number of the available SBs following the non-contiguous CA approach and $K = 12\eta$ is the number of sub-carriers per SB, with η being the SB size (i.e. number of resource blocks that constitute the SB) and *N* is the time index.
The feedback and computational complexity reduction that the Mean Channel (MC) approach achieves come at the cost of performance degradation [5]. The aim of this section

is to propose a new low complexity, low-feedback approach that achieves also improved performance. The motivation here stems from the fact that in OFDM systems adjacent sub-carriers are subject to strong correlation. To this end, the UE can calculate the PMI and RI based on the channel covariance matrix on each SB. Thus, the UE computes for each SB:

$$\boldsymbol{R}_{in} = \frac{1}{K}\sum_{i=1}^{K} \boldsymbol{H}_{kin}\boldsymbol{H}_{kin}^{H}, (2).$$

Let us first consider the selection of the RI index. The RI index is in fact the number of the parallel streams that are employed for transmission. According to the literature, the number of parallel streams that a transmission should employ is dictated by the condition of the equivalent eigen-channels of the channel matrix. A channel that corresponds in a small eigenvalue exhibits a relative bad condition and should not be used from a capacity point of view. To that end, we propose to select the RI based on the number of eigenvalues of the correlation matrix that are above a threshold. Given the assumption that the sub-carriers that are included in a SB exhibit high correlation, the eigenvalues of the channel matrices that correspond to the sub-carriers are close to the ones of the correlation matrix. Therefore, if the correlation matrix $\mathbf{R}_{in}$, admits the following decomposition:

$$\boldsymbol{R}_n = \boldsymbol{V}_n\boldsymbol{\Sigma}_n\boldsymbol{V}_n^{\boldsymbol{H}}, (\mathbf{3})$$

the RI index is computed as follows:

$$RI = \sum_{l=1}^{\min\{R_x,T_x\}} 1\{\boldsymbol{\Sigma}_n(l,l) \geq \eta\}, (4)$$

where $1\{\cdot\}$is the indicator function and $\Sigma_{\mathrm{n}}(\mathrm{l},\mathrm{l})$ is the l-th eigen value of the sample covariance matrix and the predefined threshold.
We would like now to derive the computational complexity of the proposed method that can be found in Appendix 3.2. Table 1 provides results of the comparison of the original, MC and the proposed approach. As it is shown the proposed approach requires significantly reduced complexity as compared to the former approaches. This low complexity achievement does not come with a performance degradation as described below.

Table 1: Computational Complexity Comparison

η	***Original***	***Mean Channel***	***Proposed***
1	490760	45120	16880
2	490760	24480	10360
3	490760	14160	7100
4	490760	9000	5470

In the following text, a number of representative simulations are presented for a 2x2 LTE-A system that employs CCs of 96 sub-carriers (that is equal to 1.4 MHz bandwidth per CC). In Figure 1, the achievable sum rate of the system that employs the proposed technique for PMI/RI selection is examined for different SB sizes ($K = 12\eta$). As it was expected, performance degradation is presented when the SB size increases. For comparison purposes, the performance of the original technique of [5] is also presented in the same figure for the same values of the SB size. It is evident that the proposed technique achieves identical performance to the proposed one despite the fact that it requires severely reduced computational complexity. Similar conclusions are also derived for the case of the M-best strategy as it is depicted in Figure 2, where M is the number of the best channels that are used to compute the PMI/RI granularity. It is though noteworthy that the value *M* has a great impact on the performance since a simple increase by one can increase greatly the performance in terms

of the achievable data rate. Thus, our low feedback rate channel allocation will rely on the M-best strategy.

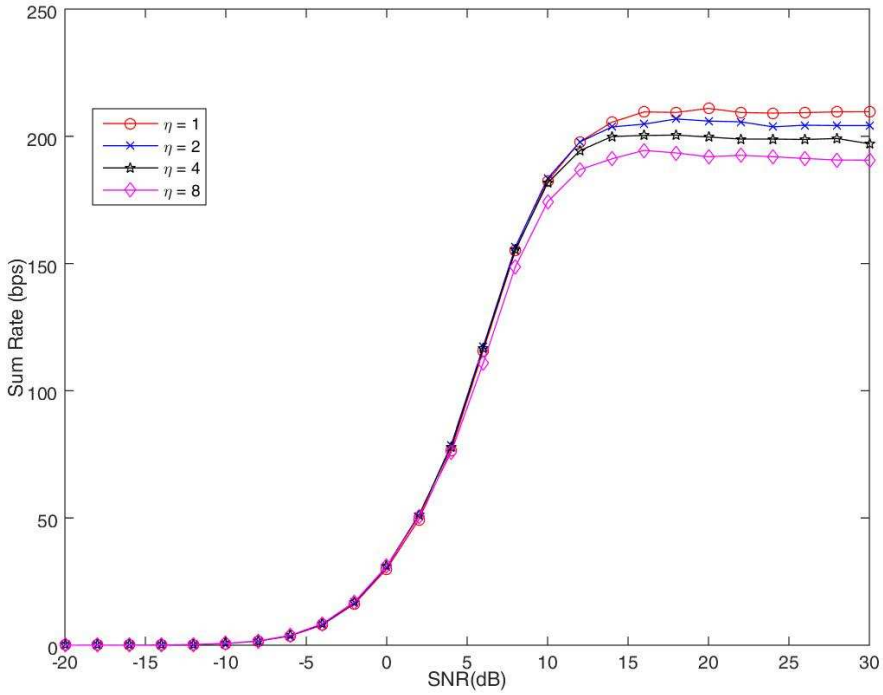

Figure 1: Sum Rate for Medium Correlation using η feedback strategy

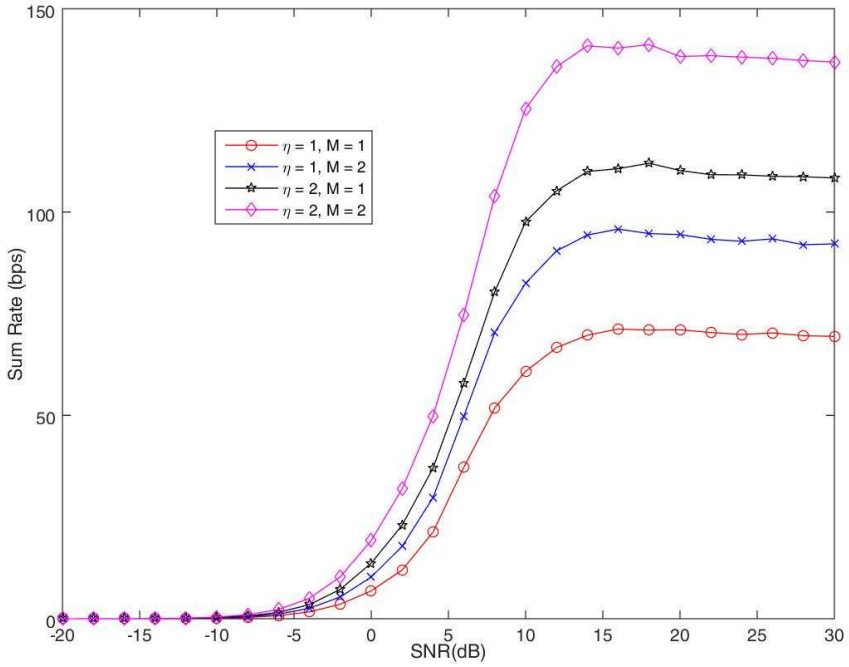

Figure 2: Sum Rate for Medium Correlation using *M* feedback strategy

3.2.2 Low-Feedback Rate Channel Allocation in Carrier Aggregation Systems

We extend our system model with multi-users with a set of K users. Each user $k \in K$ has a target throughput S_k^{QoS} that the system must ensure it is achieved. In this case, we employ a M-best feedback strategy in order to control the amount of overhead added to the system. We aim to performing CC channel allocation and decide the optimal $\bar{M}$ for all CCs. The solution approach of this problem is to minimize feedback overhead by minimizing M. Moreover η does not affect the amount of feedback overhead in this case, it only affects the achievable throughput of the users and so it should be chosen accordingly (lowest possible for maximum throughput). Over all possible CC allocation combinations, we choose the ones that firstly have M-best partial feedback that provides enough throughput to satisfy user needs and secondly choose the best solution among them, as the one that minimizes the total M for all channels. For a specific CC channel allocation, we assume a set of N_k carriers is allocated to user *k*. Then, we would have to solve the following problem for each user *k*.
In a similar manner, the problem can be defined also for the M-best selected strategy case. That is:

$$\max_{M_{kn}} \sum_{k=1}^{K} \sum_{n=1}^{N} \alpha_{kn} M_{kn}, (5)$$

subject to:

$$\sum_{k=1}^{K} S_{nk}(M_{kn}) \geq S_k^{QoS}$$

$$M_{kn} \in \{1,2,3,4\}$$

$$\sum_{n=1}^{N} \alpha_{kn} = 1, \forall k \in K$$

where α_{kn} is a binary variable that is one when the n-th channel is allocated to the k-th user and zero otherwise. To deal with the channel allocation problem, we will use the HM that can solve the considered combinatorial optimization problem as an assignment problem [6]. For each possible number of CCs per user, we compute the exact CCs that maximize the users' sum throughput. The iteration over all possible combinations of CCs number per user is a prerequisite for the application of the HM that is used afterwards to determine exactly which CCs will be assigned to each user, i.e. the CC allocation solution. Next, we solve the optimization problem for each user and if the problem can be solved for every user (the user's throughput target is achieved), we add the current carrier allocation scheme and the result $\bar{M}$ to the set of solutions *S*. After all carrier allocation schemes are checked, we select the optimal solution as:

$$s^* = arg \min_{s \in \boldsymbol{S}} \sum \bar{M}_s, (6)$$

The procedure described above is presented in Algorithm 1 below in details.

Algorithm 1 Multi-user and Multi-CC Channel Allocation

for each possible number of CCs per user combination **do**
  Compute CC allocation using Hungarian method
  for each user k **do**
    Calculate $\bar{M}_k$ so that $r_k \geq S_k^{QoS}$

end for
if Optimization problem has solution for all users **then**
Add the overall solution $s = \{\bar{M}\}$ to set S
end if
end for
Choose the optimal solution as $s^* = arg\min_{s \in S} \sum \bar{M}_s$

Now, we test the performance of a 96-subcarrier system in terms of the total amount of feedback that is obtained from the CC channel allocation solution of the problem. We test for the case of 3 users in the system and 5 and 10 available CCs. We assume that M takes values from the set {1,2}. For each of the 2 cases, we measure the sum of M of all CCs, over a set of average throughput targets for the users and several SNR cases for the users. We assume the following cases:

- Case 1. One user has low SNR at all CCs (0-6 dB), One user has medium SNR at all CCs (7-14 dB) and the last user has high SNR at all CCs (15-20 dB).
- Case 2. All users have low (0-6 dB) SNR with all CCs.
- Case 3. All users have medium (7-14 dB) SNR with all CCs.
- Case 4. All users have high (15-20 dB) SNR with all CCs.

The results of the 4 SNR cases are displayed in Figure 3 for the 5 CC case and in Figure 4 for the 10 CC case. In Figure 3, we observe how the sum of M that is relative to the amount of feedback overhead, is related to the average user throughput target. As the throughput target increases it is expected that M also increases in order to increase the user's achieved throughput. Moreover we see that in the case of low SNRs, feedback overhead increases a lot faster and finally converge with the case of different SNRs per user. For high throughput targets the medium and high SNR cases converge to a specific total M value sooner due to the better channel quality and the resulting higher throughput. Similar results are obtained for the 10 CCs case as well. In this case the average user throughput target values are increased since more carriers are available and the users can achieve higher throughputs.

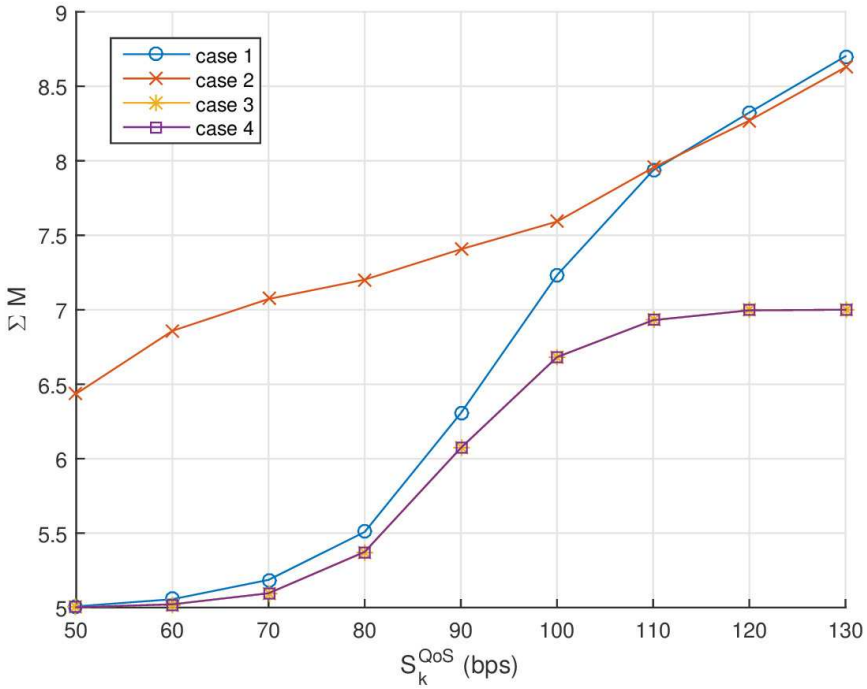

Figure 3: Total *M* for *N* = 5 CCs.

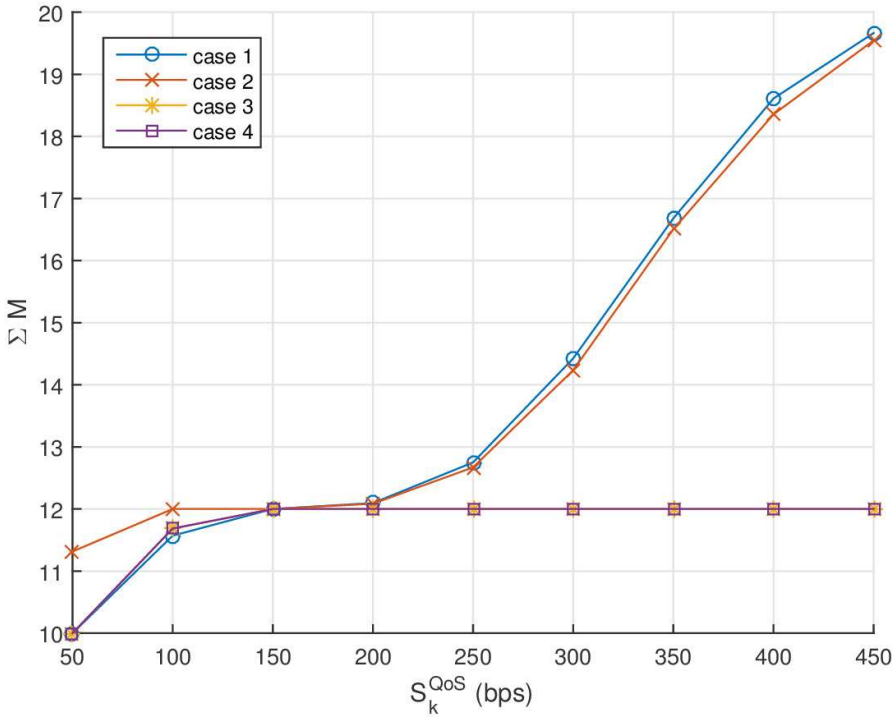

Figure 4: Total *M* for *N* = 10 CCs.

Next, we want to track the solution of the CC allocation problem for different setups. We assume that the first user has medium, the second one has high and the third one has low SNR in all CCs. We measure the number of allocated CCs of each user for different cases of throughput targets and display the results in Figure 5. The number of allocated CCs varies according to user SNR and throughput target that is expressed in bps. The results indicate that generally more CCs are allocated to the user with the lower SNR than the user with the smallest throughput target. In other words the user's SNR values in all CCs impacts the number of CCs more than the target throughput. The respective results for the 10 CCs case are displayed in Figure 6.

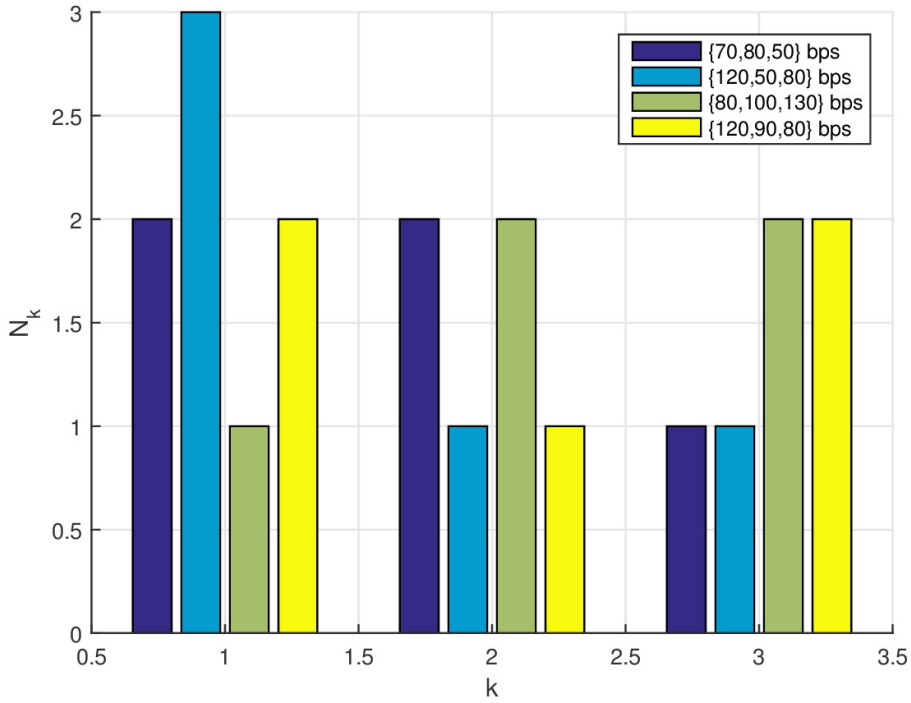

Figure 5: Component Carrier allocation with *N* = 5 CCs.

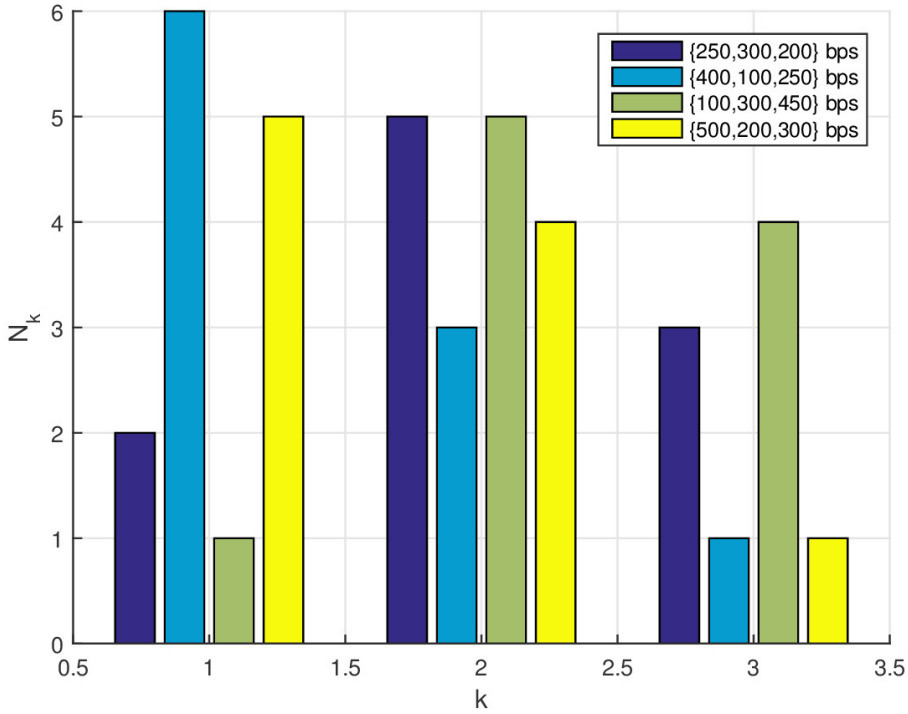

Figure 6: Component Carrier allocation with *N* = 10 CCs.

Another aspect that our solution should highlight is that the addition of CCs is going to decrease the amount of feedback overhead. More specifically, we set the throughput target of

the users to 300 bps and measured the average M (M_{avg}) value as we increased the number of CCs for 3 SNR cases: low, medium and high. The results displayed in Figure 7 indicate that the amount of feedback overhead indeed increases as we add more CCs. For a target throughput of 300 bps we clearly see that the overhead is much more in the case of low SNR carriers than the case of medium and high SNRs where performance is almost the same. To further investigate those cases we increase the target throughput of the users in Figure 8 in order to observe an increase in the performance of high SNR. Moreover we see how the overhead is not decreased significantly in the case of low SNR even with 10 CCs, since the throughput target set is too high.

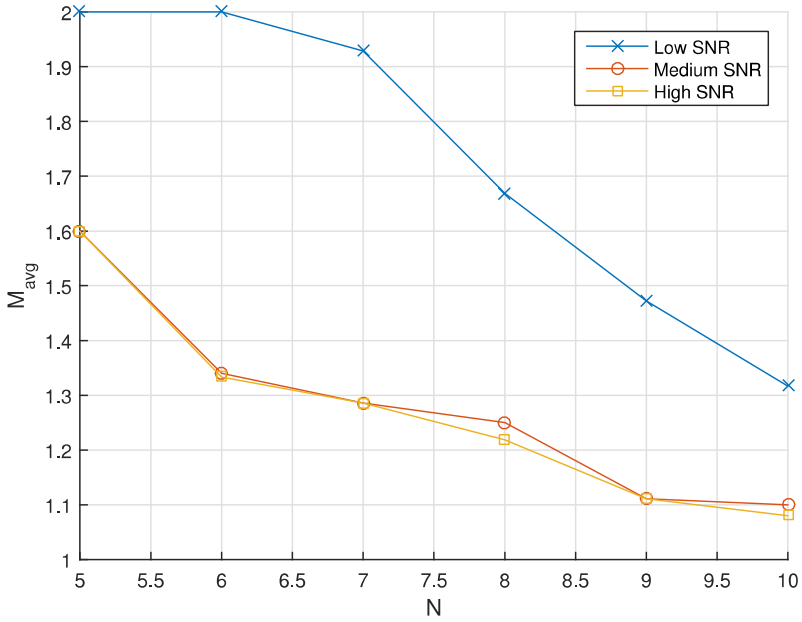

Figure 7: Average ***M*** for 300 bps target throughput.

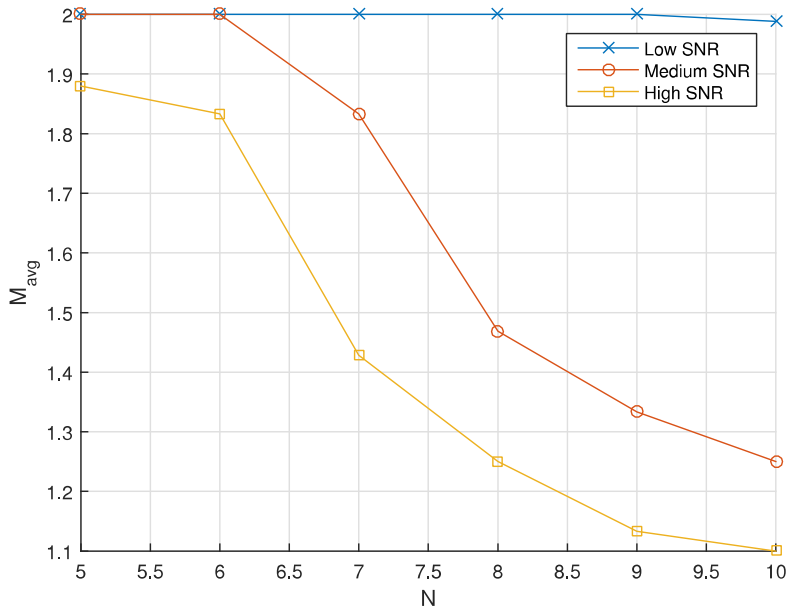

Figure 8: Average M for 500 bps target throughput.

3.2.3 Low-Complexity and Low-Feedback-Rate Channel Allocation in Multi-User Carrier Aggregation Systems

The order of complexity using the HM is too high, especially for the multi-CC and multi-user scenario involving more than 30 CCs envisioned by 3GPP [7]. Thus, we were motivated to seek for a less complex solution. To that end, a novel approach is developed in the context of SM that is recently presented in the resource allocation literature [8][9][10][11]. The idea is that each UE computes the values M_{nk} by solving the following discrete optimization

$$\text{Find the minimum } M^*, s.t. R_k(M_{kn}, \eta_{kn}) \geq R_k^{QoS}, (7)$$

Then, it starts proposing to the eNodeB to be matched with its preferred channels by sending its utility function which here is given by the targeted rate of Eq.(7). Then the eNodeB allocates the channels to the user with the maximum utility function in order to maximize its sum rate. It also informs the rest users which channels are not eligible anymore, thus each user has to plan its next proposal based on the remaining channels, The procedure follows until all the channels are allocated or all the users are satisfied. The algorithm is summed up on Algorithm 2. Each channel is proposed at least once so the worst complexity is O(nk) operations.

Algorithm 2 Low-Complexity and Low-Feedback-Rate Channel Allocation

Each user calculates the optimal M_{nk} and η_{nk} values for each one of the eligible CCs and calculates utility functions S_{nk}
if there are available channels each user does
while $R_k \leq S_k^{QoS}$ **do**
  Proposal by UE k: Request $n^* = arg\max_n S_{nk}$
  if $S_{n^*k} > S_{n^*k_1} \forall k_1 \in [1, K]$ & $k_1 \neq k$ **then**
    if n^* is allocated to another user $k_2 \neq k$ **then**
      Inform user k_2 for the releasing engagement
    end if
    Allocate n^* to user k
  end if
  for each user $k_3 \in K$ such that $S_{n^*k_3} < S_{n^*k}$ **do**
    Eliminate preference on k and disqualify the UE from proposing to n^*
  end for
end while

In correspondence to the original Multi-user and Multi-CC Channel Allocation Algorithm provided in the previous section we now present simulation results about the newly proposed Low-Complexity and Low-Feeback-Rate Channel Allocation algorithm. As before, we measure the average total M for several throughput target constraints and users' SNR profiles. Figure 9 illustrates the required results for the case of 3 user/5 CC system. The same simulation is repeated for the case of 3 user/10 CC system in Figure 10.

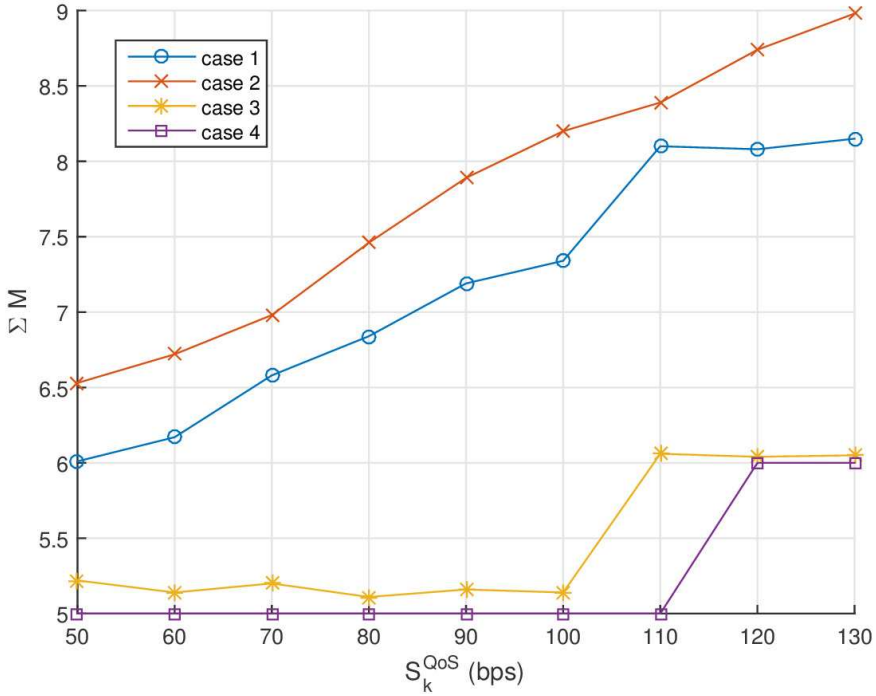

Figure 9: Total $\boldsymbol{M}$ for $\boldsymbol{N = 5}$ CCs.

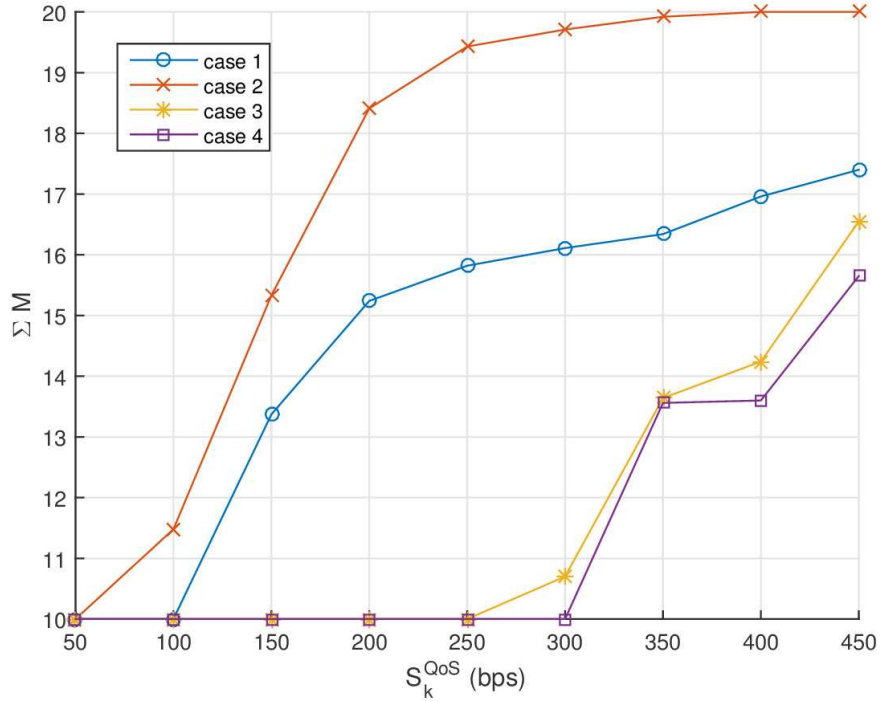

Figure 10: Total $\boldsymbol{M}$ for $\boldsymbol{N = 10}$ Cs.

Comparing the above figures to their respective ones from the original algorithm several remarks can be made. Firstly, note that the solution in many cases does not satisfy all users, since the CCs are assigned opportunistically to the "best" user and M is predetermined for each user/carrier. This case, although rare, exists when users have low SNR values with the

channels and/or high throughput target constraints. About cases 1 and 2 that represent the mixed and low SNR user cases we have a very similar to figures 4 and 5 result. As the average target throughput increases, the total M for all CCs increases. More specifically for the mixed SNR case we get a lower total M than with the original algorithm mainly for high throughput targets. On the other hand for the medium and high SNR cases we observe several differences. For $N = 5$ CCs we see an improved performance since the total M reaches up to about 6 for 130 bps target throughput, while in the original approach the corresponding result is 7. For $N = 10$ CCs, although for low target throughput rates the total M remains low, we have a rapid increase for throughput targets higher than 300 bps, resulting in total M reaching up to about 16. The reason for this imbalance between low and high throughput targets is the throughput threshold that decides M for each user/CC.

Next we measure the average M as we add more CCs to the system for low, medium and high SNR users as we did before. Firstly we observe the huge similarity of the medium and high SNR cases result of Figure 11 with the one of Figure 8. M decreases from about 1.6 to 1.1 with both algorithms. The main difference in performance is especially shown in the low SNR case where we can see that M gets the maximum value ($M = 2$) no matter how many the CCs the system has. With the original approach M drops from 2 to 1.3 obviously resulting in decreased feedback overhead.

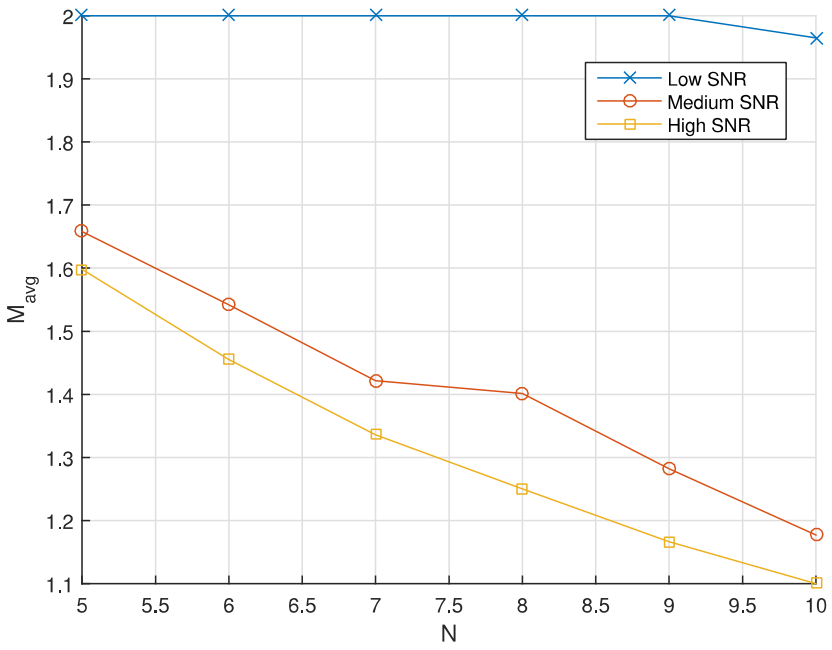

Figure 11: Average M for 300 bps target throughput.

The general conclusion about the proposed low complexity algorithm is that it works optimally for low target throughput and high SNR users, while in the opposite cases we observe some inefficiency in terms of feedback overhead, compared to the original CC allocation algorithm of the previous section.

3.2.4 Complexity Evaluation

In this section we perform numerical calculations to provide an insight on the overall complexity of the system, accounting for both PMI/RI feedback and CC allocation low complexity solutions. The results are briefly presented in Table 2 for the original PMI/RI calculation and the HM based channel allocation in Table 3 for the low complexity PMI/RI and SM channel

allocation.

Table 2: Original Channel Feedback and Channel Allocation

N/K	*PMI/RI*	*HM*	*Overall Complexity*
10/3	14722800	$2.86 * 10^6$	$17.58 * 10^6$
30/10	147228000	$6.8861 * 10^{14}$	$6.8661 * 10^{14}$

Table 3: Original Channel Feedback and Channel Allocation

N/K	*PMI/RI*	*SM*	*Overall Complexity*
10/3	14722800	30	164130
30/10	147228000	300	1641300

It is observed from the two tables above that for the low complexity channel allocation algorithm, we get a large reduction in the complexity of the order of 99% and as we increase N and/or K the complexity gain is much higher. This is due to the much better efficiency in terms of computational complexity of the SM approach compared to the HM, which in turn has to be repeated for as many times as the number of possible allocation schemes demand. Furthermore, in the case of $N=30$, $K=10$ the overall solution complexity is guided by the HM-based channel allocation and PMI/RI calculation does not have a notable impact. On the contrary the low complexity channel allocation algorithm does not heavily impact the overall complexity as shown in Table 2, since it is now guided by the low complexity PMI/RI calculations.

3.3 Achievements

The solution presented above and in the Appendix 3.2 achieved to address the objective of selective usage of a large number of non-continuous spectrum bands in HetNets dealing with the heterogeneous channel characteristics through the heterogeneous channel feedback adaptation. This objective has been defined in Section B1.1.2, point 2, of the DoW. The solution itself has tackled with the large amount of channel estimation and allocation in multi-user CA in HetNets. To this end, low-complexity and low-feedback rate algorithms have been devised and compared with original high complexity approaches.

4. LTE (Licensed) + LTE (Licensed) – HetNet deployment (RRM)

4.1 Overview

HetNet deployment in LTE licensed bands can be managed within 3GPP standards. As specifications already define aggregation of two LTE carriers in multiple scenarios (intraband continuous and non-continuous as well as interband non-continuous), focus of this section are scheduling algorithms. Scheduling is a key element of RRM – system and UE performance depend greatly on the way resources are allocated. Without proper scheduling algorithm system with CA might have worse performance (in terms of throughput) than single carrier environment with well optimized scheduler. This chapter is divided into following parts: at the beginning system-level simulator used to evaluate performance of the algorithms is

described. Then, two proposed scheduling algorithms are presented. The first one is an enhancement of Proportional Fair (PF) algorithm and the second one is a novel algorithm developed within SOLDER project. At the end of the chapter short summary and conclusions can be found.

4.2 System-Level simulator

Designed algorithms can be evaluated in different manner. During development, it is important to verify the concept as early as possible, therefore system-level simulator is used. After successful verification tests within more complex environment can be performed. Focus of this section is tool that was used to evaluate the scheduling algorithms. *"LTE MAC Lab"* [74] is a system-level simulator gradually enhanced with new functionalities in the course of SOLDER research project cooperation. The overall concept of the tool is to calculate channel parameters, set values associated with RRM functions and run the simulation. User Equipment's (UE) positions are calculated and their locations change in time in compliance with a chosen mobility model. Both large-scale propagation effects (i.e. pathloss and shadowing) and small-scale propagation effects (i.e. multipath) are taken into account. User channel conditions are updated each TTI (i.e. every 1 ms in LTE system). The same update rate is kept for physical resource assignment process - in this case PRB distribution among DL users. Modulation and Coding Scheme (MCS) can be modified in compliance with CQI feedback. The block diagram of LTE MAC Lab system-level simulator is depicted in the Figure 12.

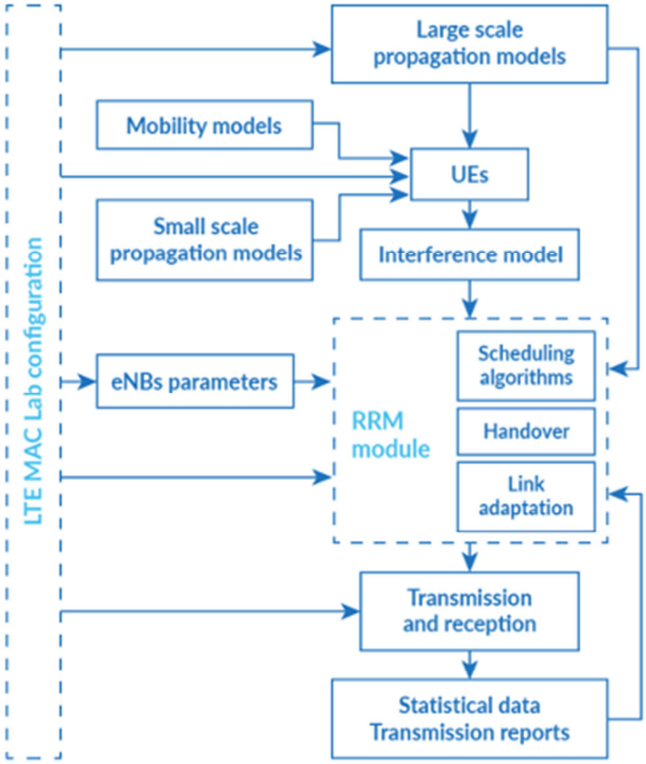

Figure 12: LTE MAC Lab building blocks

The PHY Layer is either abstracted using Exponential Effective SNIR Mapping (EESM) or Mutual Information Effective SNIR Mapping (MIESM) models. From Figure 12 it can be easily noticed that RRM module is located at the heart of the whole system. It is the entity which receives the largest volume of various data to be processed. Such information is a prerequisite for efficient radio resource distribution. RRM in LTE system predominantly occupies Me-

dium Access Control (MAC) protocol located within Layer 2 (L2). The addition of CA support to the scheduler functions (which are also RRM components) implies new complexities to be handled by the evolved NodeB (eNB). In the most basic case aggregated Component Carriers (CCs) are adjacent and come from the same band. Such configuration is denoted as *intra-band, contiguous CA*. It allows to avoid excessive computations related to propagation conditions (e.g. pathloss estimations in case of contiguous band excerpts can be assumed to be alike). However, the supposition that each Mobile Network Operator (MNO) has wide continuous frequency resources is rather unrealistic. A more proliferated scenario would be to possess fragmented spectrum within certain band or even dispersed over separate bands. These cases are labelled as *intra-band, non-contiguous CA* and *inter-band, non-contiguous CA*, respectively. They bring extra obstacles in terms of RF equipment (a necessity to simultaneously process two or more data streams which are widely spaced on frequency axis). Furthermore, distinctive propagation properties also impose additional difficulties in Link Adaptation (LA), Power Control (PC) and Handover procedures. All aforementioned factors have to be meticulously evaluated by scheduling mechanism before a decision is made which PRBs to assign to a certain user (UE).

4.3 Scheduling algorithms

4.3.1 Proportional Fair enhancement

At the beginning two schedulers' performance was compared during simulations, namely Round Robin (RR) and Proportional Fair (PF). RR scheduler assigns equal number of PRBs to each user without taking into account instantaneous channel state. If UE supports more than one CC, resources are assigned individually for each CC. On the other hand, PF in the process of scheduling considers not only channel state but also throughput achieved in the past by the certain UE. In the most basic case UE priorities can be calculated using the following formula:

$$p_{pf} = \frac{T}{R}, (8)$$

where:

p_{pf} – priority
T - achievable throughput in current TTI
R - historical average throughput

Simulations were conducted for one base station surrounded with six interfering base stations. Half of the users were able to receive data only on one CC, 25% on two CCs and remaining 25% on three CCs. Each of the CCs is equally congested. Detailed simulation parameters are shown in Table 4. .

Table 4: System-Level simulation parameters

Parameter	Value
Map size	2km x 2km
Environment	Suburban
Number of users	40
Single simulation length	1000 TTI
SNIR mapping model	EESM
Number of CC	1-3
Single CC BW	10 MHz

Carrier frequency	CC1 – 800 MHz CC2 – 850 MHz CC3 – 1800 MHz

In order to control behaviour of the PF a β parameter can be added to the formula in following way:

$$p_{pf} = \frac{T}{R^{\beta}}, \qquad (9)$$

where β is a fairness parameter.

Changes of β parameter affect fairness of the PF scheduler. Figure 13 shows peak, average and edge throughput for RR and PF. For $\beta < 1$ historical average throughput has smaller impact on priority and therefore users with good channel quality have higher priority. This is why peak throughput is very high at the price of almost zero edge throughput. In this case fairness is very low. On the other hand, increasing β above 1 privileges users with low throughput which leads to higher edge throughput.

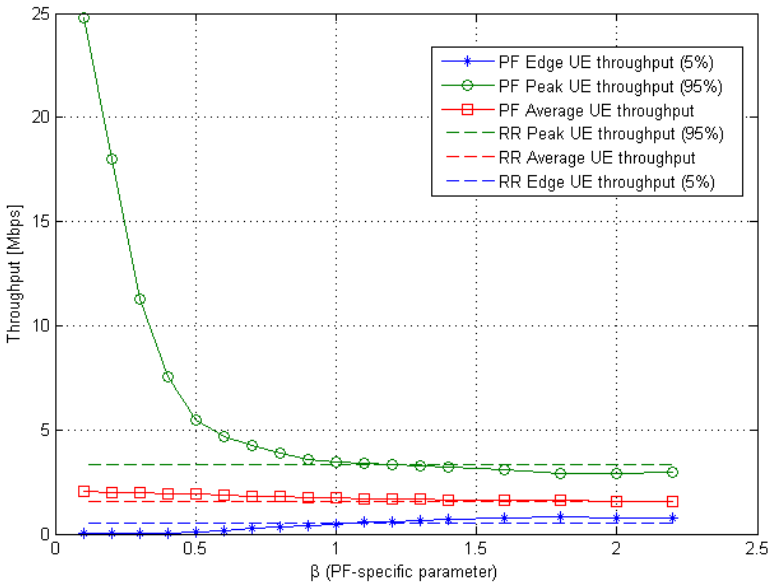

Figure 13: DL Throughput for various PF β parameter

Curves for RR scheduling maintain constant level as β is non-existent in this case. RR becomes a slightly better solution in terms of peak throughput when PF parameter β exceeds 1.5. This is due to the fact PF approach starts to prioritize the users with poor radio conditions. Thus, uniform assignments assured by RR can be more attractive with increasing PF β factor if edge throughput is not a performance indicator to be especially promoted. Figure 14 and Figure 15 depict Cumulative Distribution Functions of DL Throughput for Non-CA and CA capable users, respectively. The benefits of using CA are evident. Virtually not a single Non-CA UE exceeds the border of 1 Mbps whereas approximately 50% of CA capable users achieve more than 2 Mbps, regardless of the scheduling mechanism in use.

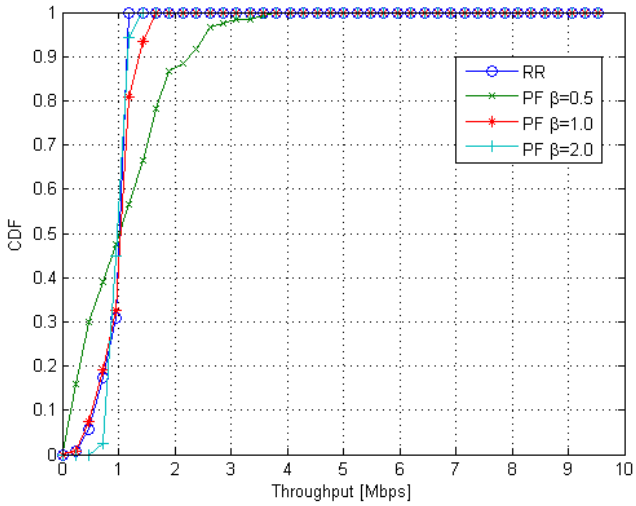

Figure 14: Cumulative Distribution Function of DL Throughput for Non-CA users

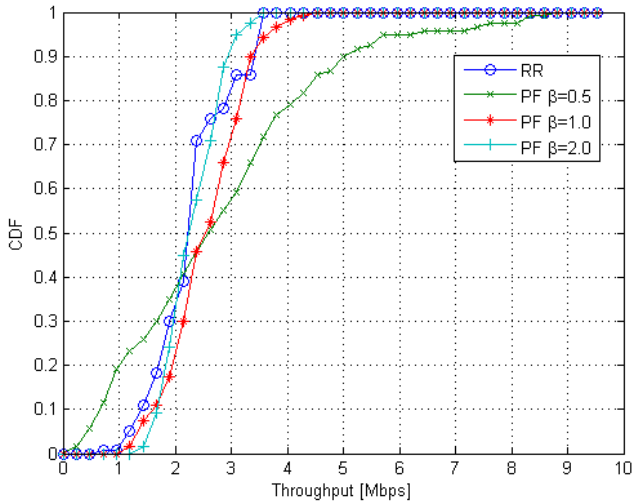

Figure 15: Cumulative Distribution Function of DL Throughput for CA users

Formula for priority calculation can be used in two ways in CA environment: separately for each CC or by calculating T and R as a sum of throughputs from different CCs. In the first approach there is no other gain from CA than simply wider bandwidth. The second case allows to control PF in one more dimension. Formula for CA case can be extended into:

$$p_{pf} = \frac{T}{R^{(\beta + N_{cc}\gamma)}}, (10)$$

where:
N_{cc} – number of used CCs
γ – CA/non-CA balance parameter

Figure 16 illustrates the performance of PF scheduler with $\beta = 1.0$ and a variable γ factor. The exponent of R ranges from approximately 0.5 to 1.5 (due to γ equals to -0.16, 0 or 0.16). Figure 16 corroborates the assumption that large R's exponent results in lower priority and thus decreases the amount of users with exceptionally high throughput.

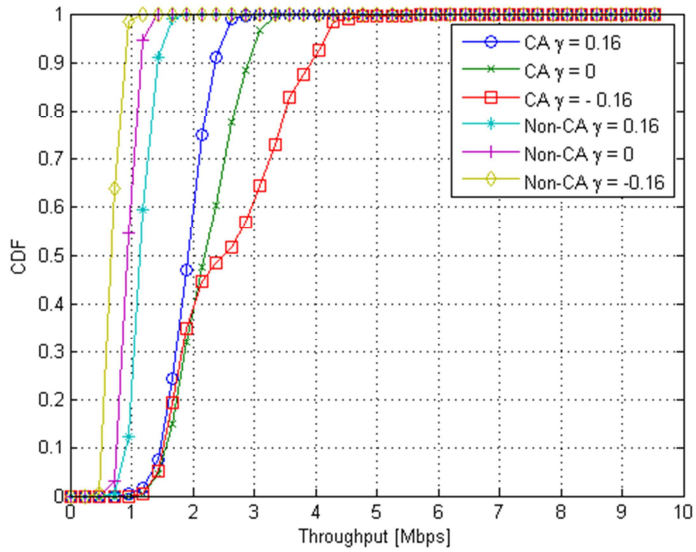

Figure 16: Cumulative Distribution Function of DL Throughput for PF scheduler with parameter

Furthermore, for a positive value of curves for CA and Non-CA case are closer to each other. Such value yields a mitigation of CA impact as Non-CA users suffer less from the fact they do not have additional frequency resources to be scheduled on. The contrary tendency is observed for . Such setting boosts CA supremacy over Non-CA users in terms of achievable DL throughput. This is due to the increased as the exponent of gets smaller with the growing number of CCs (denoted as).

4.3.2 Novel scheduling algorithm

Simulations show that even slight modification of the well-known algorithm can bring improvement and more flexibility in CA environment. Further research was conducted in order to design novel scheduling algorithm that would benefit from introducing CA even more. Final implementation of the algorithm is designed in such a way that cooperation with different LTE stacks via FAPI interface (Femto Application Platform Interface – interface defined by the SmallCell Forum, formerly known as FemtoForum, to encourage competition and innovation between suppliers) is available. In particular, scheduler will be tested with OAI stack.

Each TTI, MAC Layer sends request to the scheduler and expects decision regarding resource allocation. Scheduler decides about physical resource blocks allocation (PRB), modulation and coding scheme (MCS), activation or deactivation of secondary cells (sCell) in CA environment and a few other parameters. Algorithm consists of several steps, as presented in the Figure 17.

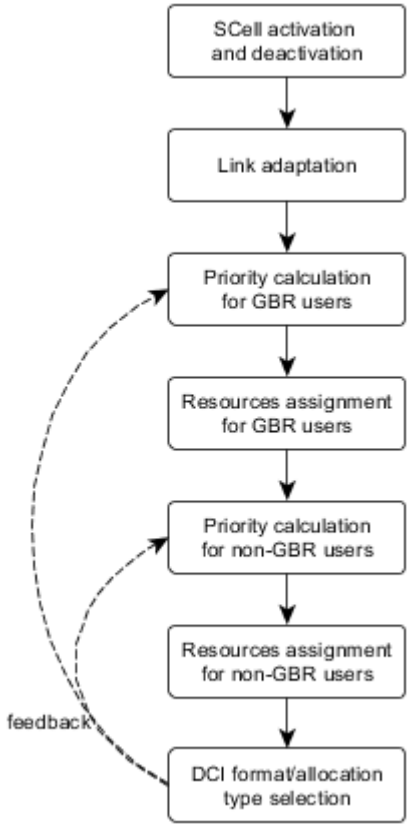

Figure 17: High-level scheduler architecture

Initial decision of the scheduler is activation or deactivation of the secondary cells for all users. If throughput demands of particular UE increased or decreased significantly scheduler should indicate to the MAC layer that proper procedure must be initiated. If user's demands does not change greatly and users with higher priorities are served with required QoS sCell activation or deactivation is not performed. Next step is link adaptation, where MCS for the user is selected. Based on historical transmission reports and previous settings of MCS scheduler adapts current value of MCS. If number of NACK exceeds assumed threshold for a certain amount of time MCS is lowered so that transmission could be more robust. Following two steps are executed twice: once for users that require guaranteed bitrate (GBR) and the second time for those, whose bitrate is not defined as guaranteed. These steps are priority calculation and resource assignment.

Priority is calculated for each PRB and for each UE. The higher the priority is the greater chance of assigning this resource to the particular user. Simplified formula for priority calculation can be presented in following way:

$$P_i = CQI_{prior} \cdot w_i \cdot r_{historical}^{-1} \cdot N_{prior}, (11)$$

where:

P_i – priority for user i
CQI_{prior} – priority related to the channel w_i – waiting time of the packet for the user i
$r_{historical}$ – historical throughput of the user i
N_{prior} – priority related to the user's buffer size (number of waiting packets)

From the analysis of the formula one can derive following conclusions:

- Better radio conditions increase priority

- Long time without transmission increases priority
- High throughput in previous TTIs decreases priority
- Long packet queue increases priority

These are not the only criterions taken into account while calculating priority. There are some other factors that have to be considered, such as not accurate CQI reporting by the UE, re-transmissions and for example UE capability. These, however, are not discussed in more details. After priority calculation, with the feedback from DCI format/allocation type selection block, resources are assigned for the users. For given PRB user with highest priority is selected with constrain that not every allocation is legal from DCI point of view – therefore feedback is required to avoid improper allocations.

When resources are allocated scheduler should create DCI and decide about its format and allocation type. Goal of the scheduler is to obtain as shortest DCI as possible in order to save resources for user data. This is the last step of the scheduling and every decision that has been made is sent to the MAC Layer, which multiplexes data from the users according to this decision. Scheduling algorithm was verified in LTE MAC Lab to prove that improvement can be expected in final implementation. Due to limitation of the simulation environment few simplification has to be made. For instance in downlink transmission base stations cannot measure radio conditions directly. UE should measure radio conditions and report this to the eNB. In the simulations there was such simplification that eNB was aware of the radio channel conditions without necessity of UE reports. This approach lowered performance of the scheduler and higher system throughputs are expected in the final form of the scheduler.

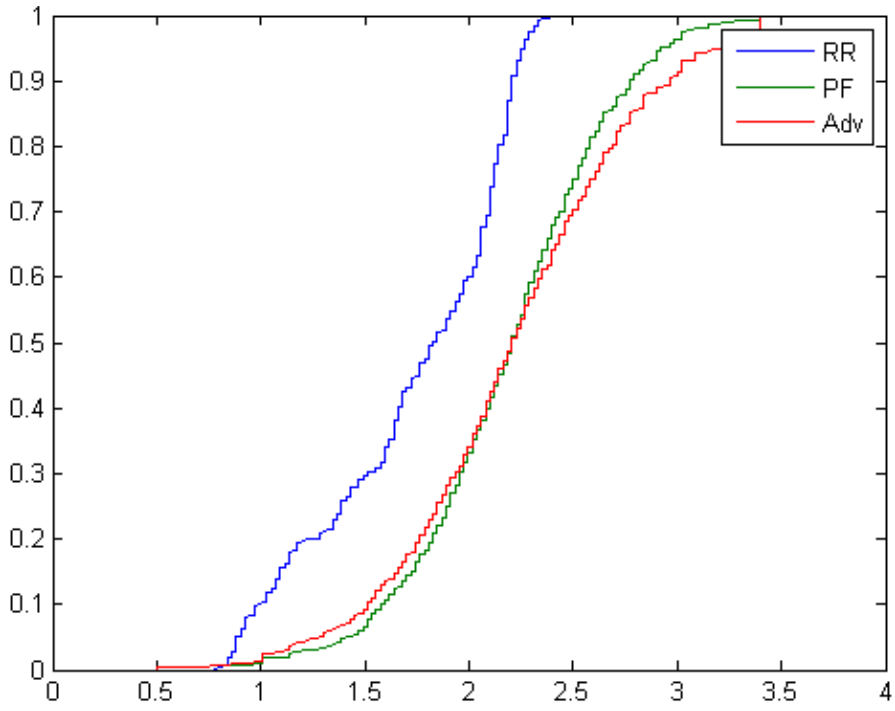

Figure 18: Throughput CDF

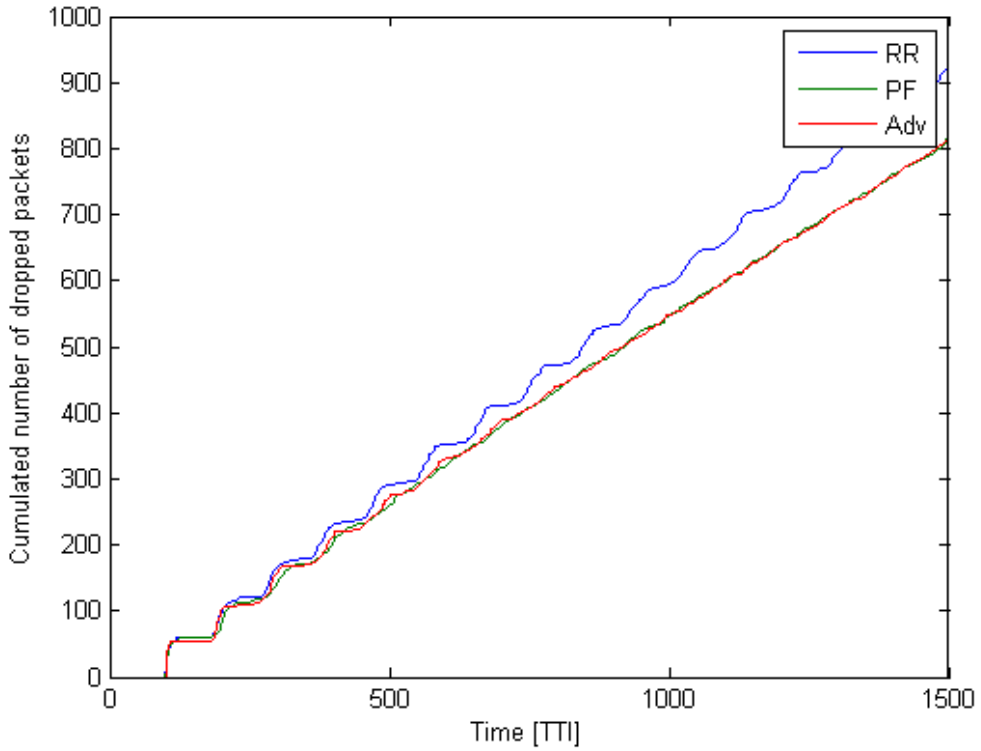

Figure 19: Number of dropped packets

One can observe that the cumulated number of dropped packets over time is nearly the same in case of PF ($\beta = 1, \alpha = 0$) and new scheduler. Scenario parameters is chosen in such a way that eNB cannot serve everyone without losing packets. This shows in better way that there is no additional degradation in novel scheduling algorithm in terms of lost packets. Round Robin scheduler obviously has worse characteristic as it does not take into account any metric related to historical throughput or packet delay. In real implementation one can expect improvement of these results for ISW's scheduler because simplifications that are introduced into system level simulator might be in favor of PF scheduler. PF scheduler has access to the detailed and exact channel condition values, while in fact its decision is based on the rough estimate of the channel, namely CQI. In terms of throughput, as in previous case, two schedulers: new algorighm and PF are better than RR. CDF shows that new scheduler more often obtains higher throughputs. For this case, results for PF scheduler are enhanced due to simplified approach described before.

4.4 Achievements

The work presented in this section is related to achieving higher and more fair throughputs in the environment with aggregated carriers. Presented algorithms can be successfully used in homogeneous or heterogeneous deployment. Conducted simulations show that novel algorithm allows to obtain higher throughput than PF without degradation in terms of dropped packets. Simulations were conducted to prove initial idea of the scheduling algorithm. Final result of this work will be completed implementation of the scheduler using well-defined interface (FAPI interface) in C language.

5. LTE (Licensed) + LTE (TVWS)

5.1 Overview

This section considers LTE in licensed spectrum aggregated with LTE in TVWS. The topic is a downlink spectrum aggregation scenario, whereby the objective is to propose novel spectrum aggregation algorithms to reduce power consumption and maximise capacity in order to fulfil the user utility requirements.

5.2 Technical Approach

We assume the existence of a Centralized Spectrum Aggregation Controller (CSAC) (as described in D2.3), or alternatively the implementation of such a concept in a geolocation database, such as highlighted in Section 9.2. Each LTE base station maintains a Channel Status Table (CST), X, which represents the status of the available channels from the CSAC such that

$$X = \begin{bmatrix} x_{1,1} & \cdots & x_{1,n} \\ \vdots & \ddots & \vdots \\ x_{m,1} & \cdots & x_{m,n} \end{bmatrix}, x_{i,j} \in \{0,1\},$$

where $x_{i,j}$ denotes the channel status on the jth channel of the i^{th} channel. If $x_{1,1}$= 1, the channel is available for the LTE system, otherwise, it is not. The CST will be updated periodically.

After that, the selected LTE and TVWS channels are aggregated and the data packets are split on the MAC layer before being transmitted on the PHY layer, as shown in Figure 20. The transport channel provides modulation and coding operation on data packets, connecting MAC and PHY layers. The split data packets are carried by different carriers with different transmit powers or transmit rates. To achieve this, FA-OFDM technique is used on both transmitter and receiver sides. Unlike traditional OFDM, FA-OFDM uses independent modulation and coding schemes for each OFDM channel based on its individual received signal-to-noise ratio (SNR). Therefore, different transmit rates and different transmit powers can be used on different channels.

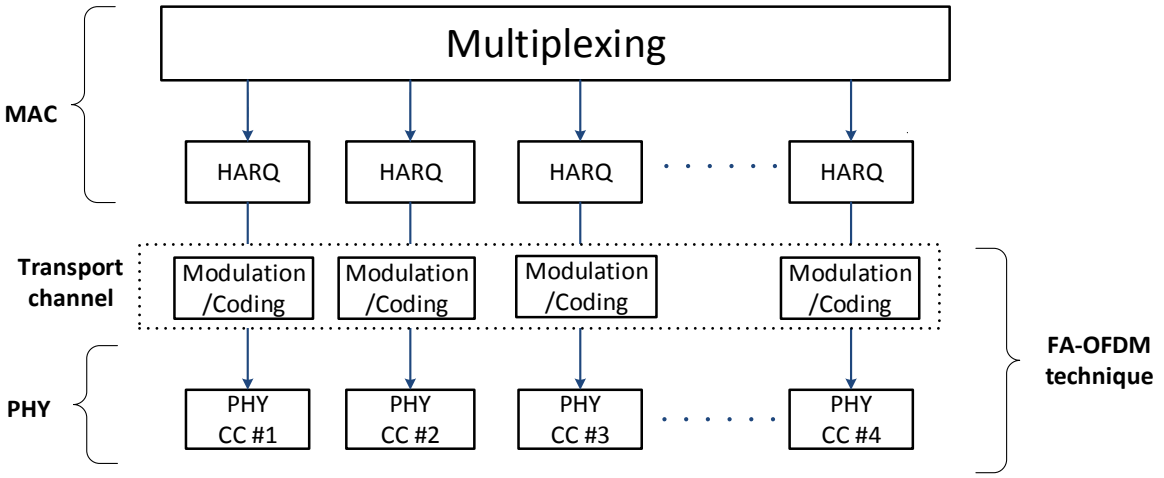

Figure 20: MAC and PHY layer structure for spectrum aggregation.

We propose two different spectrum aggregation algorithms in order to meet the power efficiency and throughput requirements of the downlink LTE network, respectively.

Algorithm 3: We aim to calculate the minimum downlink transmission power for the base station based on a rate demand for each user. The capacity of the link between the LTE base station x and a user y over the k^{th}channel is given by

$$C_{x,y}^{k} = W_{x,y}^{k} \log_2(1 + SNR_y^k),$$

where $W_{x,y}^{k}$ is the potential bandwidth of the k^{th} channel, SNR_y^k is received SNR at user y, which is given by $SNR_y^k \frac{P_{x,y}^k h_{x,y}^2}{\sigma^2}$ such that $P_{x,y}^k$ is the transmit power of x^{th} node to the y^{th} user over the k^{th} channel, σ^2 is the noise power and $h_{x,y} = F_{x,y}^k \sqrt{1/L_{x,y}}$ is the channel coefficient, where $F_{x,y}^k$ is the fading coefficient of the channel while $L_{x,y}$ is the pathloss.

For each LTE user, we assume a minimum requested rate demand R_d. Thus, the channel capacity should satisfy the following condition.

$$C_{x,y}^{k} = W_{x,y}^{k} \log_2(1 + SNR_y^k) > R_d.$$

Using the expression for SNR and solving for transmit power P, we obtain

$$P_{x,y}^{k} \geq \frac{\left(2^{\frac{R_d}{W_{x,y}^k}} - 1\right)\sigma^2}{h_{x,y}^2}.$$

Thus, the minimum required downlink transmit power from the LTE base station x to a user y over the k^{th} channel is given by

$$P_{x,y}^{min,k} = \frac{(2^{\frac{R_d}{W_{x,y}^k}} - 1)\sigma^2}{h_{x,y}^2}.,$$

Similarly, the minimum downlink transmit power for all F channels can be calculated and represented as a matrix: $\mathbf{P=}\begin{matrix} P_{1,1} & \dots & P_{1,n} \\ \vdots & \ddots & \vdots \\ P_{m,1} & \dots & P_{m,n} \end{matrix}$. The spectrum aggregation algorithm is represented as an optimization problem, given as follows.

$$\begin{aligned} &\text{P1: } \min \textstyle\sum_{i=1}^{N}\sum_{j=1}^{M} P_{i,j}x_{i,j} \\ &\text{s.t (a) } P_{i,j} \leq P_{i,j}^{a},\ \forall\, i \in N, j \in M \\ &\text{(b) } \textstyle\sum_{i=1}^{N}\sum_{j=1}^{M} C_{i,j}x_{i,j} \geq R_d \\ &\text{(c) } \textstyle\sum_{i=1}^{N}\sum_{j=1}^{M} x_{i,j} \quad \leq \quad \varepsilon \\ &\text{(d) } \textstyle\sum_{i=1}^{N}\sum_{j=1}^{M} P_{i,j}x_{i,j} \leq P_{max} \\ &\text{(e) } x_{i,j} \in \mathbf{X}_{,,}\ \forall\, i \in N, j \in M \end{aligned}$$

where $P_{i,j}^{a}$ is the maximum allowed transmit power of the jth channel of the i^{th} spectrum, P_{max} is the maximum total transmit power for the LTE base station, ε is the maximum number of channels that can be aggregated by the base station due to the hardware constraints. The constraint (a) ensures that the transmit power of each aggregated channel is limited by $P_{i,j}^{a}$ in order to avoid interference to TV users. The constraint (b) ensures that the total capacity of the aggregated channels must satisfy the minimum rate demand R_d. Lastly, the constraint (d) ensures that the maximum transmit power constraint for a LTE base station is met.

Algorithm 4: The aim of this algorithm is to maximize the aggregated channel capacity for a CR node. The channel capacity of all F channels is represented as a matrix: $\mathbf{C}=\begin{matrix} C_{1,1} & \dots & C_{1,n} \\ \vdots & \ddots & \vdots \\ C_{m,1} & \dots & C_{m,n} \end{matrix}$. The spectrum aggregation algorithm is represented as the following optimization problem.

$$\begin{aligned} \text{P2: } & \max \sum_{i=1}^{N}\sum_{j=1}^{M} C_{i,j}x_{i,j} \\ \text{s.t (a) } & P_{i,j} \le P_{i,j}^{a},\ \forall\, i \in N, j \in M \\ \text{(b) } & \sum_{i=1}^{N}\sum_{j=1}^{M} C_{i,j}x_{i,j} \ge R_d \\ \text{(c) } & \sum_{i=1}^{N}\sum_{j=1}^{M} x_{i,j} \le \varepsilon \\ \text{(d) } & \sum_{i=1}^{N}\sum_{j=1}^{M} P_{i,j}x_{i,j} \le P_{max} \\ \text{(e) } & x_{i,j} \in \mathbf{X}_{,},\ \forall\, i \in N, j \in M \end{aligned}$$

Note that the constraints have similar meaning and significance as in the optimization problem (3).

5.3 Initial Results

We conduct an initial performance evaluation of the proposed protocols using MATLAB-based simulation studies. From results in Figure 21and Figure 22, we note that transmission power increases with the rate demand. The transmit power reduces as the number of aggregated channels increase. Further, the gain achieved in reducing transmit power reduces as the number of aggregated channels increase. This is because of higher attenuation of aggregated channels. With a similar reasoning the trend in capacity curve can be explained. The capacity reaches a saturation point when the maximum allowed transmit power is reached.

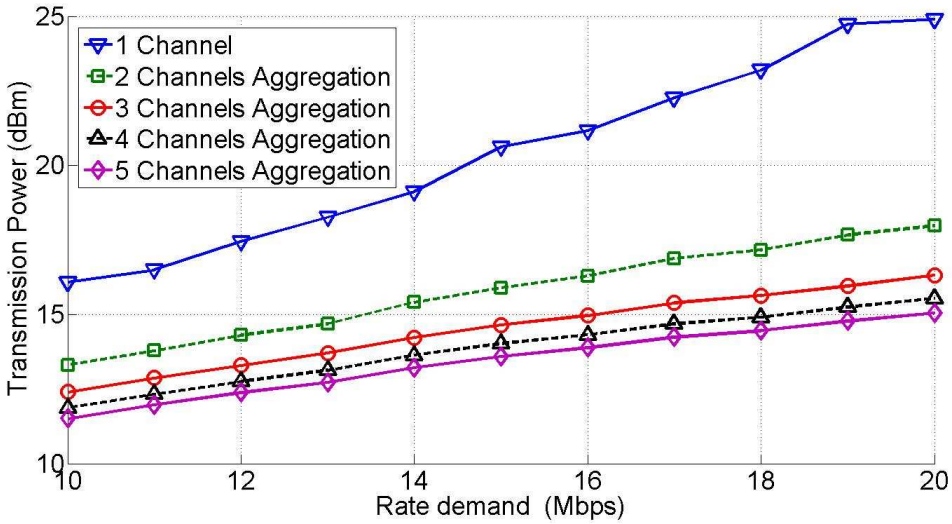

Figure 21: Transmission power consumption against rate demand

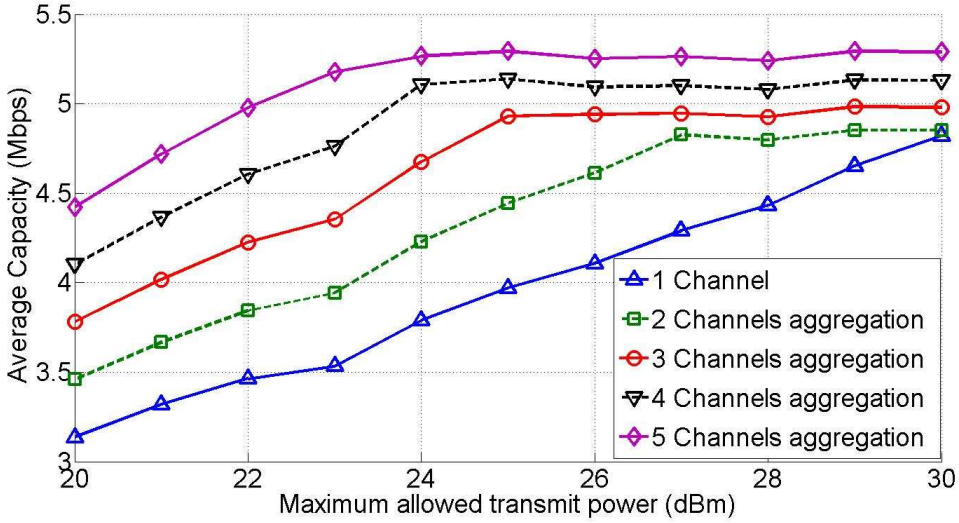

Figure 22: Average capacity against the maximum allowed transmit power per channel

5.4 Achievements

This section has presented a means for aggregation of LTE in licensed spectrum with LTE in TVWS. The solution is presented at the MAC layer as optimisation methods and algorithms with alternative purposes being to save transmission power and maximise capacity. Simulation results show considerable reductions in transmission power and increases in capacity through aggregation.

6. LTE (Licensed) + LTE (Unlicensed) – LTE-U

6.1 Overview

The use of unlicensed spectrum is becoming of interest to the network operator as a mean to offload their network (operated on licensed spectrum). We identified this trend in the previous deliverable as one of an interesting scenario for CA. Indeed, the approach followed by the standardisation is to have *assisted* operation, i.e. the operation of an unlicensed carrier is assisted by a carrier operated in the licensed spectrum, leveraging the principle of CA. This is LAA as illustrated by Figure 23.

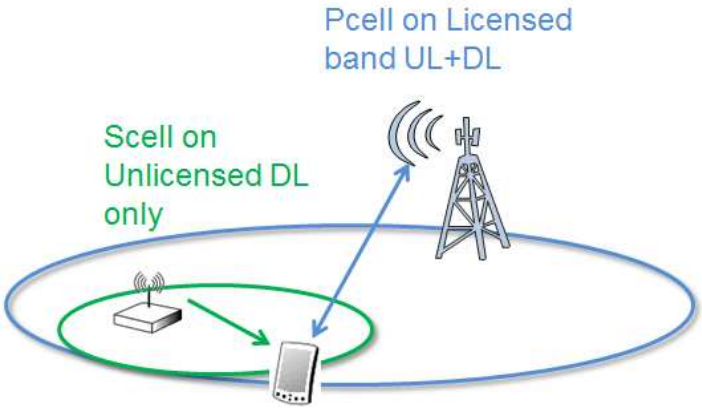

Figure 23: Illustration of LAA

The standardisation has opened a work item on LAA in June 2015, with the target to be completed in June 2016. Several events were also organized in parallel of 3GPP development, by promoters of LAA in order to evangelize the community, especially the WiFi stakeholders. The use of LTE in unlicensed spectrum requires the LTE system to be adapted to meet the regulatory constraints (especially with respect to fairness with the other users of the band, namely the WiFI). In this context, SOLDER has investigated key enablers for LAA, such as a proposal for LTE frame adaptation (see section 6.2) or how to introduce listen before talk (LBT), discontinuous transmission (DTX) carrier selection (CS) and transmit power control (TPC), which are required by the regulation in most countries.

Section 6.3 introduces the implementation LBT, DTX, CS and TPC, is presented in an open source LTE-A simulator. Having accomplished the system design and performance, we devise cognitive radio (CR) solutions for efficient CS and DTX through reinforcement learning and double Q-Learning algorithms. In this way, the CR application to LTE-A system becomes a reality. The solution in Section 6.4 deals with the resource (subcarrier) allocation problem when subcarriers can be allocated for transmission over licensed and unlicensed bands. Thereby, the system model is considered as licensed/unlicensed CA system with MIMO as well. The challenge for this model is to acquire channel knowledge for the unlicensed band, that must be provided blindly to this end. Moreover, the interference caused to the unlicensed system should be eliminated. This solution is more generic of the aggregation of HetBands and it does not stick to the LAA 3GPP concept. Simulation results reveal the achievable performance for a CA MIMO system when it is able to allocate subcarriers from both licensed and unlicensed bands.

Part of the work presented in this section can be found in the Appendix 6.3 and 6.4 with more detailed analysis results.

6.2 A proposition to modify LTE frame for LTE-U

Please note that the content of this section has been submitted for a patent filing in the second half of 2014.

LTE is a cellular system operating in licensed bands, where an operator has the exclusive usage of the allocated frequencies. The rising demand for mobile data creates the need for the use of more spectrum. A common way to increase the available spectrum is to use WiFi offloading, where instead of using the cellular network, data connectivity is provided through WiFi in unlicensed bands, and in particular the 5 GHz unlicensed spectrum.

However using WiFi for the unlicensed spectrum has several drawbacks: WiFi is not as spectrally efficient as LTE, and using WiFi requires integrating two different technologies. Some estimations put LTE as being twice as spectrally efficient as WiFi, therefore using LTE could double the available bandwidth using the same amount of spectrum resources. For this reason there is a growing interest in using LTE in unlicensed bands, which may be considered as part of LTE release 13 (the currently deployed LTE release being 9, or 10 in the most advanced deployments). For this LTE should be modified to share the unlicensed spectrum with other technologies, mainly WiFi, in a fair manner.

LTE is designed for licensed bands, so there is an assumption that an LTE channel is fully dedicated to LTE. As such, there is no current mechanism to share the spectrum with other users, and possibly other technologies. Conversely, in unlicensed bands there is a requirement to share the available capacity with other users and technologies in a fair manner.

The key principle behind this fair coexistence on an unlicensed channel is “Listen Before Talk” (LBT). With LBT, in order for a device to transmit, it will listen to the channel and only start transmission if no other transmission is on-going. However, two (or more) such devices could listen at the same time to an unused channel and decide to start transmission at the same time, leading to a collision and a failed transmission. LBT cannot avoid this issue, but is still an important mechanism to avoid collisions and share the spectrum between uncoordinated users and technologies. Such mechanisms is for instance required by regulators in most region when operating in unlicensed bands. Although not required, a number of technologies using unlicensed bands can start transmitting at any time, in order to quickly use the spectrum as soon as it is available.

LTE uses a completely different scheme: the channel usage is split into 1 millisecond subframes, with fixed time synchronization, and the eNodeB base station (eNB) centrally schedules the spectrum usage by explicitly allocating part of each subframe subcarriers to different devices UE as would be understood by the skilled person. Typically, the eNB sends allocation order to a device over the PDCCH (Physical Downlink Control CHannel) to describe an allocation in a given subframe PDSCH or PUSCH (Physical Downlink / Physical Uplink Shared CHannels). An allocation provided by the eNB has to be used.

The LTE allocation scheme is inflexible and, as is, is not suitable to share unlicensed spectrum in a fair manner. A recently developed mechanism, carrier aggregation (CA), provides a little more flexibility in that a secondary channel can be activated/deactivated within a few milliseconds (up to 8), and so does not need to be used all of the time. A primary cell (PCell) in a licensed band combined with a secondary cell (SCell) in an unlicensed band would bring more flexibility than the regular, ‘always on’ LTE used on the primary cell. But once a secondary cell is activated on the license-exempt band, the regular LTE framing and eNB scheduling is used, and is still not flexible enough. It is noted that the secondary cell could be downlink (DL) only as denoted for instance in 3GPP as supplementary DL. In the context of LTE-U (refering to LTE that has been modified and extended to work in unlicensed bands), it is assumed that the secondary cells used in the license-exempt spectrum is DL only.

There is a need for a scheme to use the LTE waveform in unlicensed bands, with minimal modification on the device side to help implementation and adoption. There is also a need to make the LTE allocation more flexible when an unlicensed band is used, while preserving most of the LTE waveform and its high bandwidth efficiency.

We propose a scheme to support a LTE extension to unlicensed bands using CA, where the primary carrier is operating in a licensed band and one or several secondary carriers may be in unlicensed bands. The proposal focuses on the modification and extensions to make to the LTE standard to support such secondary carriers in unlicensed bands. The LTE standard mechanisms apply, except for the modification described here.

We focus on using the unlicensed spectrum for a DL only LTE channel, where the traffic only goes from the eNB to the UE. The UL traffic uses the primary carrier operated in a licensed band in this case. Such proposal implies modifications at the eNB and at the UE sides compared to legacy LTE equipment.

A LTE-U capable eNB is responsible for listening to the unlicensed channel and perform listen-before-talk (LBT) before transmitting, as required for the fair use of the channel.
In order not to interfere with other users, all the usual LTE periodic transmissions are disabled in an unlicensed band outside of LTE transmissions (see below):

- The PSS/SSS are not transmitted. Synchronization on a secondary unlicensed channel is performed as described below instead;

- The PBCH carrying the LTE System Information (SI) is not transmitted. As the channel is always only a secondary cell the SI is provided to a UE as unicast data on the primary channel;
- Reference signals (RS), also called pilots, are not transmitted in unused frames, except possibly for fine time synchronization, as described below.

The end result is that when no user data transmission occurs on the unlicensed channel, no transmission is performed from the LTE-U eNB.

The structure of the proposed LTE-U transmission from an eNB in an unlicensed band is as follows:

Figure 24: proposed new LTE burst

The regular LBT process compares the measured power level on the channel to a threshold T, and will use the channel if this power is below T. The main other technology in the 5 GHz band, which is of primary interest for capacity, is WiFi. WiFi has a second power threshold W, such as W is lower than T, if it can demodulate a valid WiFi header. When decoding a WiFi header whose power level is between T and W a WiFi device will also consider the channel as used. This provides extra protection to a device transmitting a WiFi compatible header at the start of its transmission against other WiFi users in the band.
Another benefit for WiFi devices is that the WiFi header indicates the length of transmission. So after decoding a valid WiFi header a WiFi device may stop reception for the indicated transmission duration, as it knows that the channel will be used. This can be used to reduce the WiFi device power consumption
Moreover, modern WiFI transmissions use the header to signal the possible MCS or duration of the following data burst. We propose in the WiFi protection part of the LTE burst to mimic this regular WiFI header. As a result, WiFi stations could demodulate this “fake” header and determine the duration of the LTE burst that will occupy the channel.

The ‘LTE synchronization” part of the burst depicted in Figure 24, can be optionally used to ease the synchronization of the receiving device in the unlicensed band. Indeed, in regular LTE, synchronization signals (PSS, SSS) are regularly transmitted that allows the device to track its synchronization and correctly demodulate the downlink control channels.
In unlicensed band, such continuous periodic transmission cannot happen to avoid keeping the channel busy for a long (possibly infinite) period. Therefore, we propose to add optionally synchronization signal just before the LTE burst in order to give the chance to the UE to retrieve its synchronization.

Finally, the “LTE regular transmission” part of the burst depicted in Figure 24 is made of regular LTE DL control channel and DL data channel. To better protect the channel, it is proposed to only use dedicated pilot scheme (DRS) instead of having the continuous transmission of Cell specific pilots (CRS).

In this contribution we have proposed a modified LTE frame structure adapted to operation in unlicensed band. This proposal is based on consideration of fair access to the band and to comply with regulatory rules.
The next section investigates and models the use of LBT, DTX and other schemes that are likely to be mandated in the scope of LAA.

6.3 Licensed Assisted Access: Key Functionalities Analysis, Simulation and Results

6.3.1 LAA Implementation and Performance Evaluation in LTE-A System

LAA functionalities, namely carrier selection (CS), discontinuous transmission (DTX), listen-before-talk (LBT) and transmit power control (TPC), have already been introduced in the Rel.13 and initial study has been also carried out [13]. It is already recognised within SOLDER framework that the LAA concept is compatible to the aggregation of h-RATs. To this end, SOLDER has been addressed this challenge giving particular solution relying to cognitive radio principles. The fact is that this study is considered as the cognitive radio application in LTE-A system.

In particular, we first present the modeling, simulation and performance evaluation of the LAA concept into the LTE-A system. To this end, the LAA functionality implementation is provided using an open source LTE-A downlink system level simulator [16]. As a second part of our solution, we provide CR techniques application for enhanced CS, combining efficiently the DTX and TPC functionality. In particular, we apply reinforcement learning using *Q*-learning for the efficient channel occupancy time estimation under several WiFi traffic conditions. Moreover, a double *Q*-learning algorithm is devised and employed that can jointly optimize the COT learning and the interference power level adaption to maximize the achievable throughput of the aggregated unlicensed component carrier (CC). This is quite similar to the joint design of the DTX and TPC [17], since the COT drives the DTX functionality as will be shown below. We give below details about the implementation of the four LAA functionalities:

- **Carrier Selection (CS):** the eNodeB monitors WiFi traffic for the duration of each subframe of the simulation (and for the part when no LTE transmission is made). During each subframe it measures through an energy detector, the activity of WiFi users in terms of occupancy time and updates the statistics about Channel Occupancy Time (COT) for each channel. For this purpose we introduce a COT estimation module that makes all the calculations using the energy detector and signals the RF component that is in charge of carrier selection. The carrier selection decision occurs every 10 frames and if a monitored channel has a COT smaller than the current one, a channel change can occur from the next frame and so forth. This is implemented by configuring the center frequency of the transmission in the simulator.
- **Listen Before Talk (LBT):** to simulate the LBT procedure, a check is made at the beginning of a frame. The energy detector scans the current channel for a small duration of about 34 μs (prior to the beginning of the frame), and determines if there is an ongoing transmission in the unlicensed channel. If there is, no transmission is scheduled for the current frame. In the other case, LTE transmission is made for a specific number of subframes, i.e. a portion of the frame. To simulate this procedure, when the channel is busy, no LTE transmission occurs for the next 10 subframes that constitute a LTE frame by configuring a specific signal variable that controls the secondary carrier's transmission. In practice, a signal is sent to the Radio Resource Control (RRC) protocol from the LBT module to (de)activate the secondary CC but since the simulator does not implement the RRC protocol, the procedure mentioned above was followed.
- **Discontinuous transmission (DTX):** If the LBT procedure allows a LTE transmission for the current frame, the number of subframes that will be actually used is driven by the channel's COT statistics. In order to not harm WiFi activity, the LTE transmission should be active for as long the channel is not utilized by WiFi users and that is the percentage of (1-COT). This can be implemented with a signal sent from the COT estimation module to the MAC layer scheduler in order to build the proper LTE frame structure for the unlicensed carrier. The LTE frame in this case is structured with Resource Elements for the number of subframes calculated as in the example

above. In the simulator though, data processing occurs in a subframe per subframe basis, so the implementation entails a comparison of the current subrfame with the maximum subframe that should contain data. As for the synchronization of transmissions specified in [13], we do not use a specific signal but achieve synchronization by limiting transmissions in the unlicensed carrier only at the beginning of each frame by using the predefined Dedicated Reference Signals (DRS) as suggested in [13] and only in case the LBT procedure allows it.

- **Transmit Power Control (TPC):** TPC is implemented by adjusting the transmit power of the eNodeB for the unlicensed carrier by estimating the highest channel coefficient between the eNodeB and some WiFi user as shown in (6). This adjustment occurs prior to the beginning of each LTE frame and is based on the energy detector's measurements.

The flow chart of the LAA abstraction model encapsulating its overall functionality is demonstrated in Figure 25

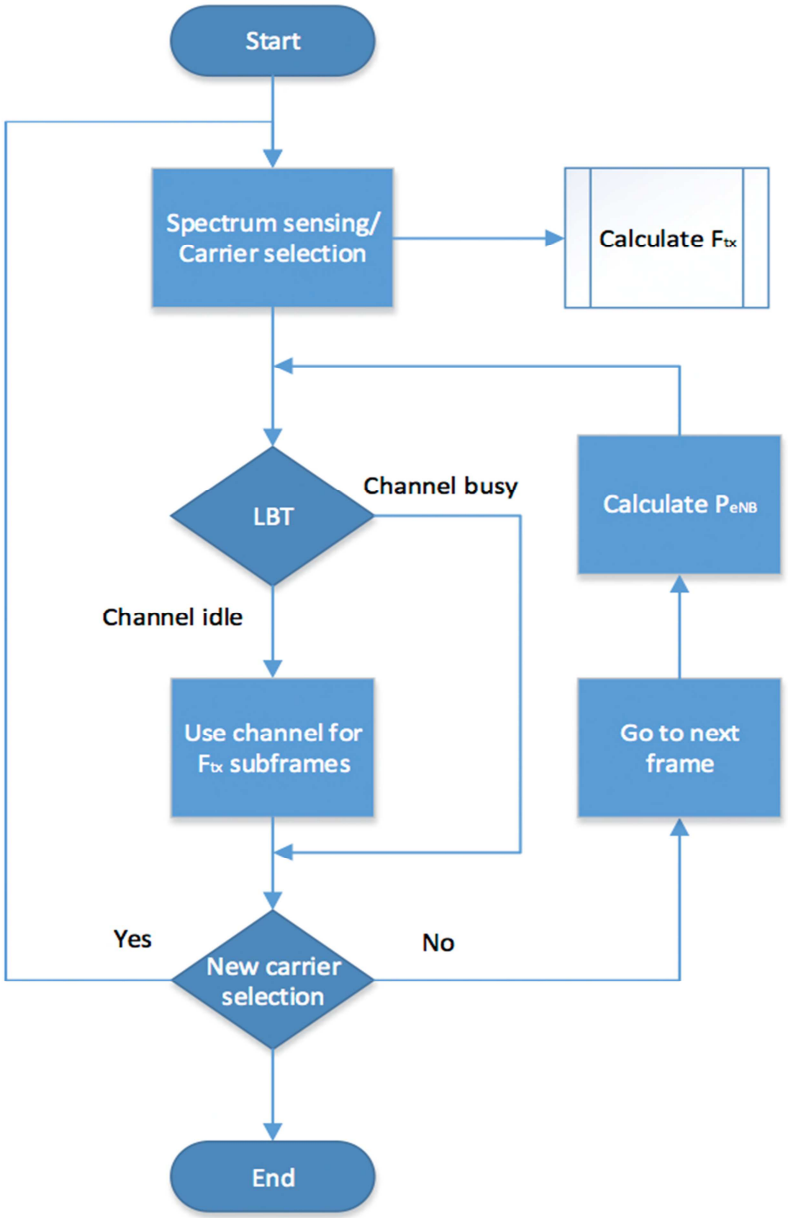

Figure 25: Flow chart of the overall LAA functionality in LTE-A system.

We now evaluate the LAA functionalities' implementation in LTE-A system. Figure 26 depicts the throughput achieved by the 5MHz licensed CC, the unlicensed 20 MHz CC and the aggregated result over different SNR values. Three cases are studied concerning the SNR of the unlicensed carrier. For two of them, a fixed SNR is considered and for one of them, the SNR is common along the x axis. For the unlicensed CC, the COT is equal to 40% and thus, there is a performance degradation. This is expected in the LTE-U CA scenario since it is utilized with DTX for protection to the primary users, i.e. WiFi users. However, the gain on the aggregated throughput is evident from the results. Moreover, although the bandwidth of the unlicensed CC is bigger than the licensed one, the throughput gain is smaller compared to the licensed one for low SNR values. At high SNR regime, the unlicensed CC provides significant increase in the aggregated throughput.

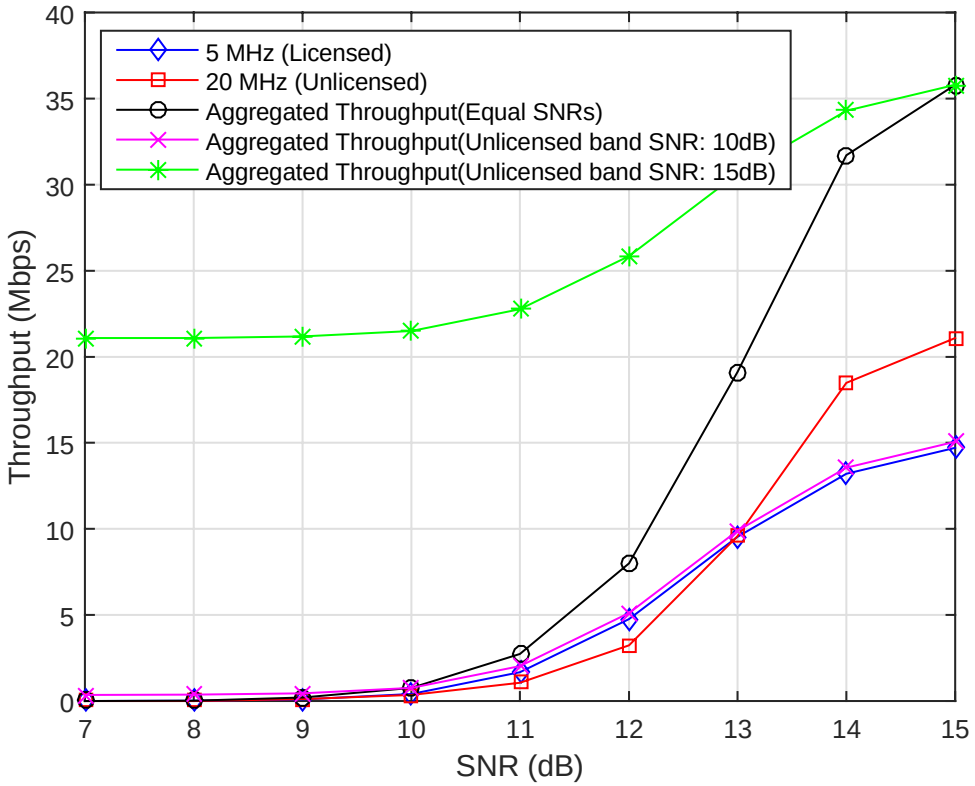

Figure 26: Throughput (Mbps) versus SNR (dB) for equal and unequal SNRs for both licensed and unlicensed bands.

Figure 27 depicts the effect of different COT values on the performance of the unlicensed CC of 20 MHz. For different COT values, we present the aggregated throughput achieved for different SNR values. It is obvious that the lowest the WiFi activity detected, the better the throughput we obtain. This is quite critical for the LAA application and it can be enhanced using advanced learning techniques being inspired by artificial intelligence to the CR networks. To this end, we provide below cognitive radio techniques that can provide the optimal spectrum exploitation within the LAA concept of 3GPP LTE-A system.

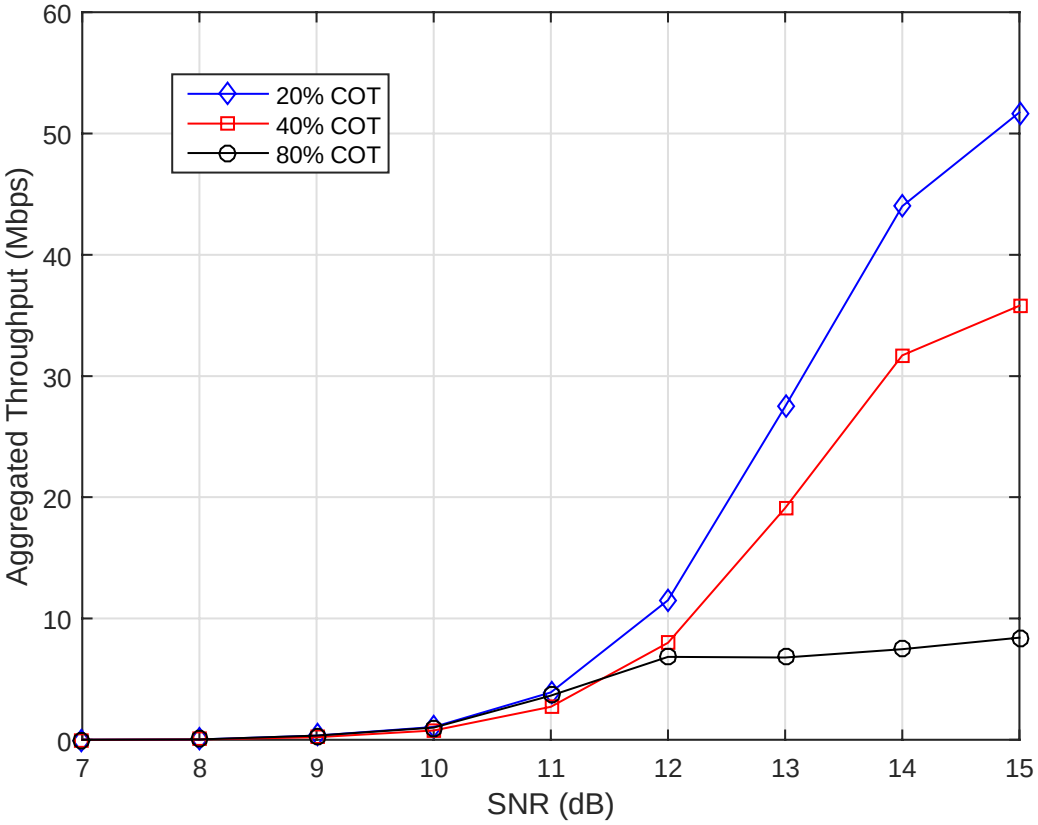

Figure 27: Throughput in Mbps versus SNR in dB for different COTs.

6.3.2 Reinforcement Learning for Enhanced Unlicensed Spectrum Aggregation

In [20][21], a taxonomy of machine learning algorithms is provided that can be applied in CR networks and systems. Taking into account this taxonomy, we can figure out that the problem of identifying the PUs activity (i.e. WiFi traffic) and adjusting LTE transmissions in the unlicensed band can be addressed with a Reinforcement Learning (RL) algorithm. The reason is that the ultimate goal is to determine a policy by which the secondary user (SU) (i.e. LTE) will choose the channel and the transmission time based on measurements taken during the sensing period. Q-learning is a RL application algorithm that determines the optimal decision making policy. An agent observes the environment and performs an action. Then, it observes the environment and decides the action of the next state based on the value of the Q function. To this end, we use below the Q-Learning technique to provide enhanced CS technique. Notably, a CS technique has not been studied and proposed in the 3GPP Rel.13 so far [13].

Let us now denote a set of states as S and decision times as t such that $s_t \in S$, meaning that the agent's state at time t is s_t. We also define a set of possible actions that the agent can perform as A and a reward function $r(s_t, a_t)$, which is based on the observation of the agent after performing action a_t when being in state s_t. A function Q_t is updated at the next decision time $t+1$ as:

$$Q_{t+1}(s_t, a_t) \leftarrow (1-\alpha)Q_t(s_t, a_t) + \alpha(r(s_t, a_t) + \gamma \max_{a \in A} Q_t(s_{t+1}, a)), \quad (19)$$

where α is the learning rate, γ is the discount factor, which indicates the effect of the future reward to the current state [22]. Similar to the work in [23], the future reward is not

considered for Q function evaluation. The goal is to decide the optimal action at the current state s_t as:

$$a_t = arg \max_{a \in A} Q_t(s_t, a). , (20)$$

This action will result in a transition to state s_{t+1} and a reward observation $r(s_t, a_t)$. Details about the Q-learning algorithm for the channel occupancy estimation can be found in our full work [14].

We now proceed with the WiFi/LTE simulation setup. The WiFi system consists of 5 channels of 20MHz at 5.8GHz spectrum area. Each channel s serves WiFi traffic modeled by a Poisson distribution with parameter λ_s. At the event of a packet arrival the following actions are taken. First, it is decided the waiting period of the Clear Channel Assessment of the WiFi system. This is a function of the time DIFS expressed in WiFi time slots as well as a necessary random backoff time in order to avoid collisions. After that a random transmission duration of the packet in WiFi time slots is calculated based on the possible physical data rates supported by the standard. WiFi transmissions occur in all 5 channels and the learning algorithm monitors COT in each LTE subframe and takes action about the LTE transmission for the next subframe accordingly. Figure 28 depicts the time partition relation between LTE and WiFi. During each $1ms$ LTE subframe, there are approximately 111 slots of $9\mu s$. At each slot, there can be several WiFi packet arrivals for each channel according to the Poisson distributions.

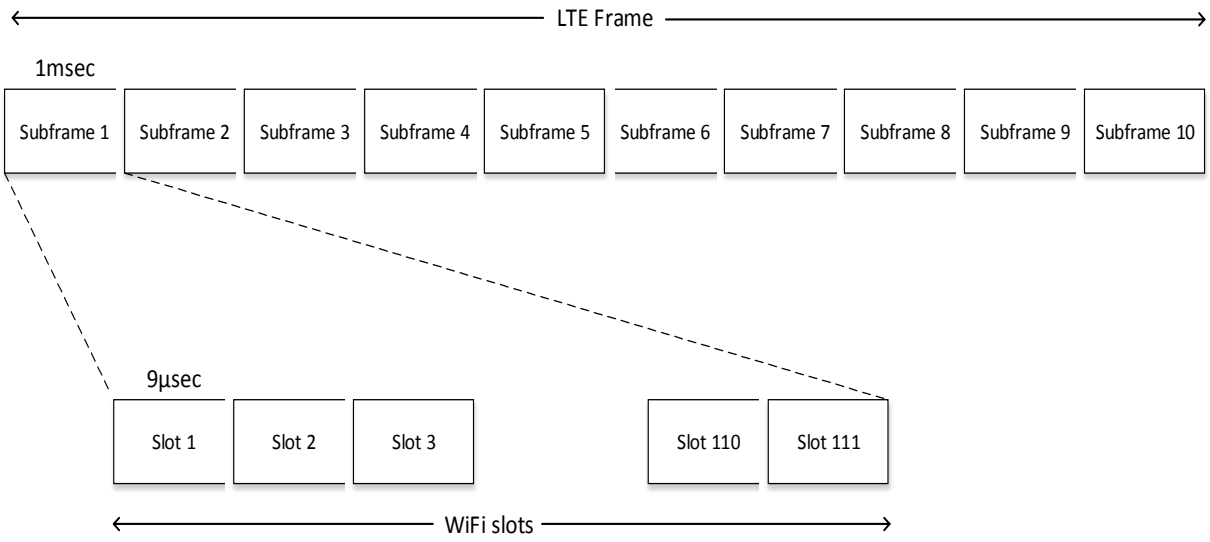

Figure 28: LTE/WiFi time slots association.

We simulate an LAA system that operates at 3MHz licensed band 20, and 5 20 MHz channels at the unlicensed band C at 5.8 GHz. The LAA implementation on the LTE Vienna Link Level simulator [16] described above is used, in order to measure the throughput gained from the aggregated signal of the licensed and the unlicensed carriers. The simulator processes the LTE signal in two different baseband streams, one for each CC, subframe per subframe. For this reason the WiFi system simulation has been embedded in the simulator's code to model WiFi transmissions so that the eNodeB can adapt to the transmissions of the WiFi system. For each iteration, i.e. a LTE transmission of 1 subframe (1ms), the behavior of WiFi transmission in all 5 channels is simulated. At the beginning of the first subframe of an LTE frame, the LBT procedure determines if a WiFi transmission is active at the current channel. If not, CA is activated for a period of time in subframes determined by either the action taken by the Q-learning algorithm or the estimated COT. For ongoing WiFi transmission, the procedure is repeated at the beginning of the next frame.

We study now the impact of LTE transmission in the WiFi system using the simulation environment described above. We evaluate the Q-learning based CS scheme and compare the results with the standard case of the WiFi system. We provide simulation results for several traffic load cases by modifying the Poisson's λ parameter. In Figure 29, we measure the percentage of packets transmitted by all WiFi stations compared to the case when no LTE transmission occur in any of the channels. This is depicted over the average number of packet arrivals per subframe. The results indicate a slight drop of the Q-learning and COT estimation methods compared to WiFi as the traffic load increases, which is expected. Moreover, we can observe that the Q-learning method outperforms the COT estimation one for higher traffic load scenarios. Thus, using the learning method, the system can be adaptive to channel traffic conditions and adjust LTE transmission better than simply estimating an expected channel idle time addressing this way the blind issue for LTE to exploit the WiFi channels.

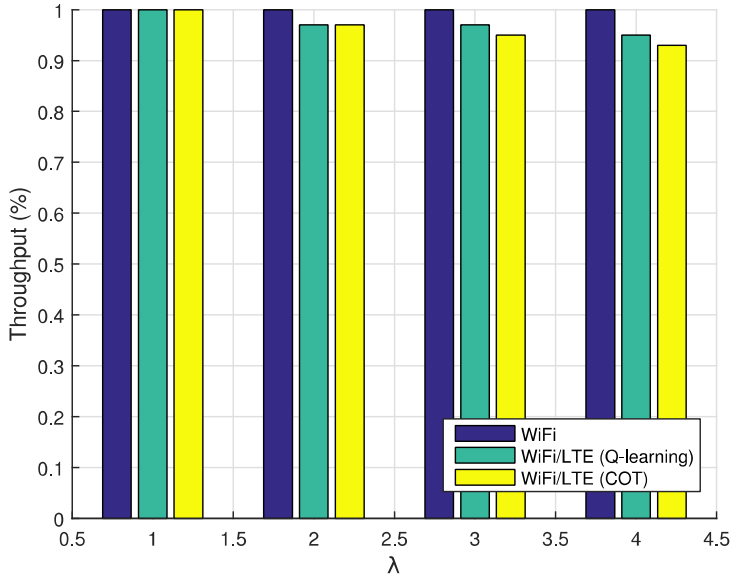

Figure 29: WiFi performance evaluation with Q-learning and COT application.

In Figure 30, we depict the throughput results of the LAA system for 3 different cases of WiFi traffic load and compare the performance of Q-learning and COT estimation for the above cases. We have already seen the superiority of Q-learning algorithm in terms of WiFi performance in the previous section and we now want to compare the two approaches under the LAA concept. The licensed CC depicted in Fig. 11 is 3MHz while the rest of the lines represent aggregated throughput results. The considered WiFi traffic cases are the same ones used to test WiFi performance and are summarized as:

- Traffic case 1: A Poisson distribution of average 1 packet arrival per LTE subframe per channel.
- Traffic case 2: A Poisson distribution of average 2 packet arrival per LTE subframe per channel.
- Traffic case 3: A Poisson distribution of average 3 packet arrival per LTE subframe per channel.

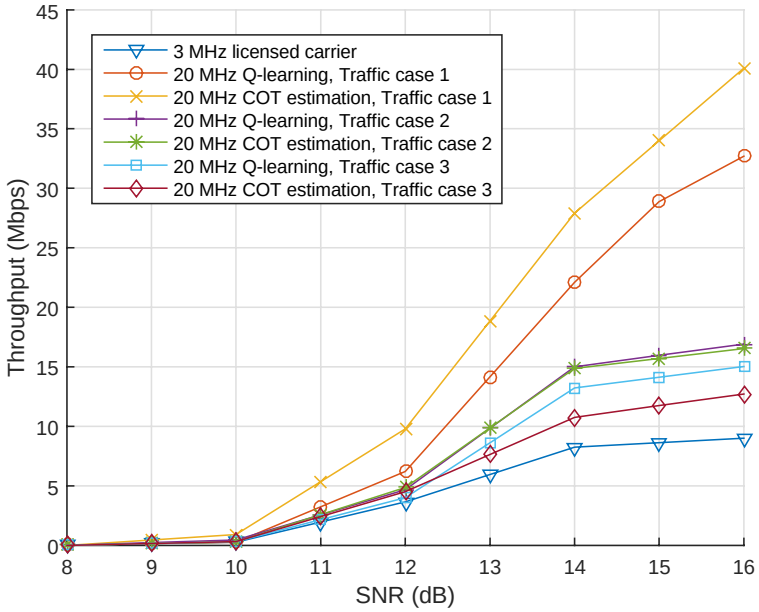

Figure 30: LTE Throughput (Mbps) vs. SNR (dB) for different WiFi traffic applying Q-learning and COT estimation.

Comparing the Q-learning and COT estimation techniques for the 3 traffic load cases, we can see that for low traffic cases (Traffic case 1) COT estimation provides significantly more throughput. As the traffic load increases though, Q-learning seems to be a better choice not only in terms of WiFi but also in terms of LTE performance. In the medium load case, the Q-learning approach provides slightly higher throughput and in the high load case (Traffic case 3), the Q-learning approach is clearly better for an average SNR value and above. Therefore, in low traffic, Q-learning is not beneficial since the best channel that is selected is sensed with large COT resulting in a large LTE transmission time. The low WiFi traffic load is not likely to be affected by the large LTE transmission time. On the other hand, if traffic load is generally high, the COT estimation at the beginning is likely to be very different than what happens later when many WiFi packets are queued due to LTE transmissions.

This results in more WiFi transmissions being congested in the small amount of time that LTE stops using the unlicensed channel. More transmissions at that time means that the probability that a WiFi transmission is active at the beginning of a frame, and thus the LBT procedure determines that an LTE transmission cannot take place, is increased. Finally, we can notice that even in high load cases, the Q-learning algorithm is not so greatly better than COT estimation due to its inherent politeness to adapt to WiFi traffic current conditions and guarantee better WiFi performance than COT estimation.

6.3.3 Double Q-Learning Method

The learning algorithm proposed in the previous section considers the COT only to perform CS. Although COT is an important and indicative parameter affecting CS, we would like to enhance learning by adding information about the interference experienced by each CC. We want to adapt the transmit power of the eNodeB according to the interference imposed to each CC through in conjunction with the COT learning. Our aim is to design a procedure, which can optimize the reward function, which is the throughput in this case, by exploiting the COT and TPC leading similar to the joint design concept of the DTX and TPC [17]. Intuitively, the more transmit power allowed at a specific CC, the better choice it makes in selecting it, since it will provide more throughput to LTE-A users and expand the eNodeB's coverage area. Under this premise, a double Q-Learning algorithm is proposed that can encapsulate

two actions per state using two different Q-functions. Details are given in the following section.

We introduce one more Q function in order to encapsulate the information about transmit power to the learning mechanism. The states are defined as previously for the candidate channels, while the action p is chosen from the set P. Similar to [18] our aim is to define a second Q function about transmit power learning and update jointly the two Q functions. The additional second Q function is defined as follows:

$$Q'_0(s,p) = \beta p, \quad (20)$$

where β is a normalization factor to adjust power levels to COT values, which is auxiliary to combine the transmit power learning with the COT one. The reward is now common for both Q functions defined as follows:

$$r(s,\{a,p\}) = \varepsilon\left(T_s^{off\,\prime} - T_s^{off}\right) + (1-\varepsilon)\beta p', \quad (21)$$

where ε is a weighting factor between the COT and transmit power terms and p' is the maximum transmit power that is calculated for the interval between after the LTE transmission and before the next Q function update. The update of Q' now is handled as follows:

$$Q'_{t+1}(s_t,p_t) \longleftarrow (1-\alpha)Q'_t(s_t,p_t) + \alpha r(s_t,p_t), \quad (22)$$

The double Q-learning algorithm is provided in Algorithm-5 below.

Algorithm 5 Double Q-learning

Initialize Q, Q' and choose s according to one of them
repeat
  Decide randomly which Q function to update
  if Q is chosen **then**
    $Q_{t+1}(s_t,a_t) \longleftarrow (1-\alpha)Q_t(s_t,a_t) + \alpha r(s_t,\{a_t,p_t\})$
    $s_{t+1} = arg\max_{s\in N} Q_t(s,a)$
  else if Q' is chosen **then**
    $Q'_{t+1}(s_t,p_t) \longleftarrow (1-\alpha)Q'_t(s_t,p_t) + \alpha r(s_t,\{a_t,p_t\})$
    $s_{t+1} = arg\max_{s\in N} Q'_t(s,p)$
  end if
until end

We evaluate and compare the double Q-learning CS algorithm with the original Q-learning algorithm that chooses the appropriate CC based only on COT information. We measure the aggregate throughput performance for the LAA in the LTE-A for different WiFi transmit power levels. We set the interference threshold at a low $I_{th} = 10dBm$ and a high $I_{th} = 20dBm$ value and the WiFi users transmit power to 1 Watt. We investigate two interference levels, where the received WiFi signal power at the eNodeB is a normal distribution with mean $\mu = 0.005$ (low) and $\mu = 0.05$ (high) respectively. The results obtained are displayed in Figure 31. We can observe that when the WiFi users interference levels are low, and thus the eNodeB can transmit with high power, the throughput result is roughly the same to the original learning algorithm because the new rewards do not change and the channel changes occur about at the same frequency. If we increase the interference caused by WiFi users though, we can see performance degradation, since now the rewards are generally smaller and channel adaptation is not that efficient. The interference threshold I_{th} plays an important role as well, since it determines along with μ of course, the eNodeB's transmit power which

as stated before affects LAA throughput performance. We see in that figure that when we use a high threshold, even with high interference, we can increase the throughput close to the levels of Q-learning. Note that the results shown in this section were taken for a high WiFi traffic case with $\lambda = 3$ where Q-learning outperforms simple COT estimation.

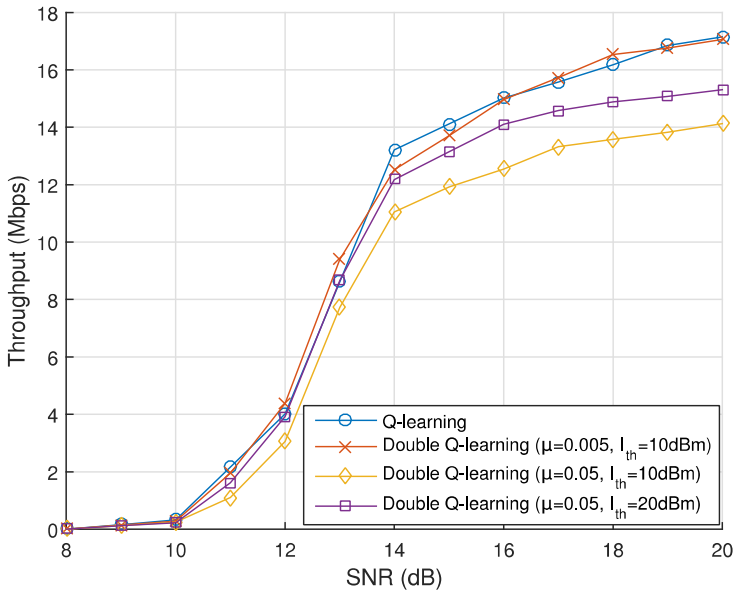

Figure 31: LTE Throughput (Mbps) vs. SNR (dB) for different WiFi power distribution with μ applying Q-learning and double Q-learning respectively.

To measure WiFi performance using the double Q-learning algorithm, we measure the received packet rate as already shown in Figure 32, only when no LTE transmissions take place, there are no losses for WiFi users while with the LAA system operating, and the WiFi packets are not received successfully with a probability proportional to the transmit power of the eNodeB. The results are depicted in Figure 32. The lost packets due to LTE transmit power are scheduled for retransmission and thus, they are counted as unsuccessful. In Figure 32, we can observe that the WiFi packet throughput decreases in case of the Q-learning application. In such a case, the LTE transmit power is fixed and the performance does not change when the interference level increases. On the other hand, with double Q-learning, the transmit power control is considered, and thus, the WiFi users are further protected resulting in performance increase compared to the original Q-learning, especially as the interference level increases. Furthermore, by increasing the interference threshold I_{th} of WiFi users, we make them less sensitive to interference, decreasing thus the chance of a packet loss and achieving even better performance.

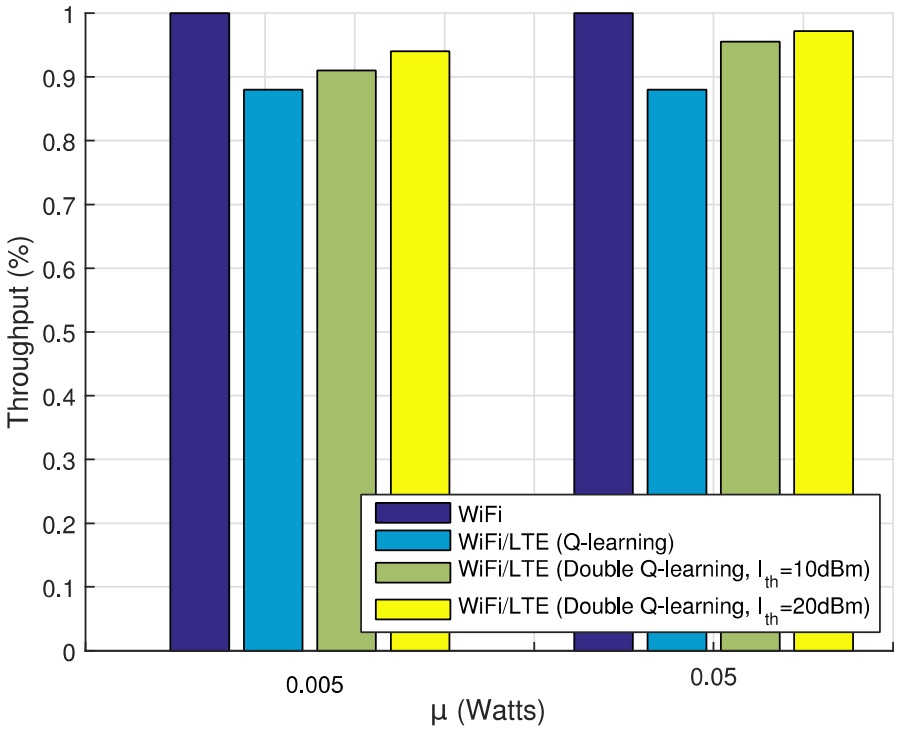

Figure 32: WiFi performance evaluation in % without and with LTE transmission.

6.4 Resource Allocation in Unlicensed/Unlicensed Carrier Aggregation System

The problem of resource allocation in licensed/unlicensed CA systems is solved in this work. A novel CA scheme is proposed for downlink MIMO Systems. The proposed approach achieves increased transmission rates by establishing the communication links via both licensed and unlicensed bands without generating or experiencing interference to/from the users of the latter bands. In particular, a rate optimization problem is specified and solved subject to the zero interference constraints, a total power constraint and a maximum number of aggregated bands constraint. Thus, a resource allocation problem is formulated for the licensed/unlicensed CA MIMO systems that is very important to unlicensed bands aggregation in LTE-A (licensed) system. It turns out that the defined problem is a Mixed Integer Non Linear Programming (MINLP) that requires an exhaustive search procedure in order to be solved. To tackle with this, an optimal low complexity method is proposed based on the Lagrange dual decomposition. Apart from the employed method, the licensed system requires also information related to the activity and the channel state of the unlicensed bands in order to derive the optimal solution. An optimal low complexity method is also provided for the solution of the latter problem. The performance of the original (MINLP) and the low-complexity proposed techniques for the perfect CSI cases are verified via indicative simulations. The extension of this work will consider the imperfect CSI and thus, a blind estimation technique will be devised and incorporated into the system.

Let us consider a typical downlink scenario in a N_U UE LTE-A system that applies a CA scheme exploiting both licensed and unlicensed CCs in order to optimize its transmission [28]. Each user form a $R_s \times T_s$ MIMO system with the eNodeB terminal. The extension to users with different number of antennas is straightforward. Each one of the available CCs is organized in Resource Blocks (RBs) which is the basic scheduling unit following the 3GPP standard. Each RB includes with its turn $N_c = 12$ sub-carriers.

Let us further assume that a UE can aggregate a maximum of K_{max} RBs out of K_U un-licensed and K_L licensed ones. The unlicensed bands are occupied by a number of MIMO

users, i.e. Wi-Fi transceivers, each one having R_p receive and T_p transmit respectively. From now and on, we adopt the CR terminology and refer to that users via the term Primary User (PU) for clarity. Each of the unlicensed RBs have at most one active PU each timeslot with probability P_A. Extension to cases having different activity probabilities and/or multiple active PUs per RBs are straightforward, though they are not shown here for the simplicity of analysis. Finally it is assumed that each one of the available RBs (both the licensed and the unlicensed ones) can be occupied by at most one UE each time following the 3GPP standards [13].

Let us move now to the actual description of the system. The input-output relationship of the $l-th$ ($1 \le l \le N_U$) user in a licensed RB k ($1 \le k \le K_L$) at a time index n ($1 \le n \le N$) within a timeslot is given by

$$\boldsymbol{y}_{lkn} = \boldsymbol{T}_{lk}^H \boldsymbol{H}_{lk} \boldsymbol{S}_{lk} \sqrt{\boldsymbol{P}_{lk}} \boldsymbol{x}_{lkn} + \boldsymbol{T}_{lk}^H \boldsymbol{z}_{lkn}\,, (23)$$

where $\boldsymbol{H}_{lk}$ is the $R_s \times T_s$ channel matrix modeled as $CN(\boldsymbol{0}_{R_s \times T_s}, \sigma_h^2 \boldsymbol{I}_{R_s \times T_s})$ which is assumed to be fixed within the timeslot following a quasi-static fading model, σ_h^2 is the channel variance, $\boldsymbol{I}_{R_s \times T_s}$ is the $R_s \times T_s$ identity matrix and $\boldsymbol{0}_{R_s \times T_s}$ is the $R_s \times T_s$ zero entries matrix, $\boldsymbol{S}_{lk}$ and T_{lk} are the $L_k^s \times T_s$ pre- and $R_s \times L_k^s$ post-coding matrices, $\boldsymbol{P}_{lk}$ is the diagonal $L_k^s \times L_k^s$ power allocation matrix, L_k^s is the number of transmitted streams, $\boldsymbol{x}_{lkn}$ is the $L_k^s \times 1$ transmitted symbols vector with covariance matrix $\boldsymbol{R}_x = \boldsymbol{I}_L$ (we follow this assumption for simplicity and without any loss of generality), $\boldsymbol{y}_{lkn}$ is the $R_s \times 1$ received symbols vector and $\boldsymbol{z}_{lkn}$ is the $R_s \times 1$ white noise random variable vector modeled as $CN(\boldsymbol{0}_{R_s}, \sigma_z^2 \boldsymbol{I}_{R_s})$ with σ_z^2 the noise variance.

In an unlicensed RB k ($K_L \le k \le K_L + K_U$), the received signal is re-written as

$$\boldsymbol{y}_{lkn} = \boldsymbol{T}_{lk}^H \boldsymbol{H}_{lk} \boldsymbol{S}_{lk} \sqrt{\boldsymbol{P}_{lk}} \boldsymbol{x}_{lkn} + \boldsymbol{T}_{lk}^H \boldsymbol{1}_k\{\boldsymbol{G}_{lk} \boldsymbol{d}_{kn}\} + \boldsymbol{T}_{lk}^H \boldsymbol{z}_{lkn}\,, (24)$$

where the $R_s \times L_p$ matrix $\boldsymbol{G}_{lk}^H$ incorporates the $R_p \times T_p$ channel matrix between the PU transmitter and the $l-th$ UE, the $T_p \times L_k^p$ pre-coding and the $L_k^p \times L_k^p$ power allocation matrix of the PU transmitter respectively where L_k^p is the number of the PU's parallel transmitted streams. The aforementioned abstracted formulation is done in the sense that the SU system receives a total signal without having any further information about the PU's transmission parameters. The indicator function $1\{\cdot\}$ that appears in Eq.(25) is defined as

$$\boldsymbol{1}_k\{\boldsymbol{G}_{lk} \boldsymbol{d}_{kn}\} = \begin{cases} \boldsymbol{G}_{lk} \boldsymbol{d}_{kn}, & if\ PU\ is\ active \\ \boldsymbol{0}_{R_p}, & if\ PU\ is\ inactive \end{cases}$$

Finally the received signal at an active PU in the $k-th$ ($K_L \le k \le K_L + K_U$) unlicensed band is given by

$$\boldsymbol{r}_{kn} = \boldsymbol{G}_k' \boldsymbol{d}_{kn} + \boldsymbol{F}_k \boldsymbol{S}_{lk} \sqrt{\boldsymbol{P}_{lk}} \boldsymbol{x}_{kn} + \boldsymbol{z}_{kn}', (25)$$

where again for simplicity we have incorporated the channel, pre-coding and power allocation matrix of the PU transmission in matrix $\boldsymbol{G}_k'$. Matrix $\boldsymbol{F}_k$ is the $R_p \times T_s$ channel matrix from the LTE-A eNodeB to the receiver of the PU and $\boldsymbol{z}_{kn}'$ is the corresponding noise vector at the PU receiver.

From the above description it is evident that the eNodeB has at its disposal a number of licensed and unlicensed bands in order to optimize the downlink communication to the available UEs in terms of the achievable overall sum rate. To that end the eNodeB should determine the optimal RB allocation among the UEs, the optimal pre- / post- coding matrices $\boldsymbol{T}_{lk}$ and $\boldsymbol{S}_{lk}$ and the optimal power allocation ones under the following constraints 1) The eNodeB / UEs will generate/exhibit zero interference from / to the PU transmissions in the unlicensed bands, 2) Each UE can aggregate at most a number of K_{max} bands and 3) The

transmissions are subject to a total transmission power constraint, P_{max} where $K = K_L + K_U$ and $tr(\cdot)$ is the trace of a matrix.

Let us now proceed to the definition of the problem. The aim is to maximize the total sum rate of the downlink transmission subject to the enumerated constraints described below and thus, the following optimization problem should be solved

$$\max_{\boldsymbol{T}_{lk},\boldsymbol{S}_{lk},\boldsymbol{P}_{lk},a_{lk}} \sum_{l=1}^{N_U}\sum_{k=1}^{K} a_{lk} N_c \log_2\left(\left|\boldsymbol{I}_{R_s} + \frac{1}{\sigma_z^2}\boldsymbol{T}_{lk}^H \boldsymbol{H}_{lk}\boldsymbol{S}_{lk}\boldsymbol{P}_{lk}\boldsymbol{S}_{lk}^H\boldsymbol{H}_{lk}^H\boldsymbol{T}_{lk}\right|\right), \quad (26)$$

$$s.t.\ \boldsymbol{F}_k\boldsymbol{S}_{lk} = \boldsymbol{0} \ \&\ \boldsymbol{T}_{lk}^H\boldsymbol{G}_{lk} = \boldsymbol{0}, \quad \forall k \in K_A \ \&\ 1 \le l \le N_U \quad (27)$$

$$\sum_{l=1}^{N_U}\sum_{k=1}^{K} a_{lk} tr(\boldsymbol{P}_{lk}) \le P_{max} \quad \& \quad \boldsymbol{P}_{lk} \ge \boldsymbol{0} \quad (28)$$

$$\sum_{k=1}^{K} a_{lk} \le 1 \quad \& \quad \sum_{l=1}^{N_U} a_{lk} \le K_{max} \quad \& \quad a_{lk} \in \{0,1\} \quad (29)$$

where Eq.(27) expresses the total sum rate of the downlink LTE-A system, the binary variable a_{lk} is set to one when the $k-th$ RB is allocated to the $l-th$ user and zero if not and $K_A \subseteq [K_L+1, K_L+K_U]$ is the set of the unlicensed bands with an active PU on them. The constraints of Eq.(29) are used to cancel the interference from/to the PUs by forcing the pre-coding matrix $\boldsymbol{S}_{lk}$ and the post-coding one to $\boldsymbol{T}_{lk}$ to be orthogonal to matrices $\boldsymbol{F}_k$ and $\boldsymbol{G}_{lk}$ respectively.

Since the eNodeB handles exclusively the interference cancellation to the PU receivers by properly design of the its pre-coding matrix, the PU systems may continue to operate as if there is no interfering user in their band. Note also that the constraints of Eq.(28) are active if at a PU user is active in the RB under consideration. The constraints of Eq.(30) control the total transmission power and force the power allocation matrices to be positive respectively and the final ones of eqs.(7) are posed in order to control the maximum number of aggregated RBs per UE, the maximum number of allowed UEs per RB (1) and to force the specified support set on the parameters a_{lk} respectively. The solution of the problem for both the perfect and the Imperfect CSI Case is described in [19].

A number of indicative simulations are provided in order to evaluate the performance of the proposed techniques. In Figure 33, the performance in terms of the achievable data rate of the proposed approach under the perfect CSI case is compared to the one of a LTE-A system that employs only a number K_L fixed licensed bands for different SNR values. At first we examine the performance for $K_L = 5$ licensed and $K_U = 10$ unlicensed RBs. The PU and the LTE-A systems are assumed to be 2×2 and 4×4 MIMO ones respectively. The channel gains of all the involved channels are generated as circular symmetric i.i.d. Gaussian variables of zero mean and unit variance, i.e. $CN(0,1)$. The performance is evaluated for two different PU activity scenarios $P_k = 0.2$ and.$P_k = 0.8$. A two user system is assumed with the maximum permitted number of aggregated RBs $K_{max} = 5$. The solution to the licensed only case is given by solving the MINLP optimization problem of Eq.(27)-(30) without the unlicensed bands constraint of Eq.(28). The proposed approach ("MINLP, $K_L = 5$, $K_U = 10$, $P_k = 0.2$" and "MINLP $K_L = 5$, $K_U = 10$, $P_k = 0.8$" curves) achieves significantly improved performance as compared to the licensed only case ("Licensed Only $N_c = 0.5$, $N_U = 10$" curve). In the licensed only case two users share only $K_L = 5$ RBs which is bellow their quota of $K_{max} = 5$ RBs. Contrariwise in the unlicensed - licensed case there are $K_L + K_U = 15$ available RBs so each one of the users can reach its quota by having also options for selecting the best possible combination of RBs that maximizes the sum rate of the system which explains the observed superiority in the performance. Note also that that the case of with the lower PU activity $P_k = 0.2$ presents better performance compared to the case where $P_k = 0.8$. This is the case since for lower P_k values there are unoccupied bands with higher probability. Thus, the LTE-A users have extra RBs without having to null out the interference

from/to the PUs that leads to loss in spatial degress of freedom. In the same figure the optimality of Algorithm 5 is verified as it achieves almost identical performance with the MINLP solutions ("Algorithm 5 in [19] $K_L = 5,\ K_U = 10, P_k = 0.2$" and "Algorithm 5 $K_L = 5,\ K_U = 10,\ P_k = 0.8$" curves). We close the study of the perfect CSI case by repeating the experiments of Algorithm 5 for the case of $K_L = 10$ licensed and $K_U = 5$ unlicensed RBs ("Algorithm 5 $K_L = 10,\ K_U = 5,\ P_k = 0.2$" and "Algorithm 5 $K_L = 10,\ K_U = 5,\ P_k = 0.8$" curves) and of the licensed only MINLP approach ("Licensed Only $N_c = 0.5$," $N_U = 10$ curve). As we can see the performance gains here are smaller (but still existent) due to fact that the system has already $K_L = 10$ available RBs which suffice for each user to reach its quota. Furthermore there are only 5 unlicensed RBs available, thus less available combinations to maximize the sum rate of the system. Of course with an increase in the number of available unlicensed RBs and/or LTE-A users one will see a corresponding increase in the sum rate of the system.

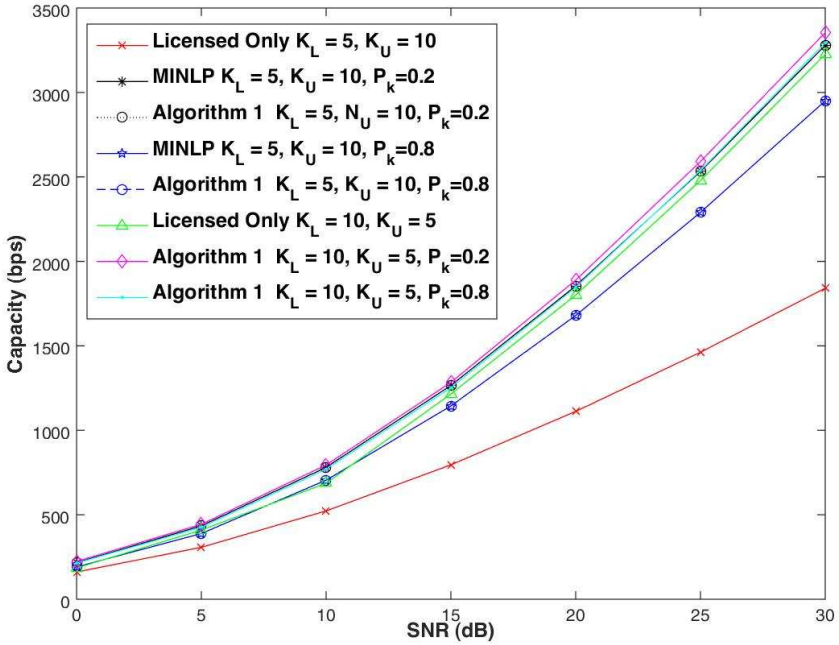

Figure 33: Performance of the proposed approach under the perfect CSI case

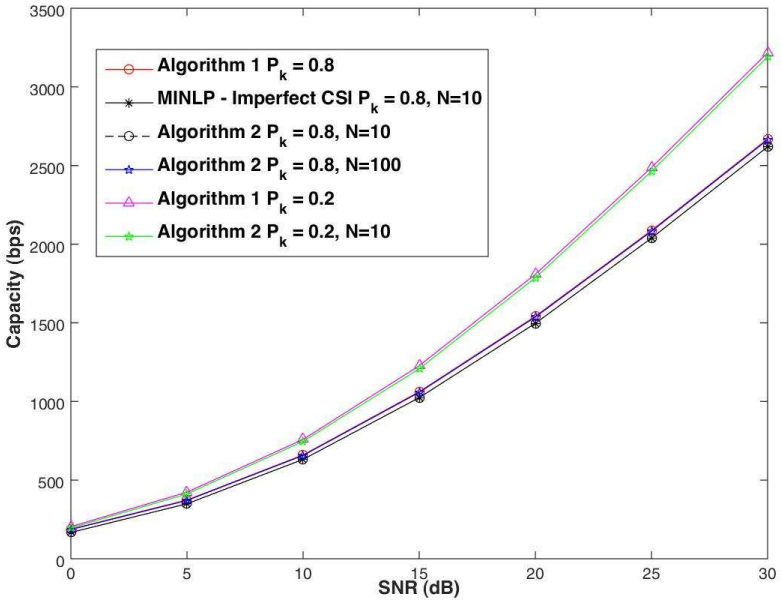

Figure 34: Performance of the proposed approach under the imperfect CSI case

In Figure 34, the performance of the proposed approach is verified for the imperfect CSI case. The simulation parameters are exactly the same to the ones of the perfect CSI case except from the numbers of licensed and the unlicensed bands which are now $K_L = 2$ and $K_U = 8$ respectively. We compare the performance of Algorithm 2 in [19] for two values of parameter $N = 10{,}100$ (recall that it is the number of samples used to estimate the require null-space matrices, see Subsec. IV.A of the Appendix 6.2) for $P_k = 0.2{,}0.8$ to the one of Algorithm 1 ("Algorithm 1 $P_k = 0.2$" and "Algorithm 1 $P_k = 0.8$" curves) [1]. As it is shown even for a very small number of $N = 10$ the performance of Algorithm 2 ("Algorithm 2 $P_k = 0.2$, $N = 10$" and "Algorithm 2 $P_k = 0.8$, $N = 10$" curves) is very close to the one of Algorithm 1. For the case of $P_k = 0.8$ there is a slighter bigger degradation since there is with higher probability an active PUs that occupying the bands. In the latter case the simulations repeated for $N = 100$ ("Algorithm 2 $P_k = 0.8$, $N = 100$" curve) and as it shown Algorithm 2 achieves almost identical performance to one of Algorithm 1 due to the improved accuracy on the estimation. The optimality of Algorithm 2 is verified by repeating the experiment for the case of $P_k = 0.8$ and $N = 10$ but using the MINLP solver of OPTI toolbox instead of Algorithm 2. As it is shown the resulting curve ("MINLP-Imperfect – CSI $P_k = 0.8$, $N = 10$") is almost identical to the corresponding one of Algorithm 2.

Finally, from Figure 35, it is evident that the CSI errors have small impact on the performance of the proposed approach. Also for low SNR values the performance is mainly dominated by the high variance noise rather than the estimation errors. In order to verify the previous statement the achievable rate of an active PU of the unlicensed band is depicted in Fig. 3 in case no LTE-A user is presented in the band and in case a 4×4 MIMO LTE-A user establishes its communication via that band for $N = 100$. As it is depicted in Figure. 31 the performance is almost identical in both cases leading us to the conclusion that a few only samples suffice in order to null out successfully the interference from/to the PUs.

[1] The authors refer to Algorithm 1 and 2 of the Appendix 6.3.

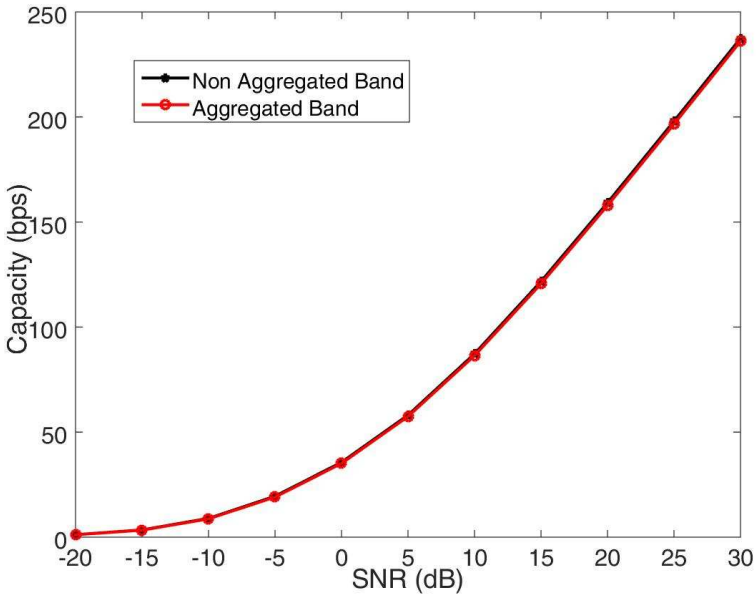

Figure 35 Impact of imperfect estimation of matrices $\boldsymbol{O_k}$ and $\boldsymbol{Q_k}$ on the performance of the users of the unlicensed bands.

6.5 Achievements

We have studied the use of CA to enable the use of LTE in unlicensed spectrum. Such use scenario is directly the case of LAA as currently being defined in the standardisation.
We have proposed to modify the LTE frame structure to define a burst that could accommodate the constraints of operation in unlicensed bands (section 6.2). Then, in Section 6.3 we have extend the cognitive radio concept to the LAA scenario, applying reinforcement learning and double Q-Learning techniques for the carrier selection and discontinuous transmission.

Section 6.4 deals with the subcarrier allocation for a licensed/unlicensed CA MIMO system. This solution provides both blind learning and interference nulling for such a system model. Such a solution addresses the efficient CA in h-RATs, where the bands belong to licensed and unlicensed bands.

7. TV White Space Aggregation

7.1 Overview

As identified in WP2 and in first deliverable of WP3, another scenario of interest for CA relates to the aggregation of TV white space (TVWS) channels. Indeed, aggregation in TVWS is often essential to the realisation of appropriate QoS in such spectrum given higher-layer traffic demands. This is due to local and in some cases temporal variations in allowed transmission EIRP on available TVWS channels, based on the presence of incumbent DTT and PMSE systems in the area. It is also potentially due to uncertain interference between white space devices (WSDs), given the range of different standards and types of systems used in TVWS, as well as the excellent propagation characteristics in TVWS. Nevertheless, it is noted that TVWS and other white space opportunities based on frameworks compliant with the European Harmonised Standard ETSI EN 301 598 [38] can present vast additional resource, and aggregation of such resources is (by definition) an essential part of the spectrum overlay that is being developed as part of the SOLDER project.

In the light of the above, this section reports some of the work that has been done within SOLDER on aggregation within TVWS, noting that some highly interesting and fundamental observations, e.g., for RF design in the context of aggregation in TVWS, have been derived from such work.

7.2 TV White Space Aggregation Assumptions and Architecture

The functionality of the TVWS framework, as has been developed by Ofcom in the UK (see, e.g., [37]) and Harmonised at the European level through the European Harmonised Standard ETSI EN 301 598 [38], can be extended to additional purposes from its core objective of protecting the primary services that are operating in TV bands. In particular, the current UK/EU framework might be extended to the white space geolocation databases also managing the resource usage *among* the WSDs, or the geolocation databases even acting as system managers dealing with connection opportunities among the secondary devices—including the most appropriate mapping of those opportunities and the associated spectrum to WSDs based on their traffic load characteristics [42]. Further, the concept can be extended to act as a management entity *in general*, not just assisting management in the scope of TVWS, but also serving the appropriate allocation of devices to spectrum or connectivity opportunities in consideration of licensed spectrum/systems and "conventional" unlicensed spectrum/systems (such as WiFi in ISM/U-NII). It is noted, however, that there are limitations as to the level at which such a management should operate. Particularly, when combining conventional licensed spectrum/systems with unlicensed and white space spectrum/systems, aggregation will generally have to be done only at high layers. In this context, there is often little that can be done technically at lower layers to assist aggregation, making such a management capability at higher layers (e.g., mapping traffic to aggregatiable link opportunities) far more relevant. When aggregating similar systems or different instances of the same system at lower layers, such a management system becomes less relevant. This is because management capabilities (including aggregation management capabilities) might often already exist in the scope of the individual systems being aggregated, or their combined scope, so it is therefore less necessary to abstract out an overarching management system for them.

In the case of management of TVWS or in some cases for resource usages in "conventional" unlicensed spectrum, a management system might be able to decide exactly which channels should be used and aggregated to achieve a given traffic demand, which should be used in view of not interfering with others users' needs to aggregate channels/spectrum to achieve their traffic demand, etc. Extending the current UK/EU TVWS framework while also building such a management architecture into that which has been proposed in Section 2 of Deliverable 2.3 [41], the management of allocation to devices—taking into account aggregation possibilities and concentrating on TVWS alone as is the scope of this section—can proceed as follows (extended from and compliant with [42], as well as content presented later in Section 9.2):

1) The Master TVWS device (typically a base station in terms of mobile network structure) sends its location information and technical characteristics/capabilities, and any information it may have on its anticipated traffic requirement, to the geolocation/management database using the standard "master specific" UK/EU TVWS framework messaging with some minor information model extensions to convey traffic requirement information.
2) The geolocation/management database performs all necessary operations for primary coexistence purposes, i.e., calculation of the allowed powers on a per-channel basis, and corresponding schedules, according to the UK/EU framework [38], [37].
3) The geolocation/management database performs a resource allocation calculation in order to ascertain which resources of those allowed according to the UK/EU TVWS framework should be allocated to which master devices. It takes into account the traf-

fic requirement of the master devices in doing this, and uses a given metric to perform this allocation—where it is noted that future additional work on the formulation of this metric may be done in view of differing requirements for different traffic types. It uses the standard "master specific" UK/EU TVWS framework messaging to convey the allowed resource usages.

4) The geolocation/management database informs the master device of the resource allocations, using the standard "master specific" UK/EU TVWS framework messaging.
5) The master device then informs the geolocation/management database of its actual use of the resource (channel/power) using the standard "master usage" UK/EU TVWS framework messaging.
6) The geolocation/management database confirms the usage of resources with the master device using the standard "master usage" UK/EU TVWS framework messaging.
7) The master device then starts actually using the allocated resources (channels/powers). In tandem it requests for parameters from the geolocation/management database using the standard "generic slave" UK/EU TVWS framework messaging.
8) The geolocation/management database calculates and returns the allowed "generic slave" channels powers according to the standard "generic slave" UK/EU TVWS framework messaging.
9) The slave TVWS devices send their information (location, technical characteristics, traffic requirements) as for the master TVWS device in step (1) to the master TVWS device, and the master TVWS device then acts on behalf of the slave TVWS devices using the extended information set including traffic requirement calculations using the standard procedures for "slave specific" parameters in the UK/EU framework.

Here, it is noted that although the precise allocation from the geolocation/management database is already known in the initial response, steps (5) and (6) are still necessary in order to be compliant with the UK/EU framework—both for the "master specific" parameters as are covered in detail in the above, and the mirrored stage of the "slave specific" parameter calculation and information transfers that naturally follow. Moreover, it is noted that the above procedure might change should the master device wish/need to obtain the precise information on traffic requirements from slave devices first before conveying its traffic requirements to the database. This change would imply the entire procedure occurring according to the Ofcom framework with the master device not conveying (and the database not taking into account) its traffic requirements, instead only the slave devices conveying this information and the database taking into account and transferring resource usages to those. An adjusted allocation can then be made for the master device based on the knowledge of the slave devices' requirements that it is supporting; this adjusted allocation can be applied to the master device on its next required periodic check with the database, noting that according to the current framework such checks are necessary at least every 15 minutes. Further, the master device might anyway reinitiate an additional resource check once it has received and conveyed information for all of its slave devices. There is nothing within the EU/UK framework, and the underlying signalling procedures, that prohibits WSDs from doing these additional polls of the database at will.

Figure 36 depicts the signalling according to the above procedure, compliantly with the UK/EU framework. This concept has been published in an expanded form (also applicable as an architecture for management in general, as indicated above), in [42]. In this context, the geolocation management entity is known as the "Trusted Non-regulatory Geolocation Database" (T-NGD). The work in [42] has also assessed capabilities achievable in TVWS through aggregation linked to this architecture; other work (e.g., [43], [44]) has extensive assessed what is possible through aggregation in TVWS in general.

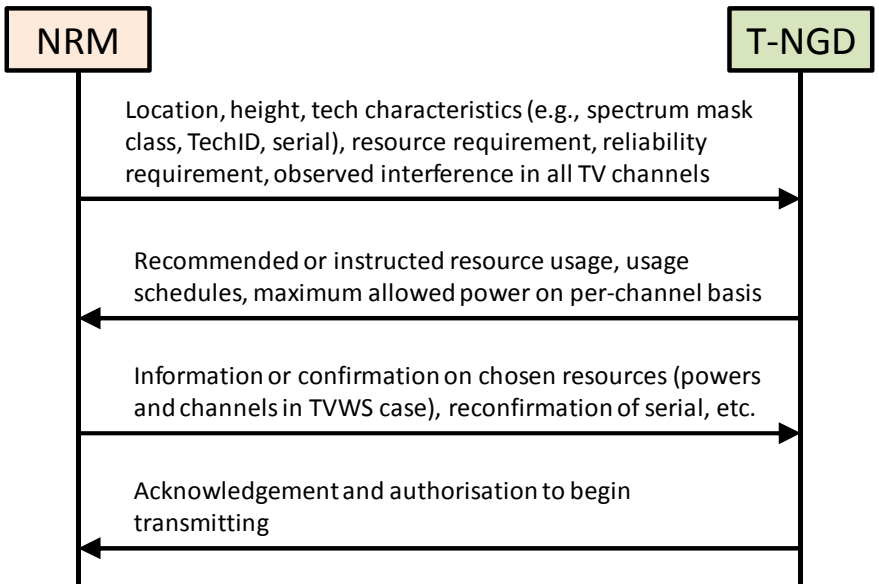

Figure 36: Signalling diagram geolocation-based management system in TVWS (in the context of our expanded work in [42] and Section 9.2). T-NGD=Trusted Non-regulatory Geolocation Database; NRM=Network Resource Manager.

7.3 Initial Assessment Results

As mentioned previously, extensive work has been done on assessing performance in TVWS, including aggregation studies, in publications such as [43], [44], [45], [42] (see also Appendix 7). Key questions are: How much white space is there, and what can be achieved using that white space? These are all the more important to answer for the UK case, which operates under significantly different rules from the US. To shed some light on this, we have investigated the available white space in the London, UK area, and also the optimum capacity that can be achieved by aggregating all of that white space. Our studies have sampled white space availability according to the UK framework in a rectangular lattice defined by the top-left corner (latitude, longitude) 51.678064, -0.506744, and the bottom-right corner 51.312133, 0.229340, with a sampling frequency of 0.01□ both in latitude and longitude. This equates to the area approximately as bounded by the London M25 orbital motorway/highway, and 2,775 sampled locations within that area. Figure 37 maps the considered area. Further, for comparison, this work has been extended and reported later in Section 7.7 to consider a much larger area of England.

We have adapted one of our implementations of the WSD-side logical requirements to methodically query Fairspectrum and obtain information on available white space, and do capacity analyses with a particular emphasis on aggregation. This work is based on the implementation of the Ofcom Framework as was the case in January 2015.

Table 5: Scenario configurations

Scenario	Transmitter Height (m)	Receiver Height (m)	Transmission Distance (m)	Path loss	Shannon Efficiency
Mobile Broadband Downlink	30	1.5	2,000	Hata Urban, large city	0.5
Indoor Wireless Local Area Networking	1	1	80	Yamada model, 8 walls, same floor, King's College Strand parameters [4]	0.5

We study two scenarios for the purpose of our availability and capacity analyses, which we term the "mobile broadband downlink" and "indoor broadband provisioning" scenarios. The mobile broadband downlink scenario is inspired by the realization that above-rooftop reception can be hampered by interference from distant DTT transmissions that are not meant to be covering the area, as reported in [43], [44], [45], and it is likely that other WSD transmissions will also cause interference in such deployment cases going into the future. This scenario is further inspired by the efforts that are being made towards the realization of LTE supplemental downlink scenarios albeit initially in the form of LAA unlicensed access in 5GHz U-NII spectrum. Given this, the downlink can typically be observed to experience far less interference than the uplink in TVWS, whereby TVWS can be a facilitator for enhancing capacity, conveniently being located extremely close to the LTE 700 and LTE 800 spectrum thereby facilitating design of LTE devices should they wish to use TVWS for a supplemental downlink. The indoor broadband provisioning scenario is inspired by the fact that TVWS channels will be much "cleaner" indoors, and indoor propagation is far better in TV bands than other bands used by WLANs such as ISM 2.4 GHz and U-NII 5 GHz.

Figure 37: The studied London M25 area for availability, capacity and aggregation studies.

The characteristics of these scenarios are given in Table 5. Note that the transmitter height is one of the parameters used by the white space database (in addition, of course, to location and other parameters such as the spectrum mask class) in assessing allowed powers on a per-channel basis, whereas the receiver height is used merely for propagation loss calculations, and the assumed Shannon efficiency of the radio interface is for capacity calculations. Moreover, propagation characteristics are deliberately set to be extremely challenging for the given scenarios, whereby the mobile broadband downlink scenario uses the most challenging variant on the Hata propagation model over a propagation distance of 2 km. The indoor broadband provisioning scenario uses a propagation model that was developed at King's College London for indoor TVWS transmissions, and parameterized at the Strand building of King's College London [46]. Particularly for this scenario and parameterization, this propagation model has been shown to perform far better than any available alternatives [46]. The transmission is over a distance of 80 m indoors and through 8 walls. It is noted that the extremely challenging nature of these characteristics mean that results in this case can be seen as something of a worst case in terms of capacity analysis.

7.4 Number of Channels available

Figure 38 maps the number of channels that are available for the mobile broadband downlink scenario (assuming a minimum allowed EIRP of 30 dBm), over the London M25 area corresponding to that presented in Figure 37, for a Class 5 device. Table 6 gives statistics over the area for all classes of devices. Figure 39 and Table 7 present the same results for the indoor broadband provisioning scenario, which assumes that a minimum allowed EIRP of 20 dBm is acceptable in assessing channel availability.

One first clear observation from these results is that Classes 1-3 are very similar in terms of availability, with availability only starting to significantly reduce for Classes 4 and 5. Moreover, it is noted that there is a very good correlation of availability with (i) the location of the London TV transmitter at Crystal Palace (marked in Figure 37), and (ii) the building density in the area. Considering (i), this is because there is one TV transmitter providing sole coverage in the area hence not other TV transmitters blocking out different sets of channels to achieve their multiplexes thereby reducing white space availability, noting that in the UK the different TV transmitters use different frequencies in order to avoid interfering with the reception of each other (content transmitted by the different transmitters can also vary significantly among the various transmitters and regions). Considering (ii), this is because of the increased propagation loss in built-up areas, thereby allowing greater availability/EIRP for WSDs in those areas. Comparing with areas such as the north-west and south-west of the assessed location, availability is reduced significantly because of the overlap of TV transmitter coverage for those areas, and the reduced propagation loss. An extreme case is presented for the Guildford location discussed later in Figure 42, whereby there is severe overlap of various TV transmitters, and availability is reduced significantly.

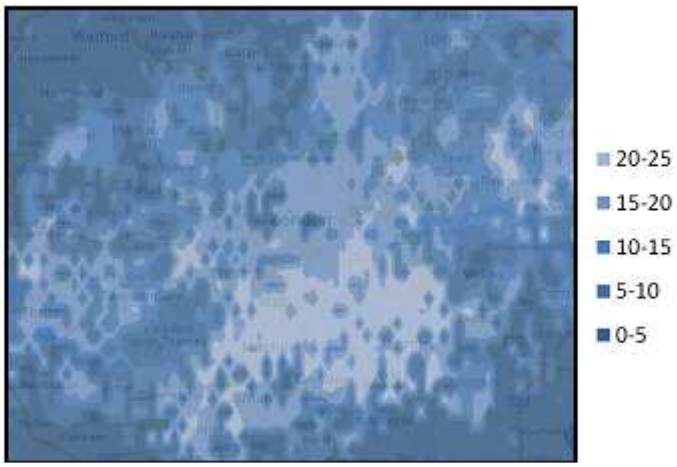

Figure 38: Number of "usable" channels available for the mobile broadband downlink scenario for a Class 5 device.

Another observation is that there are a large number of relatively small "spots" of reduced availability. These are caused by PMSE (e.g., wireless microphone) deployments, noting that PMSE is also licensed and deployment locations recorded in the UK, hence is protected to the same level as TV broadcast services. The most severe such location is part of the "West End" area of London, incidentally coinciding with the South Aldwych/Strand area and the King's College London Strand Campus, covered extensively in later discussion. This is the area about a quarter of the way down and on the right side of the letter "d" of "London" in Figure 37 to Figure 41. This reduced availability is due to PMSE usage of numerous nearby musical theatres, concert halls, TV production, among others facilities.

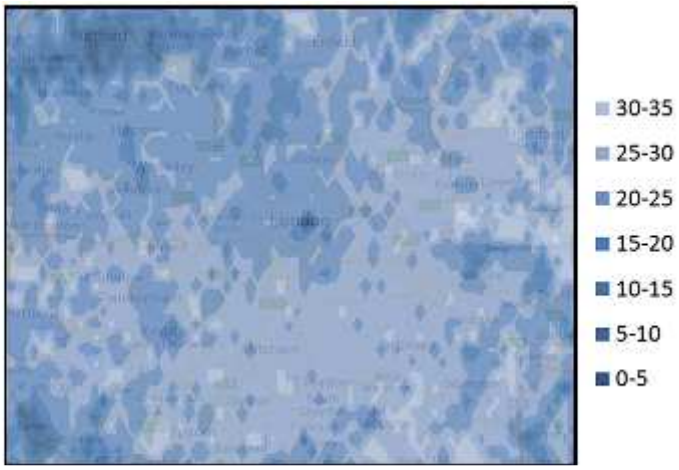

Figure 39: Number of "usable" channels available for the indoor wireless local-area networking scenario for a Class 5 device.

Concerning statistics on availability reflected in Table 6 and Table 7, it is noted that for the mobile broadband downlink scenario an average of approximately 10 to 15 channels is available depending on class; the coefficient of variation (CoV) of this number increases somewhat from 0.54 to 0.70 as the spectrum mask performance class is reduced. For the indoor wireless local-area networking scenario, an average of approximately 23 to 26 channels are available, with a coefficient of variation increasing from 0.13 to 0.22 as the spectrum mask

class quality is reduced. Hence, the indoor wireless local-area networking scenario achieves both greater availability on average, and better certainty in the availability of spectrum. There is somewhat of a reduction in such availability as the transmitter height is increased, however, that is not significant. Moreover, it is noted that the reduced EIRP requirement for the indoor wireless local-area networking scenario is the key cause of the greater certainty, leading to a reduced number of locations for which PMSE and TV primary services impact on the allowed EIRP enough to violate the 20 dBm threshold.

Table 6: Statistics on number of usable channels available for the mobile broadband DL scenario, for all device spectrum mask performance classes

Number of channels					
	Class 1	Class 2	Class 3	Class 4	Class 5
Average	15.6	15.4	15.2	12.6	10.2
STD	8.4	8.4	8.5	8.1	7.1
CoV	0.54	0.55	0.56	0.64	0.70

Table 7: Statistics on number of usable channels available for the indoor wireless local-area networking scenario, for all devices spectrum mask performance classes

Number of channels					
	Class 1	Class 2	Class 3	Class 4	Class 5
Average	25.7	25.6	25.5	24.9	23.4
STD	3.4	3.4	3.6	4.2	5.2
CoV	0.13	0.13	0.14	0.17	0.22

A further observation is that a worsening of spectrum mask class has a far more severe effect for the mobile broadband downlink scenario, as compared with the indoor wireless local-area networking scenario. This conveniently matches with the observation that white space base station deployments for the mobile broadband downlink scenario will be relatively sparse, and be able to absorb a greater expense in achieving a good spectrum mask class. Radio deployments for the indoor wireless local-area networking scenario will be very dense indeed, and typically done only by the consumer/end-user. Expense for such cases must be minimised, which seems to be viable given that deployment of a Class 5 device, for example, seems to in most cases have a relatively small effect on performance as compared with Class 1.

7.5 Achievable Capacity Through Aggregation

Next assessed are the achievable capacities for the mobile broadband downlink and indoor broadband provisioning scenarios. In all cases, a capacity calculation is done based on the allowed EIRPs in all channels, assuming the “optimal” aggregation of all channels at maximum allowed EIRP on a per-channel basis. As indicated previously, challenging propagation characteristics are assumed (see Table 5), leading to what might be seen as a “worst case” achievable capacity.

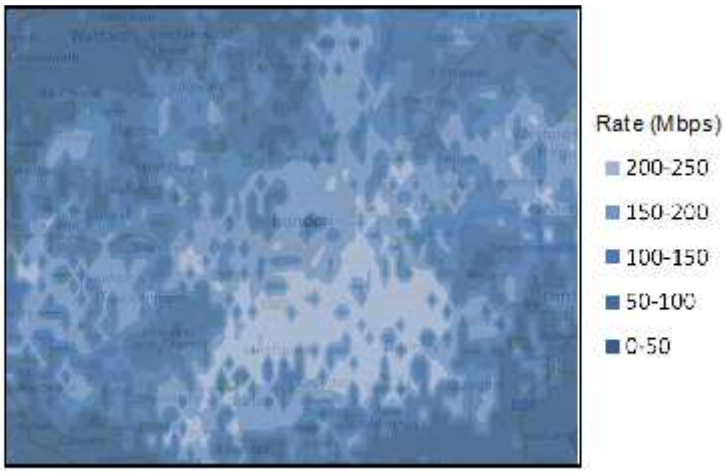

Figure 40: Capacity achievable by optimally aggregating all available channels at maximum allowed EIRP on a per-channel basis for the mobile broadband downlink scenario for Class 5 device.

Achieved aggregate capacity mapped to the locations in the London M25 area for the mobile broadcast downlink scenario is given in Figure 40, and for the indoor broadband provisioning scenario in Figure 41. Corresponding tables of statistics are in Table 8 and Table 9. It is noted that many of the same observations as are made in the analysis of available number of channels apply. However, there are some differences. For example, more of a negative effect is observed if the spectrum mask class is reduced from Class 2 to Class 3 for the mobile broadband downlink scenario. This is because there are reduced EIRPs for Class 3 devices, hence reducing the capacity that is achievable by aggregating channels at maximum allowed EIRP, however, these reduced EIRPs rarely fall below the threshold of 30 dBm to rule the channels as “not available” under this scenario as we define it.

Figure 41: Capacity achievable by optimally aggregating all available channels at maximum allowed EIRP on a per-channel basis for the indoor wireless local-area networking scenario for a Class 5 device.

Table 8: Statistics on achieved bate by optimally aggregating all available channels at maximum allowed EIRP on a per-channel basis for the mobile broadband downlink scenario, for all device spectrum mask performance classes

Achieved Rate (Mbps)					
	Class 1	Class 2	Class 3	Class 4	Class 5
Average	167.0	165.1	155.4	130.9	104.7
STD	84.2	84.4	82.5	77.4	66.8
CoV	0.50	0.51	0.53	0.59	0.64

Table 9: Statistics on achieved bate by optimally aggregating all available channels at maximum allowed EIRP on a per-channel basis for the indoor wireless local-area networking scenario, for all device spectrum mask performance classes

Achieved Rate (Mbps)					
	Class 1	Class 2	Class 3	Class 4	Class 5
Average	333.5	330.9	327.5	312.5	285.6
STD	54.9	55.6	58.8	65.4	67.9
CoV	0.16	0.17	0.18	0.21	0.24

Extending observations from the analysis of the number of channels available, Class 1 and Class 2 performances remain almost identical, both in terms of average number of channels and capacity and in terms of variability of those, although in the case of the analysis of the capacity achieved Class 3 performances are reduced somewhat. This leads to the conclusion that, given a relatively "noisy" design of WSD, there would be little benefit gained by striving for the more challenging -79 and -84 dB requirements in further-out channels than the adjacent channel, if the device already achieved -74 dB in the adjacent hence other channels. Moreover, it is noted that the -74 dB requirement in the Ofcom UK/EU case is equivalent to -55 dB in the FCC US case, due to the Adjacent Frequency Leakage Radio (AFLR) being measured for 100 kHz "chunks" in adjacent channels as compared with the 8 MHz value in the intended channel under the UK model. Hence, AFLR is already automatically 19 dB (80x) lower in a like-for-like power spectral density comparison. Devices developed and already meeting emissions requirements for the US case would therefore be classified as Class 2 or better under the UK case.

7.5.1 Aggregation Options

Next assessed is the performance that is achieved through implementing various aggregation configurations in TVWS. Figure 42 presents the achieved capacity for the mobile broadband downlink scenario against the number of channels that are aggregated for a small subset of the locations that we are taking advantage of for deployments in our trial, where it is noted that the assessment of far more locations is available in [43], [44]. Figure 42 assumes either contiguous or non-contiguous aggregation (i.e., that the radio can take advantage of all channels optimally with maximum allowed EIRP on a per-channel basis, no matter how they are distributed across the frequency band). This could be seen as feasible, for example, under an advanced radio interface such as filter-bank multi-carrier that is able to "notch out" certain channels and still use those available ones at precisely the power limit. A very simple channel selection rule ascertains the next available channel to use:

1. Choose the channel with maximum allowed EIRP according to the UK framework.
    a. If EIRP is equal among the next available channels (note, this is common under the UK framework, as EIRPs are given as integer dBm values), choose the channel of equal EIRP with the lowest frequency.

Results for the cases in Figure 42 are presented in the order of the most favorable to the least favorable for aggregation (or, indeed, often for white spaces usage in general). Considering the results for Mile End (see [43], [44] for these results), this is the best location for white spaces usage among those assessed. Performance increases almost linearly with the number of channels that are aggregated, with a slight drop-off in performance for worse performance spectrum mask classes due to increased adjacent channel leakages, either (i) ruling out some lower frequency channels at equal power for aggregation, meaning that higher-frequency (worse propagation/performance) channels have to be used at equal power, or (ii) in some rare cases causing a reduction in the allowed power in order to maintain adjacent channel leakage requirements.

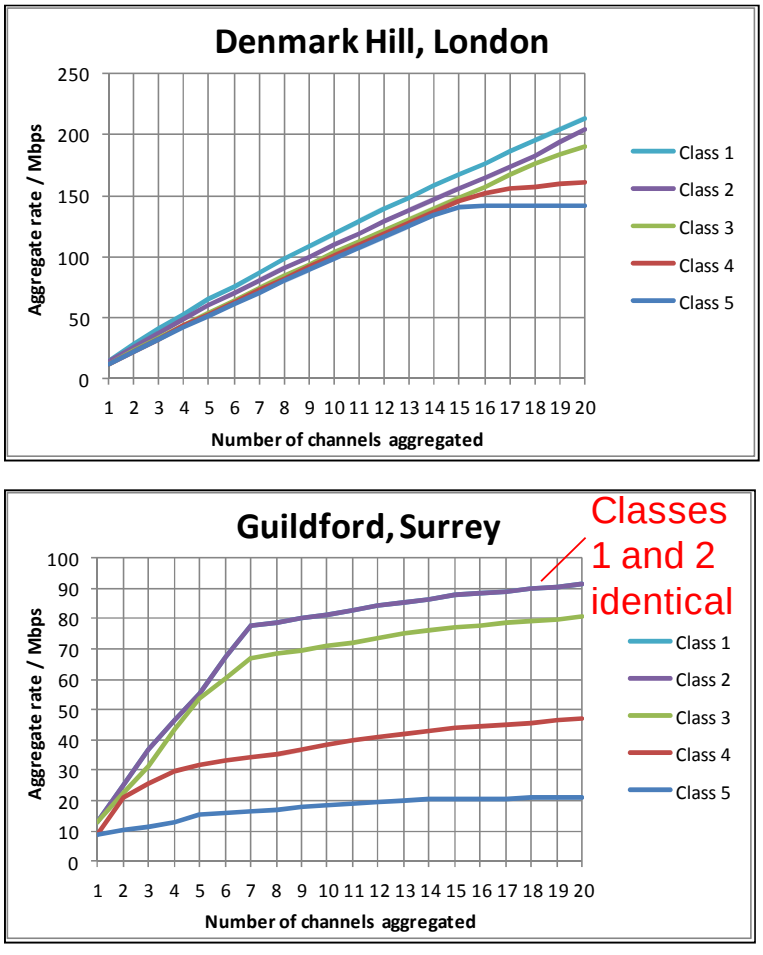

Figure 42: Capacity achievable by optimally aggregating different numbers of channels at maximum allowed EIRP on a per-channel basis for the mobile broadband downlink scenario, at some specific locations (far more extensive results are available in [43], [44]).

For the Denmark Hill case, it is possible to observe the start of cases where the limit on the number of channels that can be used for aggregation is hit, for worse spectrum mask classes, due to the adjacent channel leakage requirements. Class 4 performance here repre-

sents a worsening of the phenomena seen for Mile End case under poorer performance classes, whereas the "flat-lining" of the Class 5 case indicates that the limit has been hit. The Waterloo and South Aldwych cases (see [43], [44] for these results) show the situation where a large number of channels are ruled out due to extensive PMSE usage in the area, the South Aldwych case being perhaps the most severely affected in the whole country. Moreover, it is noted that PMSE usage is the cause of the relatively-abrupt flat-lining for the Denmark Hill case observed.

The Guildford case here represents what is seen when the limitations are largely due to DTT, Guildford white space being severely affected by overlapping DTT transmitter coverages transmitting multiplexes at different frequencies. This DTT limitation on white space usage leads to a reduction in EIRPs on many channels, but not the flat-lining that PMSE usage leads to as has been observed for the South Aldwych, Waterloo, and somewhat the Denmark Hill locations.

A further observation from these results is that, again, Classes 1 and 2 lead to very similar performance, if not identical performance. Particularly in cases where potential interference victims are more than a certain distance away (e.g., in the Guildford case) the performance is identical. This is because at more than a certain (very short) distance, the -79 and -84 dB down limitations for further-out channels than the adjacent channels no longer have an effect, as received power at the victim receivers has already dropped below the level at which unacceptable interference is caused without the need for those additional limitations.

Figure 43 represents the case where the white space device can only aggregate contiguous channels, e.g., should it have only one radio that can transmit contiguously which is of variable bandwidth. Far more extensive results, covering all of the locations referred to in this text, are available in [43], [44]. Under this case, the following algorithm has been used for choosing channels and powers:

1. For all possible sets of *n* contiguous channels.
    a. Ascertain the EIRP of the lowest allowed among the contiguous channels.
        i. Transmit on all of the contiguous channels with this equal lowest power, even if some of the contiguous channels support higher allowed power. This is necessary in order to not violate regulatory limits on a per-channel basis, assuming that the radio produces a relatively "flat" waveform over the allowed channels.
2. Perform the same operation as in Step 1 for *n*-1, *n*-2, etc., to *n*=1 contiguous channels.
3. Take the result of the highest rate among all possible sets of contiguous channels assessed in Steps 1 and Step 2 above as the achieved value for *n* contiguous channels.

One key initial observations is that except for rare examples (e.g., Guildford), class doesn't have a major effect on capacity achievable. This results, which is backed up by later results in Section 7.7, has profound implications for the design of WSDs: there is often little to be gained by striving for higher performance classes than Class 5, given the significant RF complexity that that implies. A manufacturer designing a device with the ability to aggregate 3 or more contiguous channels (bandwidth) can neglect the adjacent channel leakage increase that might often occur if the bandwidth is being increased, reducing the spectrum mask class. However, such an observation depends on the required guarantee of service for the white spaces system, as in some cases, particularly where there are a small number of dispersed channels available (e.g., the Aldwych South case, see [43], [44] for these results) or cases where multiple TV transmitters are overlapping, the out-of-channel emissions can infringe on the primary services more under the algorithm above, hence class playing a more important role. Generally, an overriding observation is that, as the number of contiguous channels available to aggregate increases, distance to primary victim receivers quickly be-

comes the limiting factor rather than the out-of-channel emissions, rendering class to be of lesser or no importance.

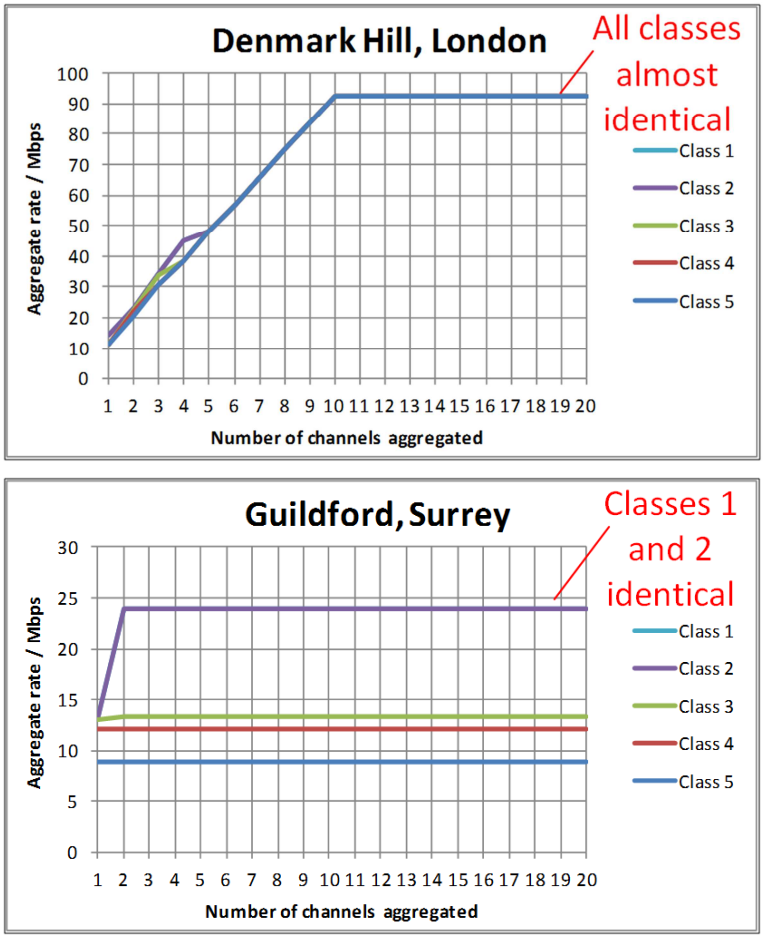

Figure 43: Capacity achievable by aggregating different numbers of contiguous-only channels for the mobile broadband downlink scenario, at some specific locations.

7.6 Will WRC 2015 Kill TV White Space?

A penultimate availability/capacity study done here is to assess the effect that WRC 2015 (which took place in November 2015) will have in a worst case scenario. At WRC 2015, the final rules and lower bound for the allocation of ~694-790 MHz to mobile broadband on a co-primary basis were decided. Should all of that spectrum be taken by mobile broadband in all locations, the effect would be that channels 49-60 would not be available for TVWSs usage. In this section, we therefore perform a further study on available channels and achievable capacity if channels 49 and above are ruled out. Exactly the same prior assumptions, parameterizations, and investigated London M25 area apply.

Results under this assumption are available in [43], [44]. One key observation is that, for the mobile broadband downlink scenario, the effect—particularly for lower classes of RF performance—could be severe. In particular, it is noted that even in some London suburb areas (not considering other further-out/challenging cases, such as the previously-discussed Guildford case) large parts of the area, particularly in the North-West and South-West suburbs, have zero channel availability with allowed power of over 30 dBm. Further, there is a significant increase in the uncertainty in the availability of both channels and achievable capacity for the mobile broadband downlink scenario.

Under the indoor broadband provisioning scenario, the effect is less severe. However, there is a reduction in both the number of available channels and achievable capacity as would be expected. The effect on the variability of availability/capacity is also less severe although is noticeable.

Regarding these results, the worst-case nature of them cannot be overemphasized. For example, in addition to the worst case lower bound consideration (which could perhaps, for international compatibility reasons, indeed result in the current assumption of 694 MHz carrying through) there are uncertainties as to whether WSD usage would remain allowed in this co-primary band, and if it were allowed, the extent to which access would be taken up by mobile operators and the resulting availability of white space in this band.

7.7 The (Slightly) Bigger Picture

Finally, we have succeeded in identifying a much larger area of England supported by the Ofcom framework and our utilized geolocation database, noting that it is challenging to extend this area as only limited locations in the UK are supported for the purpose of the Ofcom Pilot. We use this area to perform a similar assessment to Sections 7.4 and 7.5, sampled at a resolution of 0.05 degrees in latitude and longitude, leading to 2,176 sampled results being taken over the investigated area for each aspect of assessment. Figure 44 maps this area.

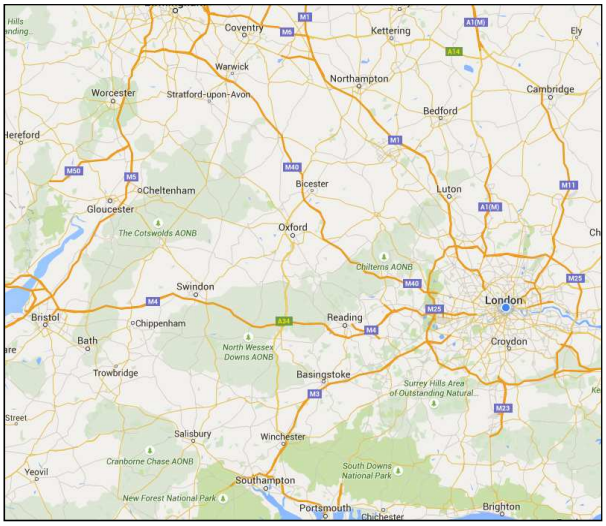

Figure 44: The investigated wider area of England for availiablity and capacity comparison studies.

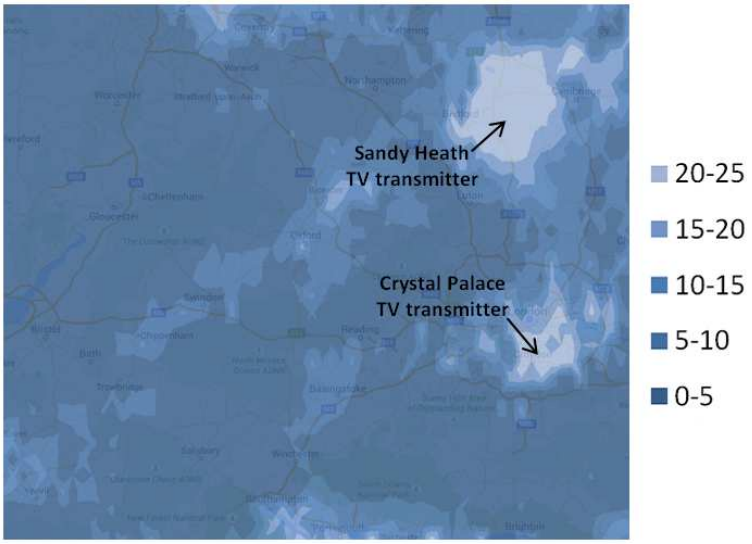

Figure 45: Number of "usable" channels available for the mobile broadband downlink scenario in the wider area of England, Class 5 device (note, far more extensive results are provided in [43], [44]).

The results in Figure 45, and the significantly more-extensive results in [43], [44], reinforce our prior assessment of the TVWS situation in the UK. For example, the same profound effect as for the Crystal Palace TV Transmitter arises from the Sandy Heath TV Transmitter, whereby due to the excellent and sole coverage of that transmitter given its extremely high power (200kW EIRP per channel) only one set of multiplexes is occupied in the area, greatly increasing white space channel availability. However, there is a far greater variability in availability than in our prior assessments for the London M25 area, particularly for the mobile broadband downlink scenario. This limits the scenario's stability for poorer mask classes, also being reflected in the capacity that can be achieved; it is noted that to be certain of achieving white space availability at all, a Class 1-3 WSD would be necessary, noting that Classes 1-5 respectively have the following probabilities of at least 1 channel being usable under this scenario: 99.2%, 98.8%, 98.2%, 88.7%, and 67.5%.

For the indoor broadband provisioning scenario, good channel availability is observed in almost all locations. For example, more than 10 channels are available in over 95% of locations even for a Class 5 device, and in 99.4% of locations for Classes 1 and 2. All classes achieve at least 1 available channel in all locations, Classes 4 and better achieve 4 available channels in all locations, Classes 3 and better achieve 5 available channels in all locations, and Classes 2 and better achieve 6 available channels in all locations. There was no distinction between Classes 1 and 2 by this performance measure. Further, if the height above ground level of the WSD is changed, these results and observations are only marginally affected; the key parameter leading to these results is the low WSD transmission EIRP under this scenario.

Results aggregating all available channels at maximum EIRP, provided in [43], [44], show very significant achievable capacity for the Indoor Broadband Provisioning scenario, and less capacity for the Mobile Broadband Downlink scenario. Like in the number of available channels assessment, this scenario takes a big hit to average performance if the wider area of England is considered, largely due to overlapping TV transmitter station coverages blocking out large numbers of TV channels. This observation strongly emphasizes the differences in this UK case compared with, for example, the US case, where in the latter a key application of such white space equipment would be broadband provisioning to hard-to-reach areas. It is

clear that in the UK case, particularly in the context of this challenging area of Southern and Central England, such broadband provisioning in TVWS would not be practical, without even taking into account the additional detriment of interference in above rooftop receiver deployments in many of these locations, which we anticipate will on average be quite severe—much as discussed in [43], [44], [45].

Although results are not provided here due to space constraints, we have also observed once again, for this wider area, that aggregating contiguous channels very quickly leads to the performances of the different spectrum mask classes being indistinguishable. For the Mobile Broadband Downlink scenario, aggregating only 3 or more contiguous channels makes the results generally indistinguishable. Moreover, in other work, we have shown that aggregating any number of contiguous channels under the Indoor Broadband Provisioning parameters leads to identical results (see, e.g., [42]). This observation again has profound implications for the design of WSDs. A manufacturer who wants to design a WSD under the Mobile Broadband Downlink scenario or similarly as a base station, need not be concerned with stringent spectrum mask requirements if it is aggregating 3 or more contiguous channels (only needing to satisfy Class 5). A manufacturer of indoor broadband, Wi-Fi or other such low power equipment need only design to the Class 5 specification of equipment, with virtually no gain being realised in achieving better class especially if the intention is to aggregate contiguous channels.

7.8 Achievements

This section has presented work on aggregation in TVWS. As well as a brief description of the architecture towards such aggregation, compliant with [42] and the later extended work in Section 9.2, it has presented some pioneering results on what is achievable in TVWS through aggregation, and fundamental observations on aggregation of discontiguous and contiguous channels affecting aspects such as RF design of devices, among other observations. This work has been one part of a pioneering pilot of white space technology within the Ofcom TVWSs Pilot in the UK, and has been presented in a number of high profile events and conference settings.

8. LTE (Licensed) + WiFi (Unlicensed)

8.1 Overview

As an alternative to the LTE-U scenario described in Section 6, operators and also the 3GPP is working on a tighter integration between LTE and WiFi without modifying the actual access technology. It is already possible to integrate WiFi into an LTE core network, but there is no seamless service handover between the two. In 3GPP Rel13 a study item on LTE-WLAN Radio Level Integration and Interworking Enhancement has been proposed that studies the possibility of aggregation of LTE and WiFi at the level of PDCP, while keeping the MAC and the PHY layer of WiFi “as is”.

8.2 Stochastic analysis of two-tier HetNets

In SOLDER we study the benefits of this scenario from a system level perspective using closed form expressions, thus avoiding averaging problems and complex system-level simulations. The methodology is based on two main analytical tools (stochastic geometry and queuing theory) as well as appropriate abstraction of different radio access technologies.
In a first work (see Appendix 8.1) we developed a flexible and accurate model in order to analyse the performance of heterogeneous cellular networks (HetNets). As performance metric we chose the average user rate. The model consist randomly located Base Stations

(both eNodeBs and WiFi's AP), with different densities, transmit powers and Radio Access Technologies (RATs). Also, the users are assumed saturated (or with infinite demands/requirements).
The proposed model provides a performance analysis of such those networks and different users' association schemes between them. Novel elements of this work are the probabilistic approach to model network topologies and the number of associated users by stochastic geometry as well as the realistic modelling of different radio access techniques, in order to calculate the rate, instead of Shannon's law, which is problematic in the case of HetNets. The results and methodology can be easily extended to other types of networks. The detailed analysis and the results could be found in Appendix 8.1.

8.3 Flow-level performance analysis of two-tier HetNets

In a second work (see Appendix 8.2) we generalised the aforementioned to K-tiers HetNets, additionally, we extend it for non-saturated users in order to provide an analytical model for flow-level performance in HetNets. Our performance metric are the median user's delay and the congestion probability of the arbitrary BS.
To achieve this, we base our analysis on two main tools: (a) stochastic geometry, to understand the impact of topological randomness and intra- and inter-tier interaction in resulting coverage area, and (b) queueing theory, to model the competition between concurrent flows within the same BS, for each RAT. For this part, modelling the RAT scheduler with the proper queue was mandatory. We apply our model to the case of the 2-tier HetNet of interest, based on LTE and WiFi, in order to further understand the performance differences of popular user association criteria, such as, offload, max SINR association, and load base association. Our results provide some interesting qualitative and quantitative insights about the impact of these association policies and different traffic intensities. The detailed analysis and the results could be found in Appendix 8.2.
Those two works modelled properly the PHY and MAC layer for our cases of interest and examine all users' cases of Scenario 0 (cf D3.1, Section8.1). We are ready to extend our study taking into account CA technology.

8.4 Achievements

We developed evaluation methodology and analytical tools to analyse the performance of two-tier HetNets composed of WiFi and LTE. These results allow us to find the best policies to aggregate these two networks.

9. Wifi (UnLicensed) + LTE (TVWS)

9.1 Overview

This section details solutions for the aggregation of WiFi in conventional unlicensed spectrum with LTE in TVWS.

As highlighted in other SOLDER Deliverables, e.g., D2.3 [41] and D4.1 [47], the primary solution for this aggregation scenario is based on higher layers. As an aspirational objective, this scenario hopes to push down towards opportunities for implementation at the MAC layer, however, such implementation is often not possible simply because WiFi (unlicensed) and LTE (TVWS) are different/independent systems operating in different bands. The maximum extent of possible aggregation at lower layers in such cases could potentially, for example, be a joint scheduling scheme or adaptation at the MAC to schedule better across the systems/bands. Of course, if the systems are coordinated and operating in the same spectrum,

such lower-layer aggregation is possible—as already covered in Section 11 of this Deliverable.

One key aspect of aggregation is its management, i.e., which resources should be aggregated in order to achieve the given traffic demand, also considering resources on a system level. Aggregation among similar systems or different instances of the same type of system at lower layers will often imply management of the aggregation (e.g., matching of traffic demands to the resource that must be used/aggregated) already being present in the overall aggregation solution, thereby not requiring a management architecture to be abstracted out—even though a mapping of overall higher-layer management to the layers of a given system, e.g., LTE, is possible as illustrated in D2.3. If aggregation is done at higher layers, however, an aggregation management solution is more sensible/viable, as also illustrated in D2.3. In such cases, the lower layer systems will inherently be operating (mostly, if not entirely) independently, not communicating with each other to map traffic to aggregated resource in the best way among them. A higher layer of management will therefore be necessary to address such tasks.

In the light of the above, Section 9.2, addresses the expansion of the management architecture for aggregation, first presented in D2.3, to the case where the functionalities are performed in (or extended from) geolocation databases. It is noted that this can also be generally applied to almost any case where TVWS is involved in the aggregation, or in likely future database-driven spectrum management scenarios that involve aggregation built on concepts such as TVWS and LSA, for example.

In Section 9.3, this section also addresses the higher-layer solution supporting aggregation of WiFi in unlicensed spectrum with LTE (MBMS) broadcast. However, it is noted that the solution presented, which heavily builds on packet-level fountain coding, can also be generally applied to aggregation involving any IP-based packet broadcast technology (without feedback) with any IP-based unicast (which does have feedback, for congestion control, and packet retransmission purposes). It is further noted that the proposed concept, with minor adaptations, might be applied at an integrated MAC layer of the broadcast/unicast technologies, where the broadcast has no feedback (e.g., as in DVB-T, for example) and the unicast does have feedback (e.g., as in ARQ—even if there is not an unlimited number of retransmission attempts of a packet). Further, these assumptions on the reliability of the underlying broadcast and unicast system do not preclude the use of such a higher-layer packet-level fountain coding-based aggregation solution, they merely affect the efficiency with which such a solution would operate as presented in its current form.

9.2 An Example Expansion of the Management Architecture Presented towards Geolocation Databases

First concentrating on such an integrated management solution, one promising basis for this, building on the architecture that has been introduced in D2.3, is the geolocation database architecture as implemented in TVWS and worked with extensively by KCL, e.g., in implementing white space devices to participate in the Ofcom TVWSs Pilot. This can be naturally extended to be also applicable to resource and aggregation management purposes. Hence, the concept and use of such a solution can apply to the TVWS-only aggregation work highlighted in Section 10, as well as to any aggregation management solution that incorporates TVWS as one the types of spectrum that is being aggregated.

First, the reasoning for the architecture and its geolocation database-basis is given as follows. There have been extremely positive moves in the US, UK, Japan, Singapore, Kenya, South Africa, Tanzania, India, and elsewhere, towards opportunistic/localized sharing of white space, particularly TVWS (see, e.g., [37], [38], and Appendix 9.2). These moves have

underpinned the realisation that geolocation databases, in some cases assisted by local and standardised/reliable sensing mechanisms, can be practical solutions to unlock spectrum for opportunistic usage. Further moves are underlining such approaches. For example, the 3.5 GHz tiered spectrum access “innovation band” in the US is based on a “Spectrum Access System” (essentially, databases or similar such cloud-implemented functionalities) supported by sensing [39]. And LSA approaches proposed in Europe, currently for spectrum sharing between mobile operators although eventually a lot wider than that, are key capabilities broadly also based on a database system that informs when/where the spectrum can be used by another operator, based on an agreement with the incumbent operator and a license (along with QoS guarantess) being awarded to the incoming/opportunistic operator [40]. Although this approach generally has far less dynamicity than others such as TVWS and in the 3.5 GHz innovation band, the licensing of the opportunistic operator and associated QoS guarantees for that operator are a beneficial trait.

Typically, database-based opportunistic secondary spectrum access systems do not resolve how the devices that are opportunistically using locally-unused spectrum will coexist, noting that there is significant potential for interference among these devices hence uncertainty in the quality of the spectrum they will see—particularly in TVWS. Such uncertainty must be resolved in order for some challenging 5G applications—such as Machine-to-Machine and the Internet of Things—to be realised with sufficient reliability of communication, and indeed to achieve the proposed “five-nines” reliability for 5G. Such a database system, in a 5G context, could be used to also manage the interference among the opportunistic devices, where it is noted that the UK/EU TVWS framework, for example, is already capable of that should it be required, only with changes to the calculations implemented in databases being necessary. Moreover, such a database system, with exactly the same messaging procedures and with small additions to the inherent information structures in communication between the white space devices and the deolocation databases, can inherently deal with aggregation—e.g., allocating resources among systems with aggregation in mind, with the context information that is already being transferred from the white space devices to the geolocation databases be enhanced to include such information as the aggregation capabilities of the white space devices (not only in TVWS, but also among other bands), and the decisions of the databases being enhanced to also convey information not only information on which resources can be used, but also information on which resources should (or must) be used and aggregated.

In addition to the above, it is noted that usage of unlicensed spectrum in general is typically very disorganised, and far better efficiency could be extracted from it through spectrum usage coordination among the unlicensed devices. Currently, mostly by chance of market dominance by a certain family of standards [48], the situation is less severe in 2.4 GHz ISM and 5GHz U-NII bands through the common use of Carrier-Sense Multiple Access (CSMA) interference avoidance schemes. Coordination of access among the 5G systems and devices that are accessing general (i.e., non-TVWS) unlicensed spectrum should also be sought, which for enhanced management purposes should be done by an integrated mechanism. The geolocation database approach of TVWS provides a good basis on which also to do this, providing the necessary tools to achieve resource usage management of unlicensed devices themselves, not only in TVWS, but also in conventional unlicensed bands. This coordination could be achieved by either the same database(s) that are operating in a trusted form under the certification of the regulator (as in TVWS), or another database that does not need to be trusted as there are no legal implications if mistakes are made in unlicensed spectrum (as long as the decisions and effects stay within the scope of the unlicensed spectrum and associated band rules). It is important to note, however, that such an untrusted geolocation database cannot be responsible for management of opportunistic secondary spectrum access as would have to be implemented by the regulator or qualified by the regulator, or for sharing among licensed users.

Using TVWS databases and the Ofcom TVWS Pilot in the UK as one pertinent example, a key observation is that the geolocation databases and the entire underlying framework are seen as a baseline that can used and extended to a range of forms of opportunistic spectrum access, also in other bands, and more generally for the imposition by the regulator of locally-optimised regulations based on geolocation and other (e.g., technical) information. This is essentially what the geolocation databases already do in a simple form in the TVWS case, varying the allowed power on a per-channel basis for each given location. The key is that to allow opportunistic secondary spectrum access, the regulator has to be involved and the geolocation databases and framework are a good automated model one to take forward the concept with the involvement of the regulator. Moreover, as has been borne out in the LSA case for example, it can even be necessary (or even beneficial) for the regulator to be involved in cases where there is a direct agreement between the incumbent spectrum user and the opportunistic user. Given all of the above, geolocation database functionality must either exist within the regulator, or be approved by the regulator and implemented by a trusted party. However, in the UK TVWS case, for example, some geolocation database calculations are done solely at the regulator for information privacy reasons, and some more computationally challenging ones (e.g., protection of PMSE services) are done by the trusted database outside of the regulator's scope. Hence, in this particular case, the workload is split between the regulatory and the (trusted) non-regulatory domains, and geolocation databases exist in both domains.

Given such observations on the capabilities of geolocation databases, it is suggested here that such an integrated system for spectrum coordination and resource allocation, taking into account the possibility to aggregating dispersed and heterogeneous resources, is based on them. This is due to: (i) the need to involve the regulator and coordinate heterogeneous spectrum usage/sharing (in accordance with needs to aggregate resources to satisfy traffic demands) in a way that the regulator can trust, (ii) the establishment and trialling of them in various contexts (e.g., TVWS, LSA and others) and likely further building on such concepts in regulatory and other circles, and (iii) the advancement of such approaches (e.g., LSA) to support mobile communications cases. Moreover, it is suggested that these databases should be of three forms: (i) a form of database in the presence of and run by the regulator, (ii) a form of database trusted and likely certified by the regulator but existing and being run outside of the scope of the regulator, and (iii) a final (optional) form of database that is untrusted, and existing and being run outside of the regulator.

9.2.1 Example High-Level Architectural View

In view of the observations in previous sections, an initial potential viewpoint on the architecture for such a management system is given in Figure 46. The geolocation databases within this architecture are depicted with a green background. They first comprise a Regulatory Geolocation Database (RGD), operating within the scope of the regulator. This is because it is essential that some information originates and stays only within that scope, and there may be privacy or other concerns that limit certain calculations to only being done inside of that scope, as described in the prior section (see also, e.g., [49]). Outside of the regulator's scope there are the Trusted Non-regulatory Geolocation Database (T-NGD) and Un-trusted Non-regulatory Geolocation Database (U-NGD). These entities take the complexity of more advanced resource sharing calculations out of the regulator's direct implementation. The T-NGD serves cases where a very high guarantee of the result of the calculations or other trustworthiness is necessary, for reasons as described in the prior section (see also, e.g., [49]). The U-NGD may be able to handle cases where no guarantee of trustworthiness or reliability is necessary, e.g., in unlicensed spectrum should a number of unlicensed terminals choose to operate under the control of such a database but where if the database makes an error, for example, no liability implications will result. It is useful to have a separate

such entity, as there is a large overhead in managing a T-NGD, including achieving certification by the regulator, and also associated implied workload at the regulator. Hence, there will be a practical limit on the number of T-NGDs that can be deployed.

Certain aspects of this proposal placed within a generalized mobile network are also depicted, strongly inspired by an author's prior work on and experience of the IEEE 1900.4 heterogeneous network/resource management standard [50] and reflected/expanded from the architecture presented in D2.3 [41]. This is with a pink background in Figure 46. Here, there are entities on both the network side (NRM) and terminal side (TRM) that deal with management through policies (the network side having overall control, but leaving some aspects for terminal TRM local decisions through the policies the NRM creates). On both sides, there are also entities that implement/enforce decisions (NRC and TRC), and obtain context information to feed back to the NRM and TRM (NRIC and TRIC) to assist in making the correct decisions based on the situation. There are of course separate RANs, for which decisions must be made and through which signalling between the network side and terminal side may take place. Further, there may be a separate signalling carrier operating outside of the mobile network, also depicted in Figure 46.

The terminals/devices operating within the unlicensed domain are illustrated with a blue background in Figure 46. Importantly, they will generally interact with the U-NGD, which could manage aspects such as better coordination of their unlicensed spectrum usages, taking into account the resource requirements of the devices and also the capabilities of the devices to aggregate resources. Further, the T-NGD might also manage this domain, e.g., should it wish to pair licensed and unlicensed resource usages such as is currently done in LTE-U/LAA or example.

It is noted that as well as managing allowed spectrum access in the sense of avoiding interference with incumbents, spectrum access among the secondary/opportunistic spectrum users might also be managed. In an advanced implementation scenario, this can take into account the resource requirements of the secondary/opportunistic users and allocate the spectrum accordingly, also taking into account the bandwidths that devices will need and the need to aggregate resources (e.g., channels) to achieve necessary capacity. Further, under an even more advanced scenario, such a database could play the role of pairing devices and their traffic requirements with link opportunities that are available in local areas, including the optimal allocation of which opportunities should be aggregated to achieve requirements.

Far more information on this architecture, including aspects such as signalling between the various elements, is provided in [51], [52], [53].

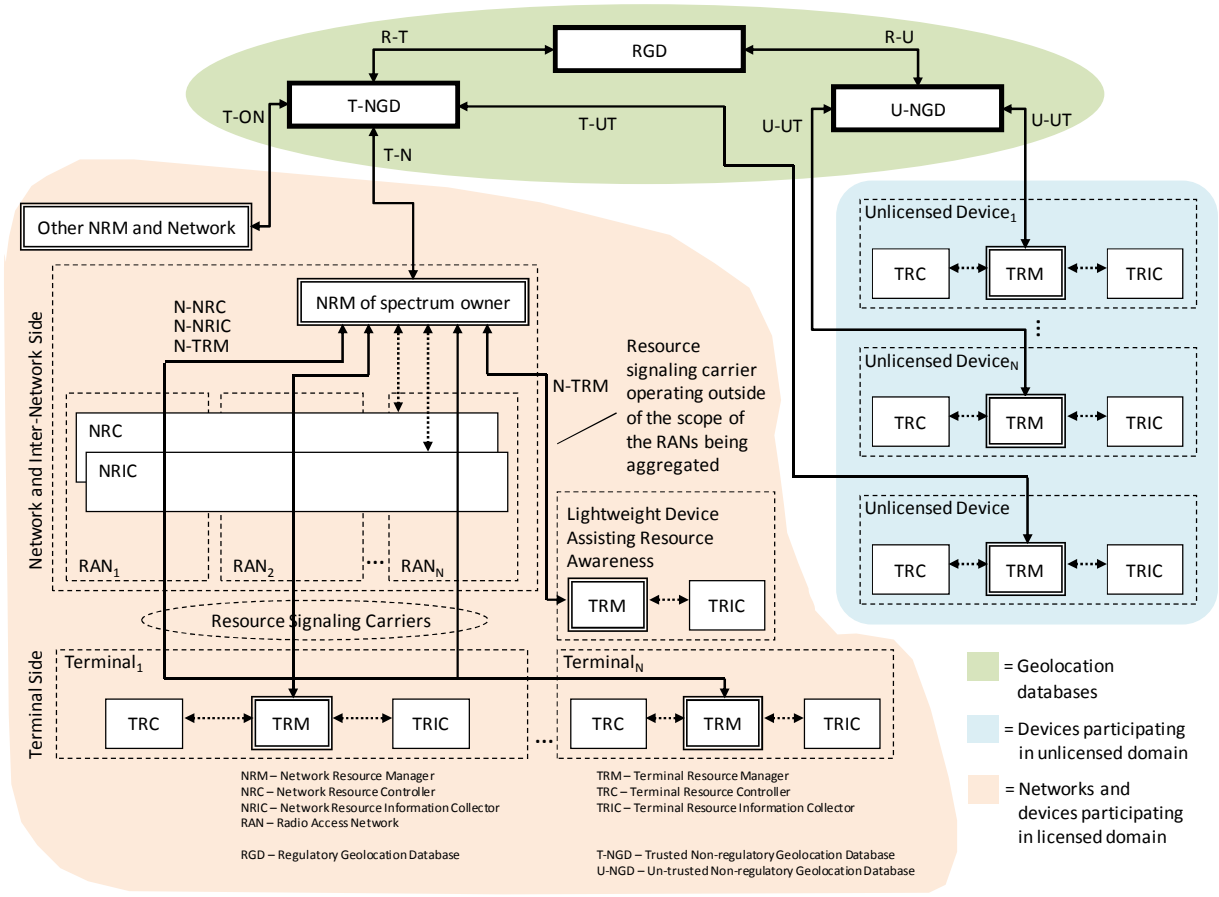

Figure 46: Example of the form that such a geolocation database-based architecture might take.

9.3 Aggregation Implementation Specifics

Regarding the initial work on the implementation aspects at the network layer and above, there are two key issues to consider: (i) coding support for the implementation, and (ii) link aggregation/bonding at the network or higher layers Although point (ii) can be implemented at lower (e.g., transport) layer with greater efficiency, it is of lesser importance and can generally easily be dealt with at the applications layer. Hence, we particularly concentrate on coding support here.

Coding support is necessary such that all information that is received over either of the interfaces (LTE TVWS or WiFi Unlicensed) is useful bearing in mind aspects such as the different (and varying) rates that information can be sent over the interfaces. Each of the WiFi flows to receivers will be operating at a different (and varying) rate, and the broadcast itself will also be operating at its own individual rate. Moreover, there is no guarantee that the packets sent over broadcast will be successful, as there is no feedback in this case to confirm their success, hence no retransmission of lost packets on the link level. In this context, packets that are transmitted over the broadcast will be useful to only a subset of the receivers, as some of them will have received them already over the WiFi interface. However, if a coded packet coded with an appropriate coding scheme is broadcast, then that packet is guaranteed to use useful to all receivers that have not already finished the file download. This underlines why a higher-layer (e.g., packet-level) coding scheme is essential to efficiently realise this aggregation scenario.

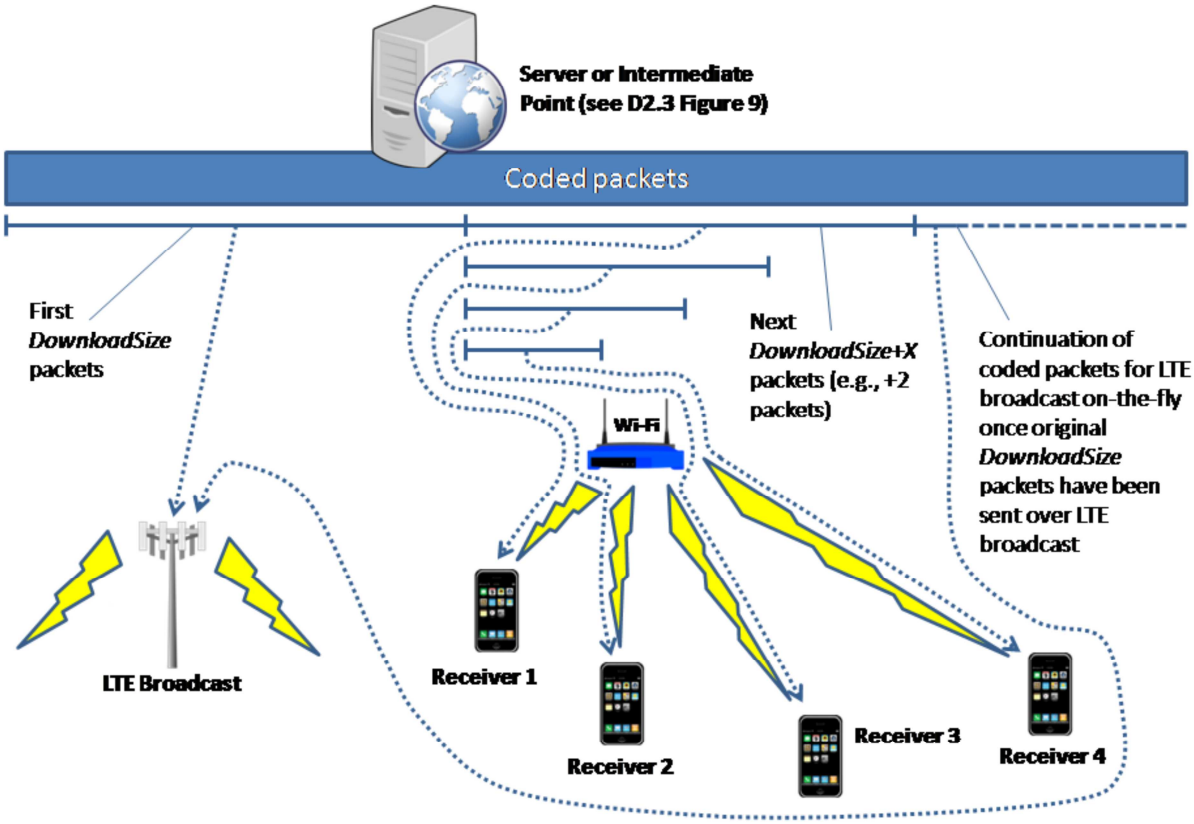

Figure 47: Mapping of fountain-coded packets to LTE Broadcast and Wi-Fi transmissions (non-systematic coding case) for different receivers of the aggregated software download.

There are a number of applications that can be mapped to this scenario, including large-scale downloads (e.g., mass-upgrades of operating systems) and layered video (e.g., enhanced resolution, or enhanced video information provisioning when a WiFi connection is available). We concentrate on the large-scale downloads cases initially here first. In this scenario, the challenge identified in the paragraph above can be addressed by coding the dataset with a form of fountain codes such as RaptorQ codes at the application layer [54], [55], typically (although not by necessity—larger coding symbols are possible) coding at the packet-level (e.g., one packet is equal to one coded symbol) to produce coded packets of the software download. This way, very large numbers of different sets of coded packets can be forwarded to the two interfaces (LTE broadcast and WiFi, in our case) and previously unused coded packets can always be transmitted and hence will always be useful. In the case of a file transfer, the *n*-packet file can typically be reconstructed from coded information as soon as slightly more than *n* coded packets have been received; in the case of RaptorQ codes, a 99.9999% decoding success rate is possible as soon as *n*+2 symbols (packets) is successfully received, irrespective of the number of symbols (packets) in the file or the loss model. Moreover, coded packets can continue being produced almost limitlessly, on-the-fly, sent as needed over the various interfaces with each transmitted packet being useful and never being a repetition. This is otherwise difficult to achieve in the multicast/broadcast case, as indicated in the above.

Using RaptorQ codes and given these above observations, Figure 47 depicts how the coded packets are mapped to the LTE broadcast and WiFi interfaces. This is assuming the entire download is coded as a single source block; in the case of RaptorQ codes this is realistic, as source blocks of up to 3.4 GB are supported (but please note that the decoding memory size

is also a key consideration here [54], [55]). Further, the case presented here is for the example of non-systematic coding; in the systematic case, the original (uncoded) download packets could be sent over the WiFi interfaces. Here, the service will send the first *DownloadSize* coded packets over LTE broadcast, then reserve and send in parallel to receivers the next *DownloadSize*+2 packets over WiFi unicast sockets. Just these 2 additional coded packets lead to only a 10^{-6} chance of failure to decode [54] should the receiver receive the packets entirely via WiFi, e.g., in supporting the extreme case where there is an infinitely better data/success rate over Wi-Fi compared with the LTE broadcast to a receiver, or perhaps the case where broadcast is not locally available. Once the *DownloadSize* packets have been sent over LTE broadcast, the LTE broadcast will continue from packet 2**DownloadSize*+3, sending coded packets on-the-fly. In parallel, the Wi-Fi sockets will keep transmitting their packet sets to users as requested by the users (clients). The application at each receiver will continually monitor the number of packets it has successfully received, then will start attempting to decode the download once it has received *DownloadSize* packets over the LTE and WiFi interfaces combined. Upon attempting to decode at *DownloadSize* received packets, there will be a 10^{-2} chance of failure. Upon attempting to decode at *DownloadSize*+1 received packets, there will be a 10^{-4} chance of failure. Upon attempting to decode at *DownloadSize*+2 received packets, there will be a 10^{-6} chance of failure [54]. The choice of number of received packets of the download at which decoding is attempted first depends on the weighting of the importance of (unnecessary) processing load, e.g., in decoding for those rare attempts in which the decoding fails, against (unnecessary) communications in transmitting/receiving additional packets. However, it is anticipated that for most likely scenarios in terms of achievable data rates of the WiFi and LTE systems, capabilities of the terminals, and characteristics and urgency of the download, it is far more likely to be preferable to wait to receive the 2 extra packets to guarantee the download (with only 10^{-6} failure probability), rather than attempting to decode early.

As soon as decoding is successfully completed, the receiver will terminate the WiFi socket and stop listening to the LTE Broadcast. The LTE broadcast will continue being transmitted, however, until it is certain that all receivers have received the broadcast, or it is thought not necessary to continue. If a feedback mechanism or other confirmation could be provided (e.g., through other communication at the application layer), then the LTE broadcast could be stopped as soon as it is confirmed that a sufficient number of receivers have received the download.

9.3.1 Use of WiFi for Feedback

A key challenge in this aggregation scenario is that it can be difficult to set the modulation and coding correctly in the LTE broadcast based on the positions of the receivers hence the signal level they will receive. In such a one-to-many transmission, there is a trade-off between catering for the worst-placed receiver hence causing a reduction to the other better channel quality receivers by lowering the modulation and/or increasing coding for that receiver, and neglecting worst-placed receivers in order to achieve a higher rate at other receivers. Moreover, in a broadcast, where there is conventionally no feedback to the transmitter, there is no knowledge on the channel quality that receivers may be obtaining, thereby not allowing feedback on channel quality hence the ability to adapt to that.

In addition to providing enhanced capacity through aggregation, through the use of WiFi links in this aggregation scenario it is possible to provide feedback on channel qualities that the receivers are seeing, and to optimise the modulation and coding of the broadcast accordingly. This could be through the WiFi providing a feedback packet on success of the broadcast every given number of packets, e.g., likely in a per-packet bitmapped form if the purpose is to assist multi-block downloads (see, e.g., [49]), or through direct information on the signal quality (e.g., SINR seen) being fed back to the transmitter. Additionally, if such feedback is pro-

vided, it facilitates implementation of the coding of the download to be across multiple blocks—which will likely still be beneficial as an option for large downloads in order to address encoding/decoding memory space issues, of if downloads are larger than the capabilities of RaptopQ codes.

The challenge if a broadcast is across multiple blocks is that the source of the download does not know whether all receivers have successfully received a block, hence, doesn't know when it is appropriate to move to transmission of coded packets on the next block instead of continually sending coding packets for the current block. If there is a record of receivers per-packet and/or per-block success status, e.g., through WiFi feedback/signalling, then the source will know when it makes sense to start moving to the next (or a next-most appropriate) block in the download. Note that the next-most appropriate block to broadcast coded packets for will be the block for which receivers have received the fewest number of packets on average. Counter-intuitively, with the WiFi progressing sequentially through the blocks of the download, the broadcast should therefore start from the last block of the download, and (initially at least) count backwards through the blocks of the download that it transmits packets for.

Based on this, the source would following this procedure:

1) Keep broadcasting coded packets on the current block until a counter is reached.
    - In parallel with this, send coded packets over WiFI for whichever block that receivers have requested (in almost always all conceivable cases this would be a sequential progression through the download, although taking into account point (3) below).
2) Based on the feedback received from receivers ideally per-packet (e.g., in a bit-mapped form for each block [49]), begin transmitting on the next appropriate block for which the least number of packets have been received on average among the receiver set.
    - If this number of packets received on average is the same among a number of the blocks, it is always best to move to the next block with that received number of the highest index (i.e., closest to the end of the download) in order to minimise the probability that the WiFi transmission for any receiver "catches up" and completes to the block currently being transmitted by the broadcast before the broadcast block reassessment counter is triggered (thereby making one of more of the broadcast packets unusable).
3) In tandem with receiving the WiFi transmissions, each receiver will monitor received packets for the current block in a common receive queue (also taking into account the received broadcast packets, if the broadcast is currently being transmitted in the same block), and will attempt decoding once n_b+X (n_b is the number of packets in the block, X could typically be 2 although depends again on processing capabilities, characteristics of the download, transmission rates and the block size) packets have been received, continually receiving packets until the decode is successful. The receiver side will not have any context information on the success of various packets/blocks at other receivers, hence in this case, it is not capable of attempting to estimate the next-best block to start receiving based on the broadcast's expected choices of block. The best estimate of next block to start receiving the WiFi on, in this "blind" receiver case is simply the next sequential block in the download, i.e., progressing in the opposite order to the broadcast's transmission of blocks.

Further work on these scenarios, including the consideration of the layered video traffic case as well as the presentation of results from this scenario, is expected to be undertaken in D3.3 and D4.2.

9.4 Achievements

This section has covered a first complete solution for the aggregation of WiFi in unlicensed spectrum with LTE in TVWS. It has also covered an optional but extremely useful case for aggregation management involving geolocation databases such as already present in TVWS. Moreover, it is noted that the solutions that are presented can easily be extended or in some cases directly applied to scenarios that involve TVWS or another futuristic geolocation database-based spectrum management solutions in the spectrum that is being aggregated, as well as any case where an unreliable IP packet-based broadcast technology is being aggregated with a reliable IP packet-based unicast technology. Further, it is noted that the reliability of the aforementioned broadcast and unicast don't preclude the use of the solutions presented in this section (particularly in Section 9.3) of this deliverable, they merely affect the efficiency of the presented solutions in their current form. The presented solutions can be further optimised should different assumptions on the reliability of broadcast and unicast, or other potential one-to-many data distribution systems, be used.

The solutions presented in this section are novel and highly-practical, e.g., in terms of their alignment with regulatory directions and standards directions in the development of systems. This practicality also serves towards their wide applicability.

10. 5G waveform (Licensed) + 5G waveform (Licensed)

10.1 Overview

In this section, we are considering FBMC PHY layer as a candidate for intra band CA. We have identified in D3.1 [56] the issues that arise when realistic transmitter front-end are taken into account. FBMC good spectral containment is a key enabling property but it requires digital techniques and digital estimation/compensation. In this deliverable we first propose a new and efficient calibration technique to compensate for radiofrequency (RF) impairments due to unavoidable ExpressMIMO2 non-idealities. Then, we address the problem of the PAPR reduction of FBMC signals. We propose two different and new approaches according to the fact that the signal to be transmitted is contiguous or non-contiguous in the frequency domain.

The work presented in this section was subject to the submission of 4 different pers [57], [58], [59] and [60]. The corresponding papers could be respectively found in Appendix 10.1, 10.2, 10.3 and 10.4.

10.2 RF impairments compensation

The ExpressMIMO2 platform uses direct-conversion (or Zero-IF) architecture for the frequency transposition. This architecture has the great advantage of lowering the number of components, decreasing the power consumption and having a small form factor. Nevertheless, Zero-IF is subjected to many drawbacks namely IQ imbalance and DC leakage. These imperfections are particularly harmful when a linearization technique has to be developed and can completely cancel out its capability. For this reason, we propose a fully digital calibration procedure to counteract the IQ imbalance and DC leakage effects.

Direct conversion, is the natural approach to upconverting (Figure 48) and downconverting (Figure 49) a signal from baseband to RF, and RF to baseband [61]. Direct conversion translates the band of interest directly to zero frequency or RF thanks to IQ modulator and demodulator, and employs low-pass filtering to suppress nearby interferers. The quadrature I and Q channels are necessary in typical phase and frequency modulated signals because

the two sidebands of the RF spectrum contain different information and result in irreversible corruption if they overlap each other without being separated into two phases.

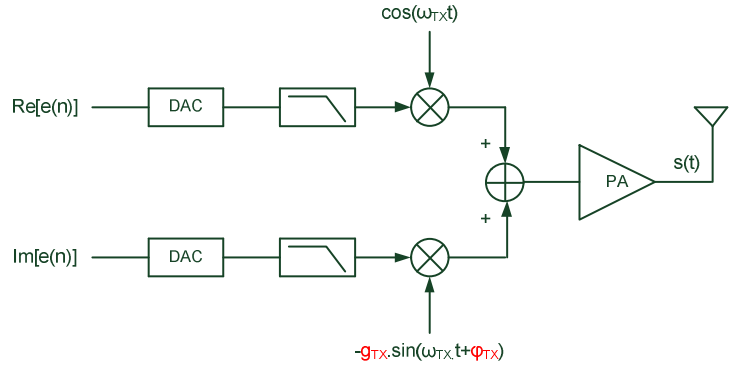

Figure 48: Zero-IF transmitter architecture impaired by IQ imbalance, g_{TX} and φ_{TX} respectively refers to the gain and phase imbalance.

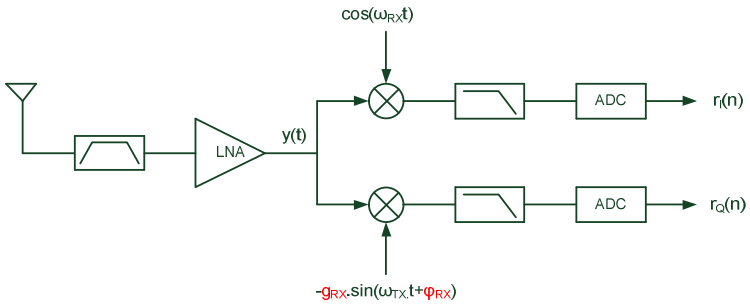

Figure 49: Zero-IF receiver architecture impaired by IQ imbalance, g_{RX} and φ_{RX} respectively refers to the gain and phase imbalance.

The IQ imbalance refers to the loss of quadrature between I and Q paths, and can be either in amplitude or in phase, and usually both. This quadrature loss is due to different phenomenons:

- It is very difficult to generate two local oscillators that are perfectly in quadrature, especially for high frequency. Moreover, the lines that connect the local oscillator with the mixer shall have exactly the same length between I and Q paths. If there is a length difference, a phase imbalance (φ_{TX}, φ_{RX}) between I and Q appears.
- The conversion gain of I and Q mixers and the variable gain amplificators shall have exactly the same level. If there is a gain difference (g_{TX}, g_{RX}), a gain imbalance between I and Q appears

Direct conversion architecture suffers also from another drawback called DC-Offset:

- The DC-Offset at the transmitter (DC_{TX}) side is also called “Carrier leakage”. It is due to the fact the mixers isolation between the ports is not perfect: there is leakages of the local oscillator that pass through the mixers are appears at their output. The digital to analog converters can also generate a DC-Offset.
- The DC-Offset at the receiver side (DC_{RX}) is also called “LO-Leakage”. The isolation between the LO port and the inputs of the mixer and the LNA is not perfect, i.e., a finite amount of feedthrough exists from the LO port to the LNA. The leakage signal appearing at the inputs of the LNA and the mixer is now mixed with the LO signal, thus producing a dc component. This phenomenon is called “self-mixing.”

DC-Offset and IQ imbalance have a sequential effect on the signal to be transmitted/received (Figure 51). At the transmitter side, the signal $e(n)$ to be transmitted is first affected by the DC-Offset and then affected by the IQ imbalance of the IQ modulator. At the receiver side, the baseband model $y_{BB}(n)$ of the received signal is first affected by the IQ imbalance of the demodulator and then affected by the DC-Offset.

Figure 50 presents an example of the impact of the IQ imbalance and DC-Offset on the transmitted signal in the case of two aggregated carriers. We can see that the impairments generate spurious, in band and out of band radiations, even if the PA is ideally linear. These effects drastically degrade the linearity of the transmitted signal. By nature, the digital pre-distortion (DPD) is not capable to pre-compensate these sources of non-linearity.

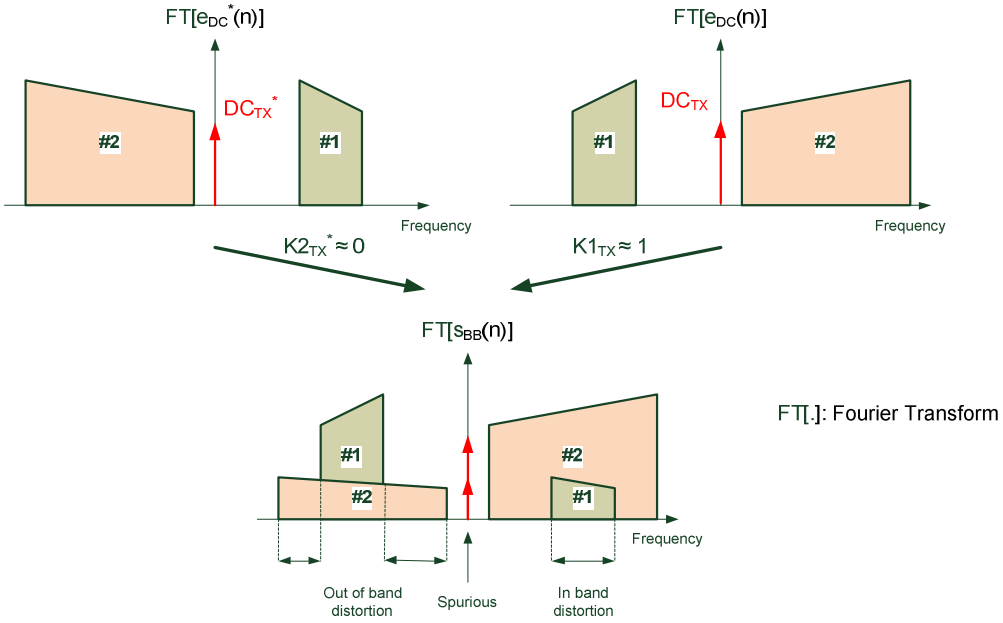

Figure 50: Effects of IQ imbalance and DC-Offset on the transmitted signal. $K1_{TX}$ and $K2_{TX}$ refer to the IQ imbalance model parameters. A perfect quadrature between I and Q paths gives $K1_{TX}$=1 and $K2_{TX}$=0.

In SOLDER, we use the receiver path as a feedback loop for DPD computation. At the receiver side, the IQ imbalance and the DC-Offset degrade the downconverted spectrum in a similar way, i.e. spurious, in band and out of band radiation are generated. In order to develop an efficient DPD, these non-linear signals shall not be interpreted as PA non linearity by the DPD.

We propose a fully digital calibration procedure to compensate the impairments of the zero-IF architecture used for both the transmitter and feedback loop. The digital compensation block diagram is presented in Figure 51. The basic idea is to digitally pre-compensate the transmitter impairments and post-compensate the feedback loop impairments, in the reverse order of appearance. Hence, the association of the pre-(post) compensation with an impaired IQ modulator (demodulator) gives an ideal IQ modulator (demodulator).

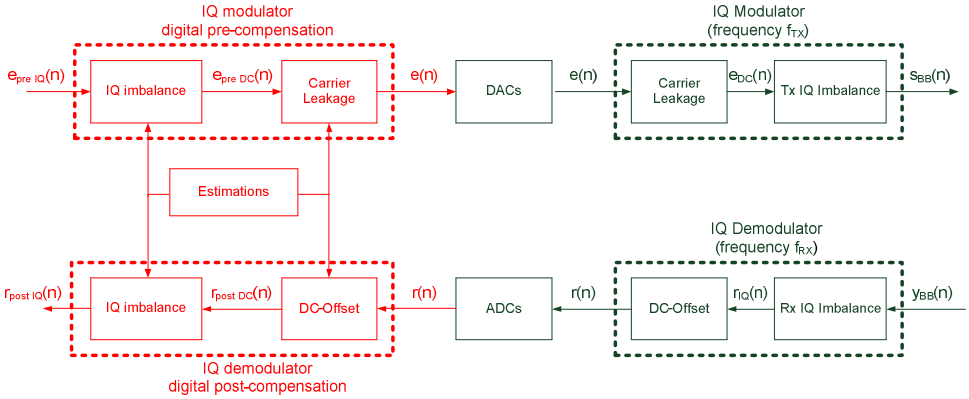

Figure 51: Block diagram of the RF impairments digital pre and post compensations

In comparison with the existing techniques, the proposed procedure used for the parameters identification (Figure 52) has the following advantages:

- **Fast**: the estimation procedure uses a single short calibration signal avoiding long adaptive algorithms such as LMS for example.
- **Exact**: the parameters estimation is unbiased and does not require any approximation.
- **Simple**: the proposed calibration does not require any extra hardware. The only modifications can be summed-up as follows: i) connect the IQ modulator output to the IQ demodulator input, ii) receiver local oscillator frequency has to be slightly shifted w.r.t. transmitter local oscillator.

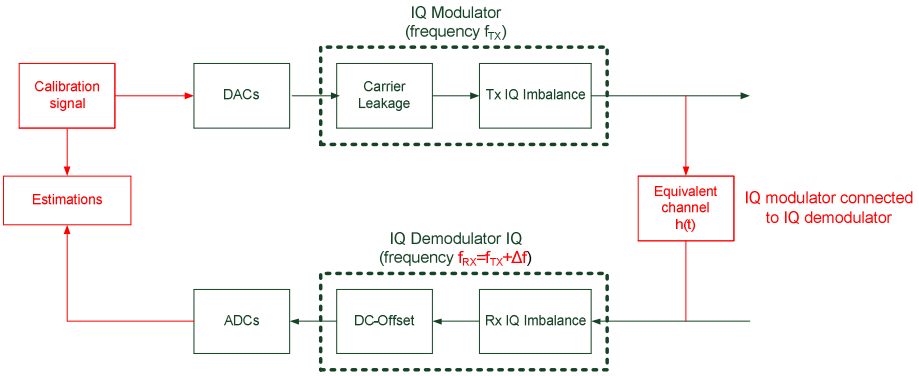

Figure 52: Block diagram of the RF impairments calibration procedure

The time structure of the calibration burst is presented in Figure 53. The first part of the burst is dedicated to the time synchronization (seq_0). Then, two different sequences (seq_1 and seq_2) are transmitted. A cyclic prefix and a cyclic suffix are appended respectively to the beginning and to the end of each sequence in order to perform frequency domain computations and to relax time synchronization procedure. seq_1 and seq_2 are used for the impairments parameters estimation. Note that in order to improve the estimation quality, seq_1 and seq_2 can be repeated N times.

Figure 53: Time structure of the calibration signal

Table 10 gives the simulation parameters used for the simulation of the proposed calibration technique. The impairments levels are set to realistic levels w.r.t. the ExpressMIMO2 platform. Note that the noise floor is supposed to model the ExpressMIMO2 thermal noise, the DACs and DACs quantization noises.

Table 10: Simulation parameters setting

Parameters		Setting
Transmitter Path	Phase Imbalance	$\varphi_{TX} = +5°$
	Gain Imbalance	$g_{TX} = +0.83\ dB$
	Image Rejection	$-23.8\ dBc$
	Carrier Leakage Level	$DC_{TX} = -20\ dBc$
Feedback Loop	Phase Imbalance	$\varphi_{RX} = +3.3°$
	Gain Imbalance	$g_{TX} = -0.43\ dB$
	Image Rejection	$-28.5\ dBc$
	Carrier Leakage Level	$DC_{RX} = -24\ dBc$
Equivalent Channel	Channel Impulse response	$h(n) = e^{j0.3\pi}.[1,0,0,0,0.1]$
	Noise Floor	$-60\ dBc$

The parameters of the proposed algorithm are given in Table 11.

Table 11: Calibration procedure setting

Parameters	Setting
Sampling Frequency	30.72 MHz
seq_1 and seq_2 duration (in samples)	256
Cyclic Prefix duration (in samples)	10
Cyclic Suffix duration (in samples)	10
Normalized frequency shift between the transmitter and the receiver local oscillators ($k_{\Delta f}$)	1 (or 120 kHz)
Normalized frequency spacing between tones of the calibration signal	3 (or 360 kHz)
Number of tones used for estimations	32
seq_1 and seq_2 repetition (N)	10

The impairments are first estimated using the multitone calibration signal presented in Table 11. Then, the estimations are transmitted to the pre and post-compensation blocks (see Figure 51). Finally, the performance of the digital pre and post-compensations are evaluated using a multitone signal that has 16 tones transmitted only on positive index carriers. With the type of signal, it is easy to measure the IQ imbalance rejection observing the image signal that is present on the negative index carriers. DC-Offset rejection performance can also be easily observed since the null carrier is not used.

Figure 54 and Figure 55 present the simulation results of the calibration procedure for respectively the transmitter path and the feedback loop. It can be observed that the IQ imbalance rejections are below -90 dBc, which provide extremely good rejection capabilities. The transmitter DC-Offset is rejected up to a level slightly below -60 dBc, whereas the feedback loop DC-Offset after calibration is well below -120 dBc.

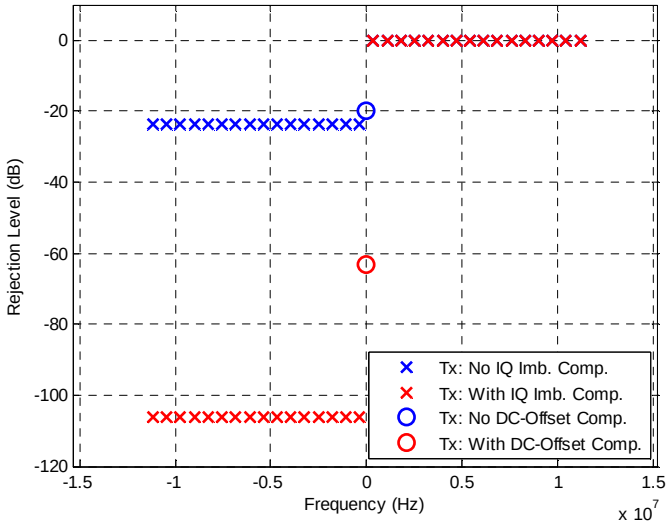

Figure 54: Performance of the calibration procedure on the transmitter path.

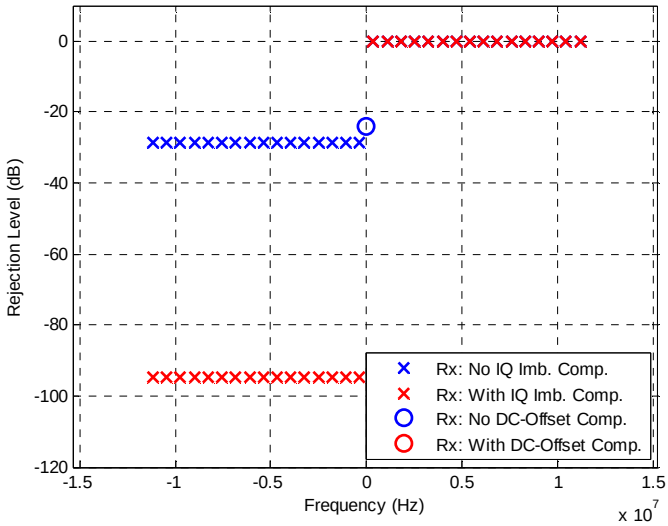

Figure 55: Performance of the calibration procedure on the feedback loop.

10.3 PAPR reduction for FBMC

A major disadvantage of a multicarrier system such as FBMC is the resulting non constant envelope with numerous high power peaks that appear when the independently modulated subcarriers are added coherently. These instantaneous power peaks produce signal excursions into the nonlinear region of operation of the PA at the RF front end, generating distortions and spectral spreading. Therefore in the sequel, we consider methods to reduce these peaks while maintaining the spectral occupation, in order to set the PA's operating point as close to its saturation point as possible.

We propose two different approaches according to the fact that the component carriers are contiguous or non contiguous.

10.3.1 Contiguous case

In this section, we consider a precoding method of peak power control for FBMC signals, using a Filter Bank as a precoder, by analogy to Single Carrier Frequency Division Multiple Access (SC-FDMA), which uses a Discrete Fourier Transform (DFT) precoding for OFDM signals [62]. Since FBMC signals have a better spectral occupation than OFDM signals, they do not need as large guard bands. Therefore we propose also to use that gained spectrum to add excess band and apply spectral shaping to the signal in order to decrease power peaks probability as much as possible.

The filter bank precoding method consists in mimicking the SC-FDMA signal generation used for uplink transmission in LTE where an M-points DFT acts as the precoder, whereas an N-points IDFT refers to the OFDM modulation (M > N) [27]. The DFT precoder can be interpreted as an OFDM demodulator appended before the main OFDM modulator. At the receiver side, the signal is first demodulated thanks to an N-points DFT and then, the signal is recovered by applying the inverse function of the precoder, namely a M-points IDFT. Following a similar approach for FBMC signal, the FBMC modulator and demodulator are referred to an Analysis Filter Bank (AFB) and Synthesis Filter Bank (SFB) respectively. The modulation/demodulation process is supposed to be performed over N subcarriers and the overlapping factor is set to K_N without loss of generality. Thus the FBMC precoding process consists in using a SFB over M subcarriers with an overlap factor of K_M, whereas the signal recovery at the receiver side is assumed by an AFB which has similar settings. The filter bank precoding approach is presented in Figure 56.

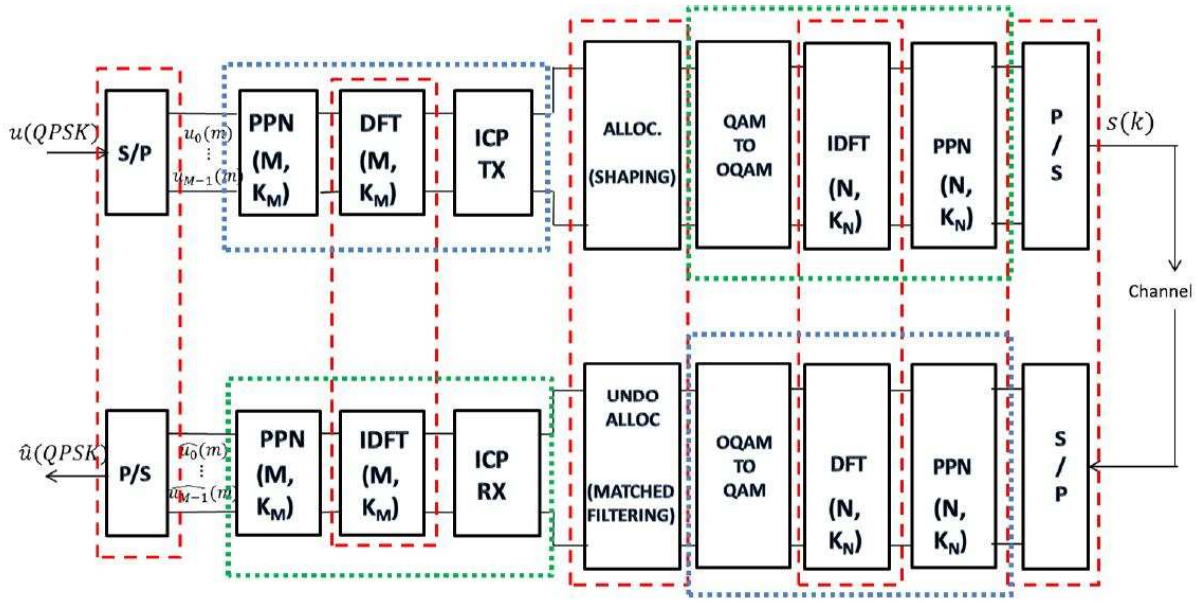

Figure 56: Transmitter and receiver of the Filter Bank FBMC, with in dotted green the SFBs, in dotted blue the AFBs, and in dashed red the blocks shared with SC-FDMA.

It is important to note that the modulator/demodulator overlap factor K_M is chosen independently of the precoder overlap factor K_N. The near perfect reconstruction quality of the FB means however that the precoding AFB will generate interference on the data symbols, which will not be entirely cancelled by the SFB. We have proposed in [58] a formalization of the interference cancellation processing (ICP) necessary to recover the transmitted information.

In order to examine the impact of the overlap factors, we simulate the instantaneous PAPR of a FBMC signal generated using different values of K_N and precoded using different values of K_M. We use the prototype filter proposed in [63], defined for K=3,...,8. We do not consider overlap factors of 1 or 2 since the near-orthogonality condition is no longer respected and data recovery becomes impossible, whether the precoding is used or not. In order to examine the impact of the overlap factors, we simulate the complementary cumulative density function (CCDF) of the PAPR using different values of K_N with K_M fixed to 4 (see Figure 57, left), and also using different values of K_M with K_N fixed to 4 (see Figure 57, right). The modulation used is QPSK for both cases. We can observe that regardless of the values of K_N and K_M picked, the PAPR reduction performances are exactly the same and the PAPR improvement at a probability of 10^{-4} is slightly greater than 3.5 dB.

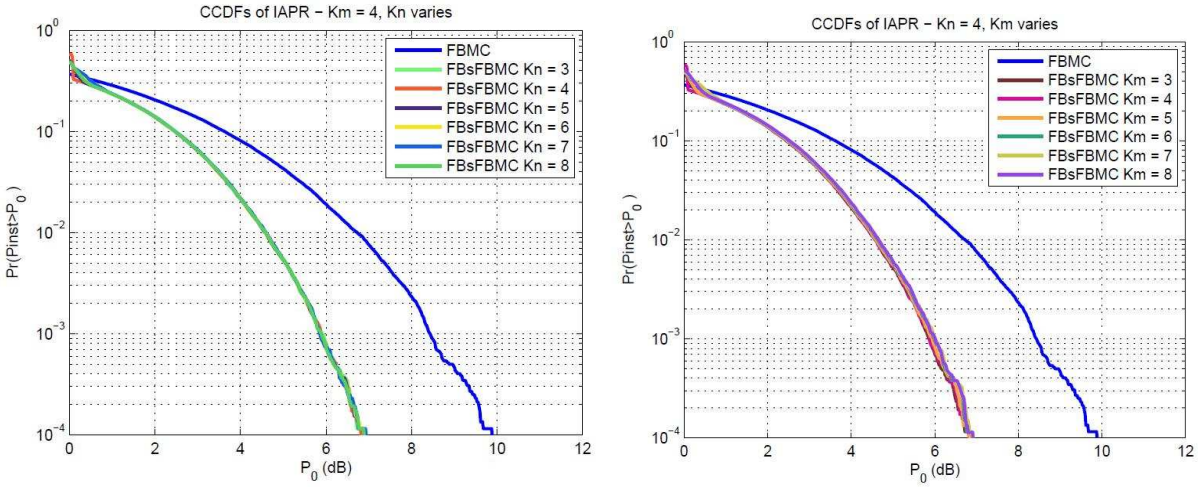

Figure 57: (left) CCDF of PAPR of Filter Bank precoding, (left) with K_M set to 4 and K_N varying from 3 to 8, (right) with K_N set to 4 and K_M varying from 3 to 8. The number of used subcarriers is M=64 over N=256 available subcarriers, QPSK modulation.

Figure 58 presents the impact of the modulation order on the CCDF of PAPR when QPSK, 16QAM and 64QAM modulations are considered. We can observe that the use of QPSK modulation gives the best performance results, whereas the performance of 16QAM and 64QAM modulations almost coincide and are worste by about 1 dB.

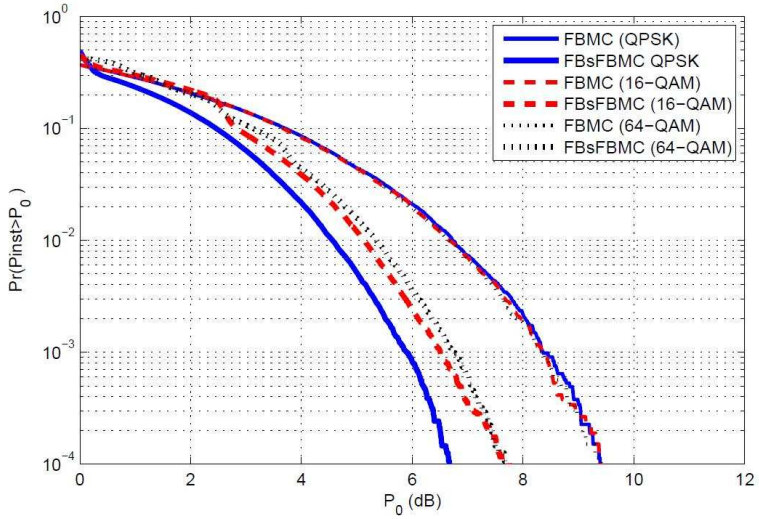

Figure 58: CCDF of PAPR of the FBMC and precoded FBMC signals, for QPSK, 16QAM and 64QAM modulations.

FBMC signals have a better spectral occupation than OFDM signals and they do not need as large guard bands. The spectrum occupation saving of FBMC can be used either to increase the data rate or, as proposed here, to decrease as much as possible the power peak probability provided by the FB precoding. For that purpose, we propose to extend the occupied spectrum from M to D subcarriers instead: the output samples from the precoder are extended to a frequency occupation of D subcarriers (with D>M) through periodic repetition, and a window is applied to them. We are considering three different windows: Raised Cosine (RC), Root Raised Cosine (RRC) and a window designed to provide optimal PAPR reduction for SC-FDMA (OPT) proposed in [64]. In Figure 59 we show the CCDFs comparison of PAPR with and without the windowing process, using QPSK modulation with M = 64, N = 256 and D = 70, i e. an excess bandwidth of about 10%.

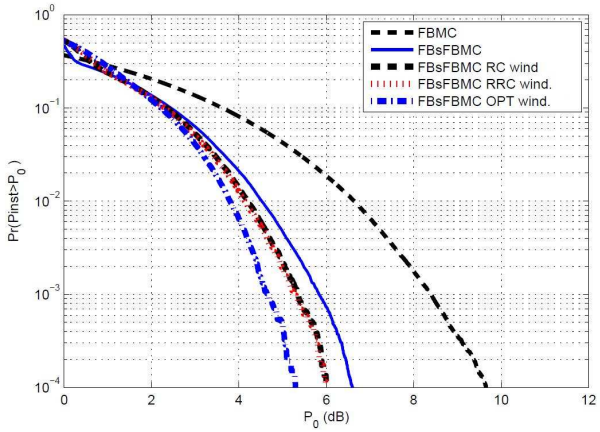

Figure 59: CCDFs comparison of PAPR with and without the windowing process, using QPSK modulation with M = 64, N = 256 and D = 70. The excess bandwidth is about 10%.

At a probability of $10^{-4,}$, the performances improvement of the FB precoding method with excess bandwidth and with RC or RRC windows is about 0.7 dB. For OPT window, the peaks are about 2 dB lower at the same probability. The CCDFs of PAPR of FB precoding with excess bandwidth show a slightly faster decrease than that of FB without excess bandwidth.

We analyse now the impact of the FB precoding on the Bit Error Rate (BER) performances (see Figure 60), considering an Additive White Gaussian Noise (AWGN) channel. At the receiver side, the matched filter is applied to the data for the RRC window case. The data on each (D-M)/2 excess band is then folded back on the regular band in order to benefit from the entire transmitted power in-band. As a consequence, the BER for RRC window is the same as in theory for QPSK modulation, since the matched filter of an RRC window is an RRC window, making the overall transfer function a raised cosine, i e. a Nyquist pulse. This is not the case for RC window since there is no matched filter at the receiver because the Nyquist criterion is applied wholly to the transmitter. Therefore the BER is worse than the theoretical one. However for the OPT window, and as proposed in [29], the data was not recovered by matched filtering. The frequency bins in the excess band were discarded, as recommended in [29], and equalization by the inverse window (in order to recover the data) was applied to the transmission band. Therefore the BER is also worse than theory since part of the transmission power has been discarded. The RRC window BER is indistinguishable from theoretical BER, and therefore is the window that gives the best BER of the three. However if the focus is on improving the PAPR, the window optimized for SC-FDMA is the best choice.

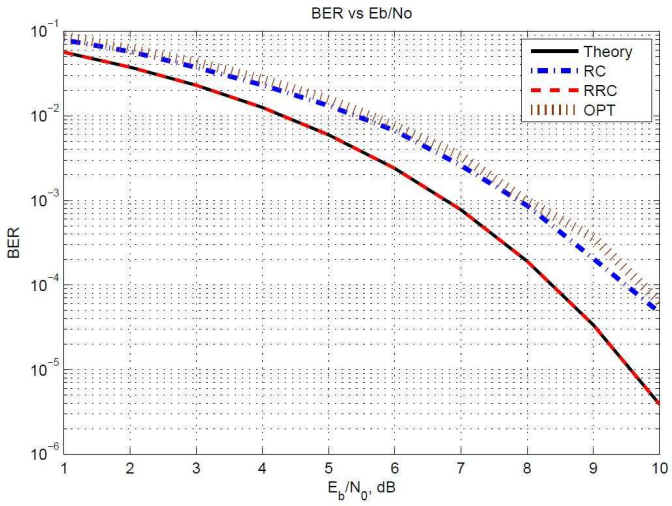

Figure 60: BERs performances for an AWGN channel with the windowing process, using QPSK modulation with M = 64, N = 256 and D = 70. The excess bandwidth is about 10%.

Figure 61 shows the PAPR at probability 10^{-4} according to the excess bandwidth ratio and the type of window. For the RC window, the PAPR decrease is continuing and almost linear. For the RRC window, the PAPR is decreased up to an excess band ratio of 0.4 after which the PAPR very slightly increases. For the OPT window, beyond an excess band ratio of 0.4, the PAPR is not reduced much. Therefore, the maximal recommended excess band ratio value is 0.4. The actual excess band ratio value will be chosen in order to provide good compromise between spectral occupation and PAPR reduction performances.

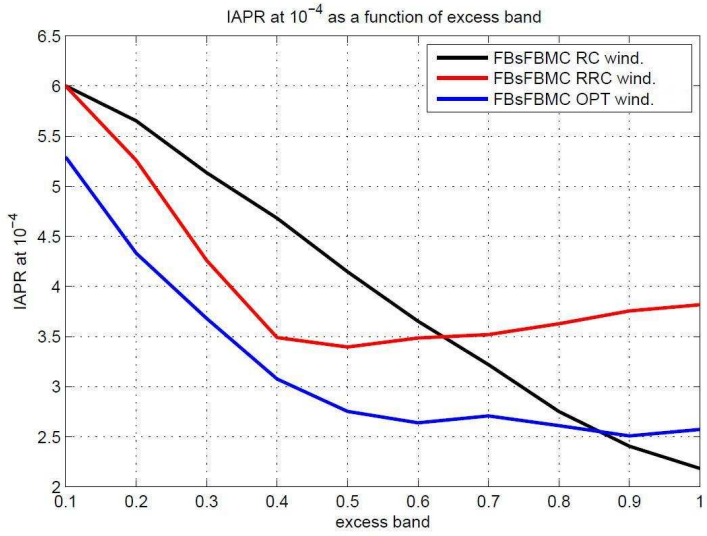

Figure 61: PAPR at 10^{-4} probability versus excess band ratio, for RC, RRC and OPT windows.

10.3.2 Non contiguous case

The previous precoding technique is inefficient when considering non contiguous transmission. For this reason, we are considering an alternative technique in this section which is a distortion-based technique. Distortion-based techniques deliberately non-linearly modify the signal [65], [66], [67], [68], [69], [70] and [71] and take benefit from the idea that some degree of distortion is generally allowed for the transmitted signals. Furthermore, distortion-based techniques operate after the modulation process and are usually less complex. The most popular, efficient and simple distortion-based techniques are clipping and filtering [67] and [71], peak windowing [68] and peak cancellation [69] and [70]. Prasad has shown in [66] that all these techniques are equivalent from the point of view of the filter design. The design of such filter is of high importance since it determines at the same time the level of out-of-band radiation of the PAPR reduced transmitted signals, but also the signal quality which is usually measured by the mean of error vector magnitude (EVM). Obviously, efficient frequency selective filters imply an important increase of the complexity due to the increase of the filter length. Many recent practical implementations recommend the use of an equiripple (ER) filter [72] since it provides a good tradeoff between frequency selectivity, EVM and complexity.

Moreover, distortion-based methods usually equally spread out the distortion generated by the PAPR reduction algorithms among all bands of the carrier aggregated signals. This can be seen as suboptimal since these bands could support different level of distortion because they might use different types of modulation and orders. In [71], Fehri has proposed a method to unequally split the distortion over different bands, but does not address the case of unequal repartition within the same band.

In SOLDER, we propose a new, simple and highly adaptive filter design that could be used for clipping and filtering, peak windowing, and peak cancelation techniques. The proposed method is designed in order to efficiently address the multiband and heterogeneous nature of the carrier aggregated signals. We show that the proposed method outperforms the performance of the well-known ER filter providing at the same time better out-of-band radiation for a given complexity, and a better control of EVM. Furthermore, we also take into account in our design method the unequal repartition of the distortion even within the same band. To the best of our knowledge, this is the first work that addresses this problem. It has to be noted

that the method proposed in this section could be applicable to contiguous case, but we recommend using precoding approach in this case since it does not increase at all the EVM and provides good PAPR results.

In our simulations, we are considering clipping and filtering technique. It is important to note that our filter design method is not limited to the clipping and filtering method and could be used for any technique that necessitates a filtering or windowing process. We consider the transmission of a non contiguous FBMC signal. The test signal is composed of three non-contiguous bands which are respectively composed of 4, 1 and 8 contiguous resource block (RB), each RB contains 12 subcarriers. The spacing between the three bands are 4 and 3 RB. Figure 63 shows the power spectral density (PSD) of the reference signal to be transmitted without PAPR reduction. The modulation of each resource RB is supposed to be heterogeneous and is arbitrarily set as follows:

- Band #1: 2 contiguous 16QAM modulated RB, then 4 contiguous 64QAM modulated RB, and finally 2 contiguous 16QAM modulated RB,
- Band #2: a single 64QAM modulated RB,
- Band #3: 4 QPSK modulated contiguous RB.

We propose to consider the LTE specifications for base station [73] to illustrate our simulation results. Nevertheless, we decide to limit the EVM degradations due to the PAPR reduction algorithm to a value that is 3% below the specifications in order to leave some room to additional EVM degradations due to radiofrequency impairments for example. Thus, the maximum tolerable EVM are 14.5%, 9.5% and 5% for respectively QPSK, 16QAM and 64QAM.

We first analyse the case of a multiband filter that is not optimized according to the heterogeneity of the EVM requirements of the signal to be transmitted. In this case, the maximum tolerable EVM is fixed to 5% by the 64QAM modulation. Thus, the PAPR reduction algorithm is set in order to reach this EVM requirement. In this case, the PAPR can be reduced to 7.3 dB. Figure 62 presents the CCDF of the instantaneous power before and after the PAPR reduction algorithm for the three analysed prototype filters. The multiband ER filter is the summation of three different ER filters of $N_h = 449$ coefficients; each filter is designed and adapted to the bandwidth of each band.

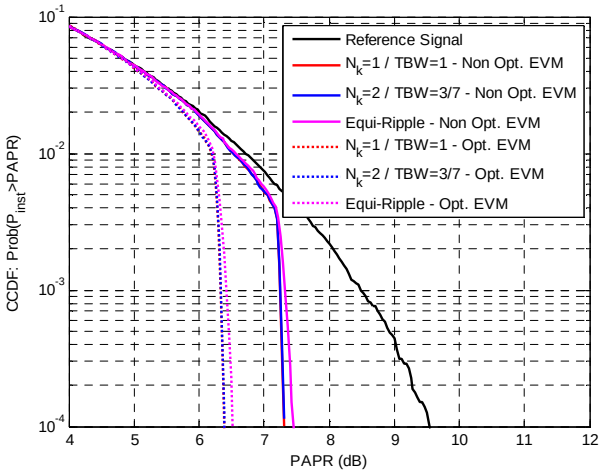

Figure 62: CCDF of the instantaneous power with/without the PAPR reduction algorithm. "Non Opt. EVM" legend refers to the multiband filter without optimization according to the EVM requirements, whereas "Opt. EVM" legend refer to the optimized filter. In any case, the performance of the two proposed filters coincide

The PSD after the PAPR reduction algorithm for the three tested prototype filters are presented in Figure 63 (left), Figure 63 (right) focuses on the PSD between and #1 and #2. We

can observe that the PSD of the PAPR reduction algorithm output can be easily controlled and adapted with N_K and TBW, which are design parameters. Obviously, a tighter filter provides better PSD results at the expense of an augmentation of the length impulse response. We can also observe that for a given filter length, the proposed prototype filter outperforms the performance of the ER filter.

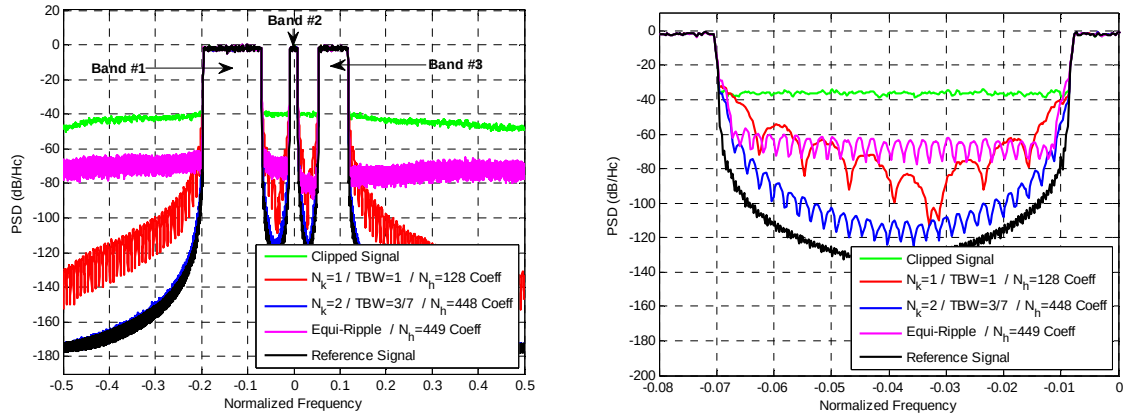

Figure 63: PSD of the signal after the PAPR reduction algorithm according to the type of prototype filter. We compare two kind of proposed prototype filters with an ER filter. (left) PSD of band #1 #2 and #3; (right) Zoom of the PSD between band #1 and #2

The mean EVM for each subcarrier index and according to the three different bands are presented in Figure 64 (up). We can observe that the mean EVM obtained with the proposed prototype filters are flat along the subcarrier index, except at the band edges. The mean EVM obtained with the ER prototype filter is affected by the filter passband ripple.

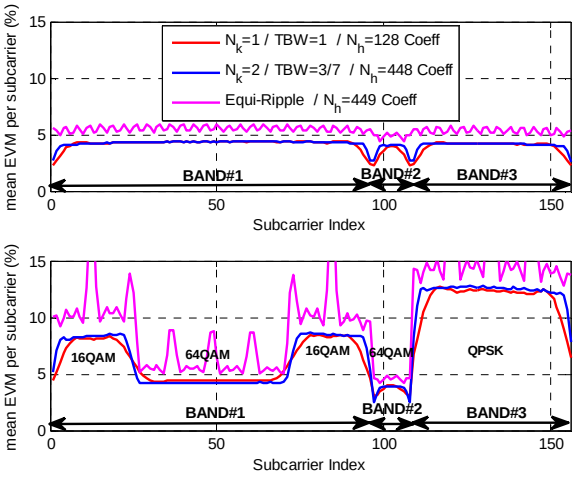

Figure 64: Mean EVM for each subcarrier index of 13 RB according to the prototype filter. Multi-band filter parameters are adapted (up) to the most constraining EVM objective (64QAM); (down) according to the EVM objective of each RB modulation

We analyse now the benefit of the multiband filter optimization according to the EVM requirements of each RB. The EVM specification of 16QAM and 64QAM modulations are respectively approximately two and three times the EVM specification of the QPSK modulation. The mean EVM for each subcarrier index and according to the three different bands are presented in Figure 64 (down). We can observe that the EVM obtained with the proposed method are perfectly adapted according to the type of modulation. On the other hand, the mean EVM obtained with the ER filter is dramatically affected and does not respect the EVM speci-

fications due to the fact that the prototype ER filter is not appropriate for the design of a multiband filter. Another important result presented in Figure 62 is that an additional PAPR reduction of 1 dB can be obtained thanks to the multiband filter optimization. Finally, the PSD at the PAPR reduction algorithm output are similar to those presented in Figure 63 and in consequence are not presented.

10.4 Achievements

We have proposed a new and efficient calibration technique to compensate for radiofrequency (RF) impairments due to unavoidable ExpressMIMO2 non-idealities. In comparison with the existing techniques, the proposed procedure has the advantages of being fast, exact and very simple to implement. Then, we have presented two different and new PAPR reduction techniques according to the type of aggregated signal. For intra-band contiguous signals, the filterbank precoding with the use of potential excess bandwidth provides excellent PAPR reduction capabilities and does not introduce any EVM degradation. For intra-band non contiguous signals, we have proposed an efficient distortion-based technique which is adaptive according to EVM requirements.
The solutions presented in this deliverable alleviate the problems that arise when considering DPD as a linearization technique to compensate for realistic transmitter front-end non linearities. The exact DPD solution that will be developed in SOLDER will be described in the next D3.3 deliverable.

11. List of prototyped techniques

In this section, we link the work developed and presented in this deliverable with the techniques which will be prototyped in WP4. Hereafter is described the relationship between each proof of concept (PoC) identified in D4.1 and this deliverable:

- PoC 1a: Aggregation of TVWS and WiFi for augmented broadcast
  The higher-layer coding solution described in Section 9 is the solution that will directly be implemented for PoC 1a in WP4. This implementation has already been done.

- Poc 1b: Aggregation of LTE in licensed and unlicensed bands
  The functionalities developed and presented in the D3.2 (section 6.3 above) about the LAA will be implemented on the SDR platform of ISI for demonstration purposes. In particular, all LAA functionalities according to 3GPP LAA concept will be implemented, namely DTX, CS, LBT and TPC. In addition to that, the learning/cognition RL algorithms will be implemented for enhanced performance of utilizing unlicensed spectrum bands.

- PoC 2: Energy efficient transmission technologies
  In this PoC, we will demonstrate the RF impairments compensation technique and also the PAPR reduction techniques for FBMC which are respectively described in sections 10.2 and 10.3.

- PoC 3a : LTE-A inter-band carrier aggregation in homogeneous networks
  This PoC will include development of Eurecom, Sequans and IS-Wireless. More specifically, section 4.3 (scheduler of CA) will be integrated with the OAI platform.

- PoC 3b: Dynamic Cognitive CA in HetNets
  LTE-A and beyond: the low complexity PMI/RI calculation (section 3) will be implemented on the SDR platform of ISI for multi-channel CA scenario. The channel allo-

cation algorithm will be also implemented selecting thiw way the best CCs that achieve the lowest feedback overhead and the highest throughput.

12. Conclusion

This report is the second report of WP3. Since CA could be addressed from many standpoints, several aspects are covered in this report:

We investigated tools and enhancement of CA where we have considered the specific problem of scaling the number of CC from 5 to 32 and identified a proposal to simplify the potential burden of DL signaling. This evolution is mostly pertinent in context of LAA or the use of higher frequency bands such as the one envisaged in 5G.

We studied solution to address the objective of selective usage of a large number of non-continuous spectrum bands in HetNets dealing with the heterogeneous channel characteristics through the channel feedback adaptation. The solution tackled with the large amount of channel estimation and allocation in multi-user CA in HetNets. To this end, low-complexity and low-feedback rate algorithms have been devised and evaluated.

The report has presented work related to achieving higher and more fair throughputs in the environment with aggregated carriers. Presented algorithms can be successfully used in homogeneous or heterogeneous deployment, and allows to obtain higher throughput than Proportional Fair algorithm without degradation in terms of dropped packets. Simulations were conducted to prove initial idea of the scheduling algorithm.

We have further studied a means for aggregation of LTE in licensed spectrum with LTE in TVWS. The solution was presented at the MAC layer as optimisation methods and algorithms with alternative purposes being to save transmission power and maximise capacity. Simulation results showed considerable reductions in transmission power and increases in capacity through aggregation.

The use of CA to enable the use of LTE in unlicensed spectrum was presented. We proposed to modify the LTE frame structure to define a burst that could accommodate the constraints of operation in unlicensed bands. We extended the cognitive radio concept to the LAA scenario, applying reinforcement learning and double Q-Learning techniques for the carrier selection and discontinuous transmission. Finally subcarrier allocation for a licensed/unlicensed CA MIMO system is discussed and the proposed solution can provide both blind learning and interference nulling for such a system model.

The report has also provided work on aggregation in TVWS. Some pioneering results are presented on what is achievable in TVWS through aggregation, and fundamental observations on aggregation of discontiguous and contiguous channels affecting aspects such as RF design of devices, among other observations.

In this deliverable, the performance of two-tier HetNets composed of WiFi and LTE has been assessed and analysed thanks to the development of an evaluation methodology and analytical tools.

We have covered i) a first complete solution for the aggregation of WiFi in unlicensed spectrum with LTE in TVWS, but also ii) an optional but extremely useful case for aggregation management involving geolocation databases such as already present in TVWS. The presented solutions can easily be extended or in some cases directly applied to scenarios that involve TVWS or another futuristic geolocation database-based spectrum management solutions in the spectrum that is being aggregated, as well as any case where an unreliable IP packet-based broadcast technology is being aggregated with a reliable IP packet-based unicast technology. The solutions are novel and highly-practical, e.g., in terms of their align-

ment with regulatory directions and standards directions in the development of systems. This practicality also serves towards their wide applicability.

At last, we tackled issues that arise using FBMC waveform as a PHY CA component when realistic transmitter front-end is taken into account. We have proposed a novel and efficient calibration technique to compensate for radiofrequency impairments due to unavoidable non-idealities. Then, we have presented two different and new PAPR reduction techniques according to the type of aggregated signal (intra-band contiguous and non-contiguous signals). Although most of the information captured in this report will be further enriched in the last WP3 deliverable, they show the promises of CA considered in its various

Appendix

The list of the appendices is the following:

Appendix 2.1: (see Appendix D3.2_Section_2.1_SEQ (R1-155917).doc)
3GPP R1-155917, “On reducing the complexity of DL control blind decoding”, 3GPP TSG-RAN WG1 Meeting #82bis, Malmö, Sweden, 05th - 09th October 2015.

Appendix 3.2: (see Appendix_D3.2_Section_3.2_ISI.pdf)
C. Tsinos, A. Galanopoulos, F. Foukalas, “Low-Complexity and Low-Feedback-Rate Channel Allocation in CA MIMO Systems with Heterogeneous Channel Feedback”, Submitted to IEEE Trans. On Veh. Techn., Oct. 2015.

Appendix 6.3: (see Appendix_D3.2_Section_6.3_ISI.pdf)
A. Galanopoulos, F. Foukalas, T. Tsiftsis, “Licensed Assisted Access: A Cognitive Radio Application in LTE-Advanced System”, Submitted to IEEE Trans. On Cogn. Communi. And Netw., Oct. 2015.

Appendix 6.4: (see Appendix_D3.2_Section_6.4_ISI.pdf)
C. G. Tsinos, F. Foukalas, T. A. Tsiftsis, “Optimal Resource Allocation for Licensed/Unlicensed Carrier Aggregation MIMO Systems”, submitted to IEEE Trans. On Wirel. Communi., Oct. 2015.

Appendix 7: (Appendix_D3.2_Section_7_KCL.pdf)
O. Holland, S. Ping, A. Aijaz, J.-M. Chareau, P. Chawdhry, Y. Gao, Z. Qin, H. Kokkinen “To White Space Or Not To White Space: That Is The Trial Within The Ofcom TV White Spaces Pilot”, IEEE DySPAN 2015, Stockholm, Sweden, September-October 2015.

Appendix 8.1: (see Appendix_D3.2_Section_8.1_EUR.pdf)
G. Arvanitakis, F. Kaltenberger, “Stochastic Analysis of Two-Tier HetNets Employing LTE and WiFi”, Submitted to IEEE ICC 2016, Kuala Lumpur, Malaysia.

Appendix 8.2: (see Appendix_D3.2_Section_8.2_EUR.pdf)
G. Arvanitakis, T. Spyropoulos, F. Kaltenberger, “An Analytical Model for Flow-level Performance in Heterogeneous Networks”, Submitted to ACM SIGMETRICS / IFIP Performance 2016, Antibes Juan-les-Pins, France.

Appendix 9.2: (see Appendix_D3.2_Section_9.2_KCL.pdf)
O. Holland, M. Dohler, “Geolocation-Based Architecture for Heterogeneous Spectrum Usage in 5G”, accepted to IEEE Globecom Workshops, San Diego, CA, USA, December 2015.

Appendix 10.1: (see Appendix_D3.2_Section_10.1_TCS.pdf)
A. Valette, S. Traverso, I. Fijalkow, M. Ariaudo, A. Cipriano, “Parameters Selection for Filter Bank Precoded Filter Bank Multicarrier Systems”, accepted to IEEE GlobeCom 2015 Workshop on 5G & Beyond - Enabling Technologies and Applications, San Diego, CA, USA, December 2015.

Appendix 10.2: (see Appendix_D3.2_Section_10.2_TCS.pdf)
A. Valette, I. Fijalkow, S. Traverso, M. Ariaudo, A. Cipriano, "Interference Cancellation for Filter Bank Precoded Filter Bank MultiCarrier", Submitted to IEEE Communications Letters.

Appendix 10.3: (see Appendix_D3.2_Section_10.3_TCS.pdf)

S. Traverso, “A New Family of Filters for PAPR Reduction of Carrier Aggregated Signals”, Submitted to IEEE WCNC 2016, Doha, Qatar.

Appendix 10.4: (see Appendix_D3.2_Section_10.4_TCS.pdf)
S. Traverso, “A Family of Square-Root Nyquist Filter with Low Group Delay and High Stop-band Attenuation”, Submitted to IEEE VTC 2016, Nanjing, China.

List of Acronyms

Acronym	Meaning
3GPP	3rd Generation Partnership Project
AFB	Analysis Filter Bank
AWGN	Additive White Gaussian Noise
BER	Bit Error Rate
CC	Component Carrier
CCDF	Complementary Cumulative Density Function
COT	Channel Occupancy Time
CQI	Channel Quality Indication
CS	Carrier Selection
CSI	Channel State Information
DFT	Discrete Fourier Transform
DTX	Discontinuous Transmission
ER	Equiripple
EVM	Error Vector Magnitude
FB	Filter Bank
FBMC	Filter Bank MultiCarrier
HM	Hungarian Method
IDFT	Discret Fourier Transform
IF	Intermediate Frequency
LAA	Licensed Assisted Access
LBT	Listen Before Talk
LMS	Least Mean Square
LNA	Low Noise Amplifier
LTE	Long Term Evolution
MLNP	Mixed Integer Non Linear Programming
OFDM	Orthogonal Frequency Division Multiplexing
OQAM	Offset Quadrature Amplitude Modulation
PA	Power Amplifier
PAPR	Peak to Average Power Ratio
PCell	Primary Cell
PMI	Precoding Matrix Indicator
PSD	Power Spectral Density
QAM	Quadrature Amplitude Modulation
RB	Resource Block
RC	Raised Cosine
RI	Rank Indicator
RL	Reinforcement Learning
RRC	Root Raised Cosine
SCell	Secondary Cell
SC-FDMA	Single Carrier Frequency Division Multiple Access
SFB	Synthesis Filter Bank
SI	Study Item
SM	Stable Matching
TPC	Transmit Power Control
TVWS	TV White Space
WI	Work Item

References

[1] LTE_WLAN_radio, RP-150510, “LTE-WLAN Radio Level Integration and Interworking Enhancement” new WID accepted during RAN#67, March 2015
[2] LTE_WLAN_radio_legacy, RP-151615, “New WI Proposal: LTE-WLAN RAN Level Integration supporting legacy WLAN“, new WID accepted during RAN#69, September 2015
[3] 3GPP RP-150771, “LTE Carrier Aggregation Enhancement Beyond 5 Carriers”, updated Work item description, June 2015.
[4] 3GPP R1-155917, “On reducing the complexity of DL control blind decoding”, 3GPP TSG-RAN WG1 Meeting #82bis, Malmö, Sweden, 05th - 09th October 2015.
[5] S. Schwarz, M. Wrulich and M. Rupp, Mutual Information based Calculation of the Precoding Matrix Indicator for 3GPP UMTS/LTE, International ITG Workshop on Smart Antennas (WSA 2010).
[6] H. Kuhn, “The Hungarian method for the assignment problem,” Naval Res. Logist. Quart., vol. 2, no. 1/2, pp. 83–97, Mar. 1955.
[7] 3GPP Release 13, Web: http://www.3gpp.org/release-13.
[8] Mochaourab, R.; Holfeld, B.; Wirth, T., "Distributed Channel Assignment in Cognitive Radio Networks: Stable Matching and Walrasian Equilibrium," in Wireless Communications, IEEE Transactions on , vol.14, no.7, pp.3924-3936, July 2015.
[9] Li Huang; Guangxi Zhu; Xiaojiang Du; Kaigui Bian, "Stable multiuser channel allocations in opportunistic spectrum access," in Wireless Communications and Networking Conference (WCNC), 2013 IEEE , vol., no., pp.1715-1720, 7-10 April 2013.
[10] A. Leshem, E. Zehavi and Y. Yaffe "Multichannel opportunistic carrier sensing for stable channel access control in cognitive radio systems", IEEE J. Sel. Areas Commun., vol. 30, no. 1, pp.82 -95 2012.
[11] B. Holfeld, R. Mochaourab and T. Wirth "Stable matching for adaptive cross-layer scheduling in the LTE downlink", Proc. IEEE VTC, pp.1 -5 2013.
[12] Y.Huang and B.D.Rao, Performance Analysis of Heterogeneous Feedback Design in an OFDMA Downlink with Partial and Imperfect Feedback, IEEE Trans. on Sig. Processing, vol.61, no.4, pp. 1033-1046, Feb. 2013.
[13] 3GPP TR 36.889 TSG RAN, "Study on Licensed-Assisted Access to Unlicensed Spectrum", Rel.13, v13.0.0, June 2015.
[14] A. Galanopoulos, F. Foukalas and Th. Tsiftsis, Unlicensed Spectrum Aggregation: A Cognitive Radio Application in LTE-A Systems, submitted to IEEE Trans. On Cog. Commun. And Net., Sep. 2015.
[15] F. F. Digham, M.-S. Alouini, and M. K. Simon, On the energy detection of unknown signals over fading channels, IEEE Trans. Commun., vol. 55, no. 1, pp. 21..24, Jan. 2007.
[16] C. Mehlfuhrer, M. Wrulich, J. Colom Ikuno, D. Bosanska and M. Rupp, "Simulating the Long Term Evolution Physical Layer", Proc. of the 17th European Signal Processing Conference (EUSIPCO 2009), Aug. 2009.
[17] A. Cheng, H. Jin, J. Li, Y. Yu and M. Peng, Joint Discontinuous Transmission and Power Control for High Energy Efficiency in Heterogeneous Small Cell Networks, IEEE PIMRC 25th, Sept. 2014.
[18] van Hasselt, Hado, "Double Q-learning", Advances in Neural Information Processing Systems, pp. 2613-2621, 2010.
[19] C.Tsinos, F.Foukalas and Th. Tsiftsis, Resource Allocation for licensed/ unlicensed carrier aggregation systems, submitted to IEEE Trans. Wirel. Communi., Sept. 2015.
[20] M. Bkassiny, Y. Li, and S. Jayaweera, "A survey on machine-learning techniques in cognitive radios," Communications Surveys Tutorials, IEEE, vol. 15, pp. 1136-1159, 3rd Quarter 2013.

[21] L. Gavrilovska, V. Atanasovski, I. Macaluso, and L. DaSilva, "Learning and reasoning in cognitive radio networks," Communications Surveys Tutorials, IEEE, vol. 15, pp. 1761-1777, 4th Quarter 2013.
[22] M. Li, Y. Xu, and J. Hu, "A q-learning based sensing task selection scheme for cognitive radio networks," in Wireless Communications Signal Processing, 2009. WCSP 2009. International Conference on, pp. 1-5, Nov. 2009.
[23] K.-L. Yau, P. Komisarczuk, and P. Teal, "A context-aware and intelligent dynamic channel selection scheme for cognitive radio networks," in Cognitive Radio Oriented Wireless Networks and Communications, 2009. CROWN-COM '09. 4th International Conference on, pp. 1-6, June 2009.
[24] Feifei Gao; Rui Zhang; Ying-Chang Liang; Ying-Chang Liang, "Optimal design of learning based MIMO cognitive radio systems," Information Theory, 2009. ISIT 2009. IEEE International Symposium on , vol., no., pp.2537,2541, 28 June – 3 July 2009.
[25] Xin Kang; Ying-Chang Liang; Nallanathan, A.; Garg, H.K.; Rui Zhang, "Optimal power allocation for fading channels in cognitive radio networks: Ergodic capacity and outage capacity", Wireless Communications, IEEE Transactions on , vol.8, no.2, pp.940-950, Feb. 2009.
[26] 3GPP TSG RAN Meeting #66, "LTE Carrier Aggregation Enhancement Beyond 5 Carriers," Document, RP-142286, pp. 1–9, Dec. 2014.
[27] J. Andrews, F. Baccelli, and R. Ganti, "A tractable approach to coverage and rate in cellular networks," Communications, IEEE Transactions on, vol. 59, no. 11, pp. 3122–3134, Nov. 2011.
[28] H. Dhillon, R. Ganti, F. Baccelli, and J. Andrews, "Modeling and analysis of k-tier downlink heterogeneous cellular networks," Selected Areas in Communications, IEEE Journal on, vol. 30, no. 3, pp. 550–560, April 2012.
[29] H. Dhillon, M. Kountouris, and J. Andrews, "Downlink coverage probability in mimo hetnets," in Signals, Systems and Computers (ASILOMAR), 2012 Conference Record of the Forty Sixth Asilomar Conference on, pp. 683–687, Nov, 2012.
[30] X. Lin, J. Andrews, R. Ratasuk, B. Mondal, and A. Ghosh, "Carrier aggregation in heterogeneous cellular networks," in Communications (ICC), 2013 IEEE International Conference on, pp. 5199–5203, Jun. 2013.
[31] X. Lin, J. Andrews, and A. Ghosh, "Modeling, analysis and design for carrier aggregation in heterogeneous cellular networks," Communications, IEEE Transactions on, vol. 61, no. 9, pp. 4002–4015, Sept. 2013.
[32] G. Arvanitakis, "Distribution of the number of poisson points in poisson voronoi tessellation," Eurecom, Tech. Rep. RR-15-304, 2014.
[33] OpenAir Interface, www.openairinterface.org.
[34] S. Sesia, I. Toufik, and M. Baker, LTE - the UMTS long term evolution: from theory to practice. Chichester: Wiley, 2009.
[35] AirMagnet and inc, "802.11n Primer," Whitepaper, pp. 1–15, Aug. 2008.
[36] G. Bianchi, "Performance analysis of the ieee 802.11 distributed coordination function," Selected Areas in Communications, IEEE Journal on, vol. 18, no. 3, pp. 535–547, March 2000.
[37] Ofcom, "Implementing TV White Spaces," statement, February 2015, accessible at http://stakeholders.ofcom.org.uk/consultations/white-space-coexistence/statement, accessed May 2015.
[38] ETSI, "White Space Devices (WSD); Wireless Access Systems operating in the 470 MHz to 790 MHz frequency band; Harmonized EN covering the essential requirements of article 3.2 of the R&TTE Directive," v1.1.1, April 2014.
[39] FCC, "In the Matter of Unlicensed Operation in the TV Broadcast Bands, Additional Spectrum for Unlicensed Devices Below 900 MHz and in the 3 GHz Band, Second Memorandum, Opinion and Order," September 2010 (see also Third MO&O from April 2012).

[40] GSM Association, “GSMA Public Policy Position: Licensed Shared Access (LSA) and Authorised Shared Access (ASA),” February 2013. Accessible at http://www.gsma.com/spectrum/licensed-shared-access-lsa-and-authorised-shared-access-asa, accessed February 2015.
[41] SOLDER Deliverable 2.3, “System-Level Requirements for Scenarios and Use Cases,” April 2015.
[42] O. Holland, M. Dohler, “Geolocation-Based Architecture for Heterogeneous Spectrum Usage in 5G,” IEEE Globecom 2015 Workshops, San Diego, CA, USA, December 2015.
[43] O. Holland, et. al., “To White Space Or Not To White Space: That Is The Trial Within The Ofcom TV White Spaces Pilot,” IEEE DySPAN 2015, Stockholm, Sweden, Sept.-Oct. 2015.
[44] O. Holland, “Some Are Born With White Space, Some Achieve White Space, And Some Have White Space Thrust Upon Them,” submitted to IEEE Transactions on Cognitive Communications and Networks, Sept. 2015.
[45] O. Holland, et al., “Some Initial Results and Observations from a Series of Trials within the Ofcom TV White Spaces Pilot,” IEEE VTC 2015-Spring, Glasgow, UK, May 2015.
[46] W. Yamada, …, O. Holland, et al., “Indoor Propagation Model for TV White Space,” CROWNCOM 2014, Oulu, Finland, June 2014.
[47] SOLDER Deliverable D4.1, “PoC Scenarios and system interfaces,” April 2015.
[48] IEEE Std 802.11™-2012, http://standards.ieee.org/getieee802/download/802.11-2012.pdf, accessed July 2015.
[49] O. Holland, A. H. Aghvami, “Bitmapped NAK feedback aggregation for improved reliable multicast scalability,” IEEE Globecom 2005, St. Louis, MO, USA, Dec. 2005.
[50] Buljore, S. Harada, H. ; Filin, S. ; Houze, P. ; Tsagkaris, K. ; Holland, O. ; Nolte, K. ; Farnham, T. ; Ivanov, V. “Architecture and enablers for optimized radio resource usage in heterogeneous wireless access networks: the IEEE 1900.4 working group,” IEEE Communications Magazine, Vol. 47, No. 1, Jan. 2009.
[51] O. Holland, M. Dohler, “Standards for Spectrum Sharing to Realize 5G Capacity,” IEEE ComSoc 5G Rapid Reaction Standardization Working Meeting, Piscataway, NJ, April 2015.
[52] O. Holland, M. Dohler, “Standardized Geolocation-Based System for Spectrum Sharing and Heterogeneous Access Management to Support 5G,” IEEE CSCN 2015, Tokyo, Japan, October 2015.
[53] O. Holland, M. Dohler, “Geolocation-Based Architecture for Heterogeneous Spectrum Usage in 5G,” IEEE Globecom 2015 Workshops, San Diego, CA, USA, Dec. 2015.
[54] M. Luby, A. Shokrollahi, M. Watson, T. Stockhammer, “RaptorQ Forward Error Correction Scheme for Object Delivery,” IETF Meeting 77, Anaheim, CA, USA, March 2010.
[55] M. Luby, et. al., “RaptorQ Forward Error Correction Scheme for Object Delivery,” IETF RFC 6330, Aug. 2011.
[56] SOLDER deliverable D3.1 “Initial report of heterogeneous Carrier Aggregation in LTE-A and Beyond”, Oct. 2014.
[57] A. Valette, S. Traverso, I. Fijalkow, M. Ariaudo, A. Cipriano, “Parameters Selection for Filter Bank Precoded Filter Bank Multicarrier Systems”, accepted to IEEE GlobeCom 2015 Workshop on 5G & Beyond - Enabling Technologies and Applications.
[58] A. Valette, I. Fijalkow, S. Traverso, M. Ariaudo, A. Cipriano, "Interference Cancellation for Filter Bank Precoded Filter Bank MultiCarrier", Submitted (24/07/2015) to IEEE Communications Letters.
[59] S. Traverso, “A New Family of Filters for PAPR Reduction of Carrier Aggregated Signals”, Submitted (31/08/2015) to IEEE WCNC 2016, Doha, Qatar.
[60] S. Traverso, “A Family of Square-Root Nyquist Filter with Low Group Delay and High Stopband Attenuation”, Submitted (27/08/2015) to IEEE VTC 2016, Nanjing, China.
[61] A. A. Abidi, "Direct-conversion radio transceivers for digital communications", IEEE J. Solid-State Circuits, vol. 30, pp. 1399-1410 1995.

[62] H. G. Myung and D. J. Goodman, “Single Carrier FDMA, A New Air Interface For Long Term Evolution,” Wiley Series On Wireless Communications And Mobile Computing, Wiley, December 2008.
[63] S. Mirabbasi, and K. Martin, “Overlapped Complex-Modulated Transmultiplexer Filters with Simplified Design and Superior Stopbands,” IEEE Transactions on Circuits and Systems, vol. 50, no. 8, August 2003.
[64] G. Yuen and B. Farhang-Boroujeny, “Analysis of the optimum precoder in SC-FDMA,” IEEE Transactions on Wireless Communications, Vol. 11, No 11, pp. 4096-4017, November 2012.
[65] S. H. Han and J. H. Lee, “An overview of peak-to-average power ratio reduction techniques for multicarrier transmission,” IEEE Wireless Commun. Mag., vol. 12, no. 12, pp. 56–65, Apr. 2005.
[66] R. Prasad, “OFDM for Wireless Communication Systems,” Artech House, 2004.
[67] X. Li and L. J. Cimini Jr., "Effects of clipping and filtering on the performance of OFDM," IEEE Commun. Lett., vol. 2, no. 5, pp.131-133, May 1998.
[68] O. Väänänen, J. Vankka and K. Halonen, “Effect of Clipping in Wideband CDMA System and Simple Algorithm for Peak Windowing,” World Wireless Congress, pp.614-619, 2002.
[69] J. Song and H. Ochiai, “A low-complexity peak cancellation scheme and its FPGA implementation forpeak-to-average power ratio reduction,” EURASIP Journal on Wireless Communications and Networking., vol. 2015, pp 1-14, Article ID 10.1186.
[70] Inc Xilinx, LogiCORE IP Peak Cancellation Crest Factor Reduction v3.0. (Xilinx, Inc., 1–38, 2011).
[71] B. Fehri, S. Boumaiza and E. Sich, “Crest Factor Reduction of Inter-Band Multi-Standard Carrier Aggregated Signals,” IEEE Trans. Microw. Theory Techn., vol. 62, no. 12, pp 3286-3297, Dec. 2014.
[72] I. W. Selesnick and C. S. Burrus, “Exchange algorithms that complement the Parks-McClellan algorithm for linear-phase FIR filter design,” IEEE Trans. Circuits Syst. II , vol. 44, no. 2, pp 137–143, Feb. 1997.
[73] Technical Specification Group Radio Access Network; Base Station (BS) radio transmission and reception, Release 11.2; 3GPP TS 36.104 V11.2 (2012-11).
[74] http://is-wireless.com/lte-mac-lab/, Specification and Overview.